Contributions to the Direct Time Integration in Wave Propagation Analyses

by

GUNWOO NOH

S.M. Mechanical Engineering
Massachusetts Institute of Technology, 2011
B.S. Mechanical Engineering
Korea Advanced Institute of Science and Technology, 2009

Submitted to the Department of Mechanical Engineering
in Partial Fulfillment of the Requirements for the Degree of

DOCTOR OF PHILOSOPHY IN MECHANICAL ENGINEERING

at the

MASSACHUSETTS INSTITUTE OF TECHNOLOGY

September 2013

Signature of Author .....
Department of Mechanical Engineering
August 10, 2013

Certified by. . . . . .
Klaus-Jürgen Bathe
Professor of Mechanical Engineering
Thesis Supervisor

Accepted by. . . . . .
David Edgar Hardt
Professor of Mechanical Engineering
Chairman, Departmental Committee on Graduate Students

Contributions to the Direct Time Integration in Wave Propagation Analyses

by

Gunwoo Noh

Submitted to the Department of Mechanical Engineering
on August 10, 2013 in Partial Fulfillment of the
Requirements for the Degree of Doctor of Philosophy in
Mechanical Engineering

ABSTRACT

This thesis intends to contribute to the computational methods for wave propagations. We review an implicit time integration method, the Bathe method, that remains stable without the use of adjustable parameters when the commonly used trapezoidal rule results in unstable solutions. We then focus on additional important attributes of the scheme. We present dispersion properties of the Bathe method and show that its desired characteristics for structural dynamics are also valuable for wave propagation problems. A dispersion analysis using the CFL number is given and the solution of some benchmark problems show that the scheme is a method for general use for structural dynamics and wave propagations. Finally, we propose a new explicit time integration method for the analysis of wave propagation problems. The scheme has been formulated using a sub-step within a time step to achieve desired numerical damping to suppress undesirable spurious oscillations of high frequencies. With the optimal CFL number, the method uses about 10% more solution effort as the standard central difference scheme but significantly improves the solution accuracy and a non-diagonal damping matrix can directly be included. The stability, accuracy and numerical dispersion are analyzed, and solutions to problems are given that illustrate the performance of the scheme.

Keywords
Direct time integrations, Structural dynamics, Wave propagations, Numerical damping, Numerical dispersion

Thesis Committee Members
Professor Klaus-Jürgen Bathe (Committee chair); *email:* kjb@mit.edu
Professor Tomasz Wierzbicki; *email:* wierz@mit.edu
Professor Raúl A. Radovitzky; *email:* rapa@mit.edu

Acknowledgements

I would like to express my deepest gratitude to my advisor, Professor Klaus-Jürgen Bathe, for his extraordinary guidance, support, and kindness. It has been a truly fantastic experience to work with a brilliant researcher who has a great attitude. It also has been a pleasure to work under this wonderful teacher, who is very patient and always understands and encourages his student. Professor Bathe has been a true educator to me, and this dissertation would not have been possible without his invaluable mentorship.

I also wish to express sincere gratitude to my other thesis committee members, Professors Tomasz Wierzbicki and Raúl A. Radovitzky, for their valuable advice and insights into the work presented herein. Undoubtedly, their suggestions have strengthened the quality of my work. I also deeply appreciate their kind encouragement during my time at M.I.T.

I also thank all my friends in the Finite Element Research Group. I will never forget the breakfast burritos that we had after overnights in our office, the jokes we used to tease each other with in our own language, and the beers we had for no reason, although their advice on my research may have been of less importance. It is also impossible to imagine my graduate life without my friends in MIT MechE, KGSA-ME and the KGSA basketball team.

They all made my time at M.I.T. very special.

I also deeply appreciate the Samsung Scholarship Foundation for their generous financial support for the last four years.

Finally, and most importantly, I offer my most valuable appreciation to my family for their unconditional support and endless love. Without them, I would have very little today. I am forever grateful, and I proudly dedicate this dissertation to them.

Contents

List of Figures

List of Tables

Chapter 1

Introduction

In the solutions of structural dynamics and transient wave propagation problems, direct time integration with finite elements is widely used and can be categorized into two groups: explicit and implicit methods. The method is explicit unless the solution procedure requires factorization of the "effective stiffness" matrix, in which case it is implicit [1–3].

In general, each method type has its own advantages and disadvantages. Implicit methods can be designed to have unconditional stability, so that the time step size can be selected solely based on the characteristics of the problem at hand. However, implicit methods require much larger computational costs per time step than explicit methods do, since explicit methods can be designed to require only vector calculations with the diagonal mass matrix. However, an explicit method can only be conditionally stable. Hence, explicit methods can be very effective when the time step size required by the stability limit is either greater than or not much less than that required to describe the problem, as in wave propagation analyses, for example [1–5].

However, the solutions of the transient wave propagation using the above procedures may

deteriorate due to dissipation and dispersion errors, which are caused by spatial and temporal discretization [1]. Spurious oscillations, especially for high wave numbers, ruin the accuracy of the solution [6–11]. These oscillations are from dispersion error, which is also related to Gibb's phenomenon or pollution effect. As a wave travels, the errors from the difference between numerical wave velocities and physical wave velocity accumulate, also affecting the dissipation error by dispersing the wave, whereby the solution becomes more erroneous.

Hence, there has been a considerable effort to reduce the dispersion errors. First, by improving spatial discretization, dispersion errors can be reduced. Most straightforwardly, a fine mesh with a very small time step size can be used. This strategy requires that the time step be selected carefully, depending on the element size; otherwise, the solution errors remain large, even with a fine mesh [1, 12, 13]. Different types of higher-order spatial discretization [14–24] may be used to improve the solution accuracy. However, the use of higher-order spatial discretization can be very computationally expensive and may not have the generalizability of the traditional finite element procedures using low order elements.

The errors from spatial and temporal discretization appear concurrently, and they affect each other in the solutions of transient wave propagation. Dispersion errors from spatial discretization, temporal discretization, and the coupled influence of both discretization errors have been analyzed for some cases [25–30]. Analyses of these errors have led to the

use of linear combinations of consistent and lumped mass matrices [26, 31–35]. By balancing the effect of the consistent and lumped mass matrices, these approaches may considerably reduce the dispersion error in one dimensional analysis. However, by this technique alone, good accuracy in general higher dimensional wave propagation problems is difficult to achieve.

Other approaches have been introduced to minimize dispersion errors. These use the mass and stiffness matrix from the modified integration rule [30, 35, 36] and shift the numerical integration points from conventional Gauss or Gauss-Lobatto integration points in the calculation of mass and stiffness matrices. However, different integration rules than those commonly used have been proposed, and these rules may also depend on the material properties, which renders these approaches impractical.

To improve the solution of wave propagation problems, another category of approaches have been introduced that filters the resulted spurious modes. First, to minimize spurious oscillations by pre/post-processing, a digital filter [37] and time integration for the filtering stage [35, 38] have been introduced. However, the filters are only applicable to specific points in space and time. Hence, these techniques do not lend themselves to analyses requiring a solution for all times and over the complete solution domain, for example, for making a movie of the calculated displacements and stresses.

Numerical dissipations are used in many direct time integration methods to improve the solution by suppressing high frequency spurious wave modes [1, 2, 39, 40]. Using this strategy, accurate solutions are difficult since the introduced numerical dissipation should be large enough to suppress the high frequency spurious waves, while good accuracy for the low frequency waves should be simultaneously ensured. However, this approach can be very effective since the solution procedure does not require any additional computational cost and can be used for structural dynamics and wave propagation problems in a uniform manner.

A number of implicit time integration methods have been proposed, the trapezoidal rule and the alpha methods are now being the most commonly used [1, 41]. As is well known, the trapezoidal rule is unconditionally stable in linear analysis, second-order accurate, and, regarding time integration errors, shows no amplitude decay and acceptable period elongation [1]. However, the dispersion errors in the high frequency modes may ruin the solutions significantly in the wave propagation analysis since the trapezoidal rule is non-dissipative. Moreover, the method may become unstable in nonlinear analyses, in which case momentum and energy are clearly increased. Hence, researchers have sought more effective time integration schemes.

To introduce some damping into a time integration method, adjustable parameters are employed, and this approach has been used in the design of the alpha methods [41]. In these methods, the parameters have to be selected based on the characteristics of the problem

solved. Since inappropriate parameters may result, adjustable parameters itself may render the approach ineffective.

Recently, the Bathe method [42–44] has been presented and shown to result in remarkably accurate solutions by having damping properties to limit the solution error for physical wave modes, and by almost discarding the high spurious modes [45]. With its optimal CFL number, the method results in very small numerical dispersion error in all the participating wave modes by practically eradicating the high spurious modes, which cannot be well represented spatially. Furthermore, the capabilities in structural dynamics and unconditional stability render the Bathe method very attractive as a general method for structural dynamics and wave propagation problems [42–46].

Among explicit methods, the central difference method is still the most widely used scheme. It has the highest stability limit of any second-order accurate explicit method [47, 48]. The central difference method uses a matrix factorization for systems with a non-diagonal damping matrix [49, 50]. However, since the central difference method is a non-dissipative method, the solution accuracy can be ruined by the dispersion errors in the high frequency modes.

The development of dissipative explicit methods has been heavily pursued [51], and schemes have been presented by Newmark [52], Chung and Lee [3], Zhai [53], Hulbert and Chung [4] and Tchamwa and Wielgosz [54]. The Tchamwa-Wielgosz method, Newmark

explicit method, and the Zhai explicit scheme with high-frequency dissipation are only first order accurate, and the latter two decrease the solution accuracy in the low frequency domain.. Comparative studies [55, 56] show that the remaining dissipative explicit methods are second-order accurate but often provide less accurate solutions than the Tchamwa-Wielgosz method.

This thesis presents a study of the Bathe method for structural dynamics and wave propagation problems, demonstrating that the characteristics that the Bathe method possesses are valuable, and then presents a novel and improved explicit time integration method for wave propagation analysis. In Chapter 2, the characteristics of the Bathe method in linear structural dynamics are reviewed and discussed. In Chapter 3, the properties of the Bathe method in the solution of wave propagation problems are analyzed. In Chapter 4, based on Chapters 2 and 3, a new explicit time integration method for wave propagation for significantly improved solutions is proposed. We note that most of the presented content in this thesis is similar (and in parts identical) to that published in their previous papers [44, 45, 57]

Chapter 2

A review of an implicit time integration scheme in structural dynamics

This Chapter comprises a study of the Bathe method in structural dynamics, comparing its performance with the trapezoidal rule and two additional members of the Newmark family of methods that may be considered for solutions. First, the basic equations of the Bathe are briefly reviewed and some basic properties of the time integration method are presented. Then, the scheme is applied, along with the other methods, in the solution of a simple linear "model problem" to illustrate some important and valuable properties of the method, increasing insight into the method [44].

2.1. The basic equations of the Bathe method

The governing finite element equations, in linear analysis, to be solved are

$$\mathbf{M}\ddot{\mathbf{U}}+\mathbf{C}\dot{\mathbf{U}}+\mathbf{K}\mathbf{U}=\mathbf{R} \quad , \tag{2.1}$$

with initial conditions where $\mathbf{U}$ and $\mathbf{R}$ are the nodal values of the solution and the vector of externally applied nodal forces, and $\mathbf{M}$, $\mathbf{C}$, $\mathbf{K}$ are the mass, damping and stiffness matrices, respectively. The time integration scheme obtains the solutions at time $t+\Delta t$ using some previously calculated solution variables up to time t, with the predefined time step size Δt.

In the Bathe method, the complete time step Δt consists of two equal-length sub-steps. The trapezoidal rule is used in the first sub-step, and in the second sub-step the 3-point Euler backward method is employed. The resulting equations are

$$ {}^{t+\Delta t/2}\dot{\mathbf{U}} = {}^{t}\dot{\mathbf{U}} + \left[\frac{\Delta t}{4}\right]\left({}^{t}\ddot{\mathbf{U}} + {}^{t+\Delta t/2}\ddot{\mathbf{U}}\right) \quad , \tag{2.2} $$

$$ {}^{t+\Delta t/2}\mathbf{U} = {}^{t}\mathbf{U} + \left[\frac{\Delta t}{4}\right]\left({}^{t}\dot{\mathbf{U}} + {}^{t+\Delta t/2}\dot{\mathbf{U}}\right) \quad , \tag{2.3} $$

$$ {}^{t+\Delta t}\dot{\mathbf{U}} = \frac{1}{\Delta t}{}^{t}\mathbf{U} - \frac{4}{\Delta t}{}^{t+\Delta t/2}\mathbf{U} + \frac{3}{\Delta t}{}^{t+\Delta t}\mathbf{U} \quad , \tag{2.4} $$

and

$$ {}^{t+\Delta t}\ddot{\mathbf{U}} = \frac{1}{\Delta t}{}^{t}\dot{\mathbf{U}} - \frac{4}{\Delta t}{}^{t+\Delta t/2}\dot{\mathbf{U}} + \frac{3}{\Delta t}{}^{t+\Delta t}\dot{\mathbf{U}} \quad . \tag{2.5} $$

Equations (2.2) to (2.5), with the equilibrium at time $t+\Delta t/2$ and $t+\Delta t$, result in the time-stepping equations as

$$\left(\frac{16}{\Delta t^2}\mathbf{M}+\frac{4}{\Delta t}\mathbf{C}+\mathbf{K}\right)\,{}^{t+\Delta t/2}\mathbf{U}={}^{t+\Delta t/2}\hat{\mathbf{R}}\ , \tag{2.6}$$

where

$${}^{t+\Delta t/2}\hat{\mathbf{R}}={}^{t+\Delta t/2}\mathbf{R}+\mathbf{M}\left(\frac{16}{\Delta t^2}{}^{t}\mathbf{U}+\frac{8}{\Delta t}{}^{t}\dot{\mathbf{U}}+{}^{t}\ddot{\mathbf{U}}\right)+\mathbf{C}\left(\frac{4}{\Delta t}{}^{t}\mathbf{U}+{}^{t}\dot{\mathbf{U}}\right)\ , \tag{2.7}$$

$$\left(\frac{9}{\Delta t^2}\mathbf{M}+\frac{3}{\Delta t}\mathbf{C}+\mathbf{K}\right)\,{}^{t+\Delta t}\mathbf{U}={}^{t+\Delta t}\hat{\mathbf{R}}\ , \tag{2.8}$$

and

$${}^{t+\Delta t}\hat{\mathbf{R}}={}^{t+\Delta t}\mathbf{R}+\mathbf{M}\left(\frac{12}{\Delta t^2}{}^{t+\Delta t/2}\mathbf{U}-\frac{3}{\Delta t^2}{}^{t}\mathbf{U}+\frac{4}{\Delta t}{}^{t+\Delta t/2}\dot{\mathbf{U}}-\frac{1}{\Delta t}{}^{t}\dot{\mathbf{U}}\right)+\mathbf{C}\left(\frac{4}{\Delta t}{}^{t+\Delta t/2}\mathbf{U}-\frac{1}{\Delta t}{}^{t}\mathbf{U}\right). \tag{2.9}$$

Eqs. (2.6) and (2.8) are used successively for each time step to solve for the required solution over the complete time domain considered with the initial conditions corresponding to initial time known. Prior to the time integration, a time step Δt is defined, and the "effective stiffness matrices" defined in Eqs. (2.6) and (2.8) are factorized. For each time step, the calculation of the effective load vectors and forward-reductions and back-substitutions are performed [1].

Table 2-1 *Step-by-step solution using the Bathe integration method*

A. *Initial calculation*

1. Form stiffness matrix $\mathbf{K}$, mass matrix $\mathbf{M}$, and damping matrix $\mathbf{C}$
2. Initialize ${}^{0}\mathbf{U}$, ${}^{0}\dot{\mathbf{U}}$ and ${}^{0}\ddot{\mathbf{U}}$.
3. Select time step Δt and calculate integration constants:

$$a_0 = \frac{16}{\Delta t^2}; \quad a_1 = \frac{4}{\Delta t}; \quad a_2 = \frac{9}{\Delta t^2}; \quad a_3 = \frac{3}{\Delta t};$$

$$a_4 = 2a_1; \quad a_5 = \frac{12}{\Delta t^2}; \quad a_6 = -\frac{3}{\Delta t^2}; \quad a_7 = -\frac{1}{\Delta t}$$

4. Form effective stiffness matrices $\hat{\mathbf{K}}_1$ and $\hat{\mathbf{K}}_2$:

$$\hat{\mathbf{K}}_1 = \mathbf{K} + a_0\mathbf{M} + a_1\mathbf{C}; \quad \hat{\mathbf{K}}_2 = \mathbf{K} + a_2\mathbf{M} + a_3\mathbf{C}$$

5. Triangularize $\hat{\mathbf{K}}_1$ and $\hat{\mathbf{K}}_2$: $\hat{\mathbf{K}}_1 = \mathbf{L}_1\mathbf{D}_1\mathbf{L}_1^T$; $\hat{\mathbf{K}}_2 = \mathbf{L}_2\mathbf{D}_2\mathbf{L}_2^T$.

B. *For each time step:*

<First sub-step>

1. Calculate effective loads at time $t + \Delta t/2$:

$${}^{t+\Delta t/2}\hat{\mathbf{R}} = {}^{t+\Delta t/2}\mathbf{R} + \mathbf{M}(a_0\,{}^{t}\mathbf{U} + a_4\,{}^{t}\dot{\mathbf{U}} + {}^{t}\ddot{\mathbf{U}}) + \mathbf{C}(a_1\,{}^{t}\mathbf{U} + {}^{t}\dot{\mathbf{U}})$$

2. Solve for displacements at time $t + \Delta t/2$:

$$\mathbf{L}_1\mathbf{D}_1\mathbf{L}_1^T\,{}^{t+\Delta t/2}\mathbf{U} = {}^{t+\Delta t/2}\hat{\mathbf{R}}$$

3. Calculate velocities at time $t + \Delta t/2$:

$${}^{t+\Delta t/2}\dot{\mathbf{U}} = a_1({}^{t+\Delta t/2}\mathbf{U} - {}^{t}\mathbf{U}) - {}^{t}\dot{\mathbf{U}}$$

4. If required, evaluate accelerations at time $t + \Delta t/2$:

$${}^{t+\Delta t/2}\ddot{\mathbf{U}} = a_1({}^{t+\Delta t/2}\dot{\mathbf{U}} - {}^{t}\dot{\mathbf{U}}) - {}^{t}\ddot{\mathbf{U}}$$

<Second sub-step>

1. Calculate effective loads at time $t + \Delta t$:

$${}^{t+\Delta t}\hat{\mathbf{R}} = {}^{t+\Delta t}\mathbf{R} + \mathbf{M}(a_5\,{}^{t+\Delta t/2}\mathbf{U} + a_6\,{}^{t}\mathbf{U} + a_1\,{}^{t+\Delta t/2}\dot{\mathbf{U}} + a_7\,{}^{t}\dot{\mathbf{U}}) + \mathbf{C}(a_1\,{}^{t+\Delta t/2}\mathbf{U} + a_7\,{}^{t}\mathbf{U})$$

2. Solve for displacements at time $t + \Delta t/2$:

$$\mathbf{L}_2\mathbf{D}_2\mathbf{L}_2^T\,{}^{t+\Delta t}\mathbf{U} = {}^{t+\Delta t}\hat{\mathbf{R}}$$

3. Calculate velocities and accelerations at time $t + \Delta t/2$:

$${}^{t+\Delta t}\dot{\mathbf{U}} = -a_7\,{}^{t}\mathbf{U} - a_1\,{}^{t+\Delta t/2}\mathbf{U} + a_3\,{}^{t+\Delta t}\mathbf{U}$$

$${}^{t+\Delta t}\ddot{\mathbf{U}} = -a_7\,{}^{t}\dot{\mathbf{U}} - a_1\,{}^{t+\Delta t/2}\dot{\mathbf{U}} + a_3\,{}^{t+\Delta t}\dot{\mathbf{U}}$$

The same effective stiffness matrix in Eqs. (2.6) and (2.8) may be advantageous to use in linear analysis. The same effective stiffness matrix is achieved by using the value $(2-\sqrt{2})\,\Delta t$ instead of $1/2\,\Delta t$ in splitting the full time step Δt, (see ref. [42]). In that case, the equilibrium equations are considered at time $t+(2-\sqrt{2})\Delta t$, and only one factorization of an effective stiffness matrix is required. In addition, less memory is needed if the matrix can be kept in-core.

On the other hand, in nonlinear analysis, the use of the different effective stiffness matrices in each sub-step does not increase the solution effort. This is because, in nonlinear analysis, Newton-Raphson iterations are used with new tangent stiffness matrices in each iteration. The resulting solution procedure of the Bathe method is summarized in Table 2.1.

2.2. The stability and accuracy properties

Some properties of the method can be analyzed through the following equation [1]:

$$\begin{bmatrix} {}^{t+\Delta t}\ddot{x} \\ {}^{t+\Delta t}\dot{x} \\ {}^{t+\Delta t}x \end{bmatrix} = \mathbf{A} \begin{bmatrix} {}^{t}\ddot{x} \\ {}^{t}\dot{x} \\ {}^{t}x \end{bmatrix} + \mathbf{L}_a\,{}^{t+\Delta t/2}r + \mathbf{L}_b\,{}^{t+\Delta t}r \quad , \tag{2.9}$$

where $\mathbf{A}$ is the integration approximation and $\mathbf{L}_a$ and $\mathbf{L}_b$ are load operators.

$$\mathbf{A}=\begin{bmatrix} -4\omega\Delta t\left(24\xi+7\omega\Delta t\right) & \omega\left(-288\xi+14\xi\omega^2\Delta t^2-144\omega\Delta t+5\omega^3\Delta t^3+48\xi^2\omega\Delta t\right) \\ -4\Delta t\left(-12+\omega^2\Delta t^2\right) & 144-47\omega^2\Delta t^2-8\xi\omega^3\Delta t^3-24\xi\omega\Delta t \\ 4\Delta t^2\left(7+2\xi\omega\Delta t\right) & \Delta t\left(144-5\omega^2\Delta t^2+80\xi\omega\Delta t+16\xi^2\omega^2\Delta t^2\right) \end{bmatrix}$$

$$\begin{bmatrix} \omega^2\left(24\xi\omega\Delta t+19\omega^2\Delta t^2-144\right) \\ \omega^2\Delta t\left(-96-24\xi\omega\Delta t+\omega^2\Delta t^2\right) \\ -19\omega^2\Delta t^2+144+168\xi\omega\Delta t+48\xi^2\omega^2\Delta t^2-2\xi\omega^3\Delta t^3 \end{bmatrix}, \tag{2.10}$$

$$\mathbf{L}_{\mathbf{a}}=\frac{1}{\beta_1\beta_2}\begin{bmatrix} -4\omega\Delta t\left(24\xi+7\omega\Delta t\right) \\ -4\Delta t\left(-12+\omega^2\Delta t^2\right) \\ 4\Delta t^2\left(7+2\xi\omega\Delta t\right) \end{bmatrix}, \tag{2.11}$$

$$\mathbf{L}_b=\frac{1}{\beta_2}\begin{bmatrix} 9 \\ 3\,\Delta t \\ \Delta t^2 \end{bmatrix}, \tag{2.12}$$

with

$$\beta_1=16+8\xi\omega\Delta t+\omega^2\Delta t^2; \qquad \beta_2=9+6\xi\omega\Delta t+\omega^2\Delta t^2, \tag{2.13}$$

ω and ξ are the natural frequency and the damping ratio, respectively. The spectral radii of various methods for case $\xi=0$ are shown in Fig. 2-1.

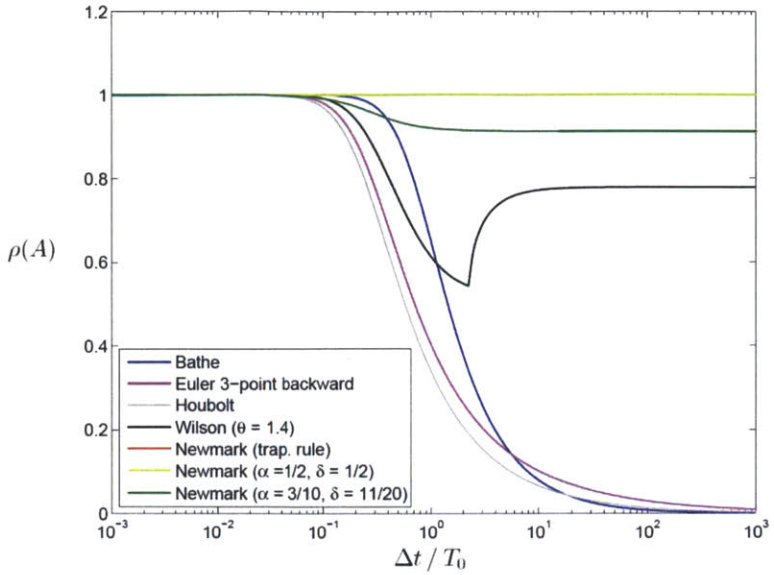

Figure 2-1 **Spectral radii of approximation operators, case $\xi = 0$, for various methods; $\rho(\mathbf{A}) = 1.0$ for the Newmark trap. rule and when $\alpha = 1/2, \delta = 1/2$ in the Newmark method**

The equations used in the Newmark schemes are [1]

$$ {}^{t+\Delta t}\dot{\mathbf{U}} = {}^{t}\dot{\mathbf{U}} + \left[(1-\delta)\,{}^{t}\ddot{\mathbf{U}} + \delta\,{}^{t+\Delta t}\ddot{\mathbf{U}} \right] \Delta t \tag{2.14} $$

and

$$ {}^{t+\Delta t}\mathbf{U} = {}^{t}\mathbf{U} + {}^{t}\dot{\mathbf{U}}\Delta t + \left[(\frac{1}{2} - \alpha)\,{}^{t}\ddot{\mathbf{U}} + \alpha\,{}^{t+\Delta t}\ddot{\mathbf{U}} \right] \Delta t^2 , \tag{2.15} $$

where the parameters α and δ used are given in Fig. 2-1.

An important point is that the Bathe method gives the value of $\rho(\mathbf{A})$ almost 1.0 up to $\Delta t / T \approx 0.1$, and the value rapidly decreases thereafter. This shows a very desirable

property of time integration since it indicates unconditional stability, highly accurate integrations up to $\Delta t / T$ is 0.1, and, thereafter, strong numerical damping in the response for which $\Delta t / T$ is larger than about 0.3. It is observed that the use of $2-\sqrt{2}$ instead of $1/2$ for the splitting of the time step results in practically the same curve of $\rho(\mathbf{A})$. The properties of the method for the various splitting ratios are discussed in Appendix A1.

The amplitude decays and period elongations are shown in Figures 2-2 and 2-3, respectively, which show the accuracy properties of the scheme. Very small amplitude decay and period elongation are observed in the Bathe method for reasonable time step values. For example, the solution accuracy for period calculations in the Bathe method with $\Delta t / T = 0.1$ is similar to that of the trapezoidal rule with $\Delta t / T = 0.07$.

Moreover, the numerical damping shown by its spectral radii (Fig. 2-1) results in improved stability characteristics in nonlinear analyses [42, 43]. Section 2.3 presents a discussion of the importance of this numerical damping, which is very small for reasonable $\Delta t / T$ values and is large for large $\Delta t / T$ values, in linear structural dynamics analysis.

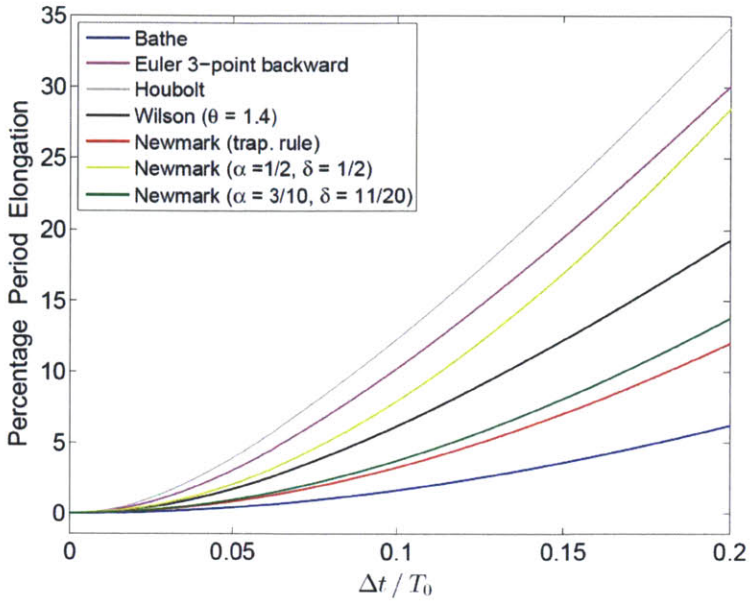

Figure 2-2 **Percentage period elongations for various methods**

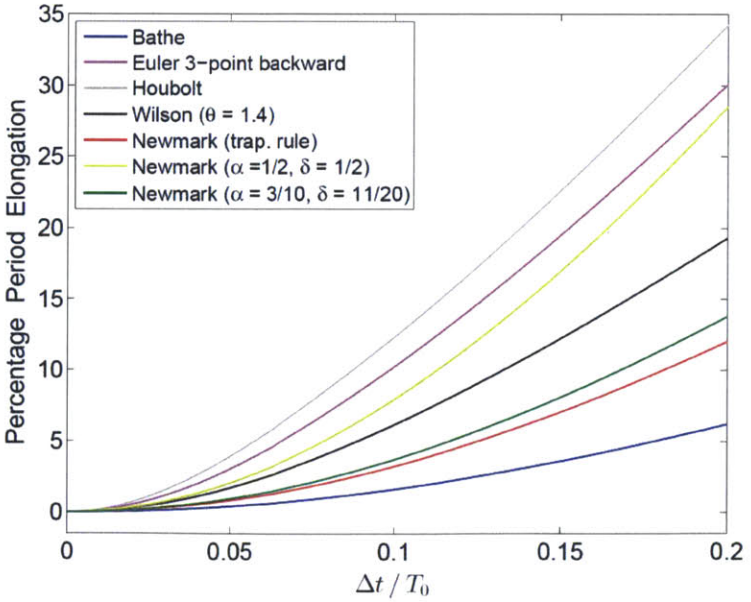

Figure 2-3 **Percentage amplitude decays for various methods; results for Newmark (trapezoidal rule) and Newmark ($\alpha = 1/2, \delta = 1/2$) are identical**

2.3. A demonstrative solution

This Section considers the solution of a simple three degree-of-freedom spring system, as shown in Fig. 2-4, to deepen insight into the Bathe method. Since the prescribed displacements are applied on node 1 over time, as given in Figure 2-4, the governing equation for the unknown displacements u_2 and u_3 is

$$\begin{bmatrix} m_2 & 0 \\ 0 & m_3 \end{bmatrix} \begin{bmatrix} \ddot{u}_2 \\ \ddot{u}_3 \end{bmatrix} + \begin{bmatrix} k_1 + k_2 & -k_2 \\ -k_2 & k_2 \end{bmatrix} \begin{bmatrix} u_2 \\ u_3 \end{bmatrix} = \begin{bmatrix} k_1 u_1 \\ 0 \end{bmatrix}, \tag{2.16}$$

where the reaction becomes

$$R_1 = m_1 \ddot{u}_1 + k_1 u_1 - k_1 u_2 . \tag{2.17}$$

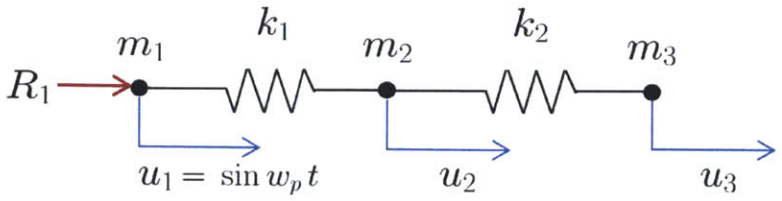

Figure 2-4 **Model problem of three degrees of freedom spring system**
$k_1 = 10^7, k_2 = 1, m_1 = 0, m_2 = 1, m_3 = 1, \omega_p = 1.2$

Note that this very simple problem is used as a "model problem" to represent a much more complex structural system that includes the stiff and flexible parts. For example, the left

very stiff spring in the model problem represents almost rigid connections or penalty factors used, while the right flexible spring is used to represent the flexible parts of the complex structural model.

An important point is that the almost rigid parts in the complex model, which are frequently idealized by artificially stiff truss or beam elements, play an important role; however, the detailed response within these parts should not frequently be included in the overall system response. This is because, in practice, the highly stiff parts have often no physical meaning, simply being used to provide constraints. Hence, a response that corresponds to very high artificial frequencies would not be included in a mode superposition analysis.

The stiff spring could be idealized as a rigid link reducing the system to only two degrees of freedom. However, in practice, such stiff elements are varied in many parts of complex finite element models and may not be reducible. The system in Fig. 2-4 is used as a "model system" to study the behavior of the numerical solution for such complex structural systems when obtained by the direct integration schemes.

As must typically be done in a complex many degrees-of-freedom structural analysis, zero initial conditions for the displacements and velocities at nodes 2 and 3 are used, and the system is solved for the response over 10 seconds. For the solution, the time integrations are applied to Eq. (2.16), and the reaction is calculated using Eq. (2.17).

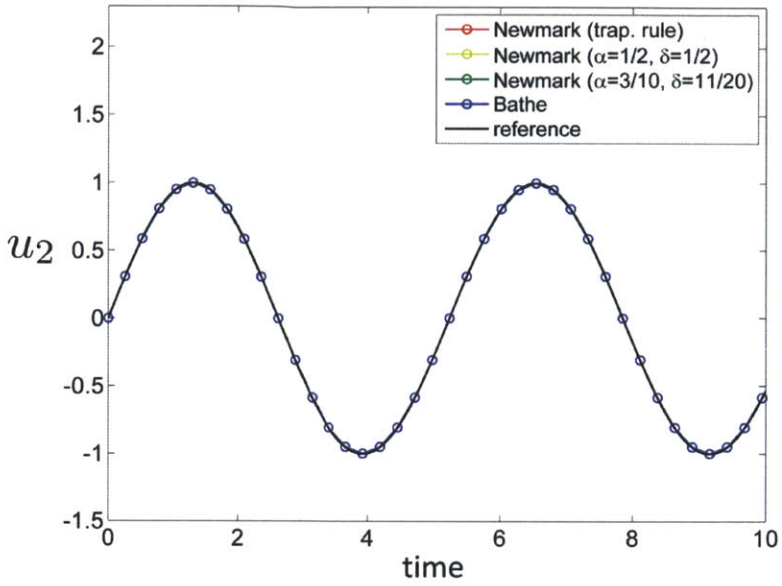

Figure 2-5 **Displacement of node 2 for various methods**

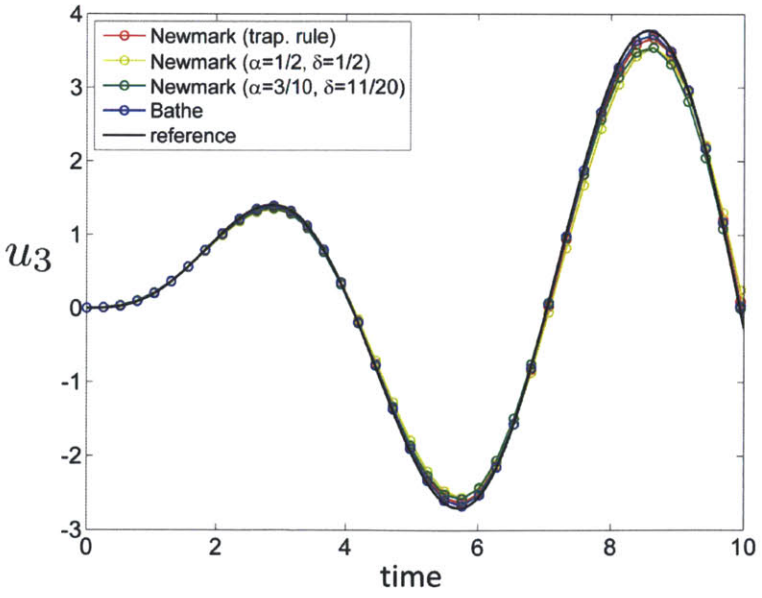

Figure 2-6 **Displacement of node 3 for various methods**

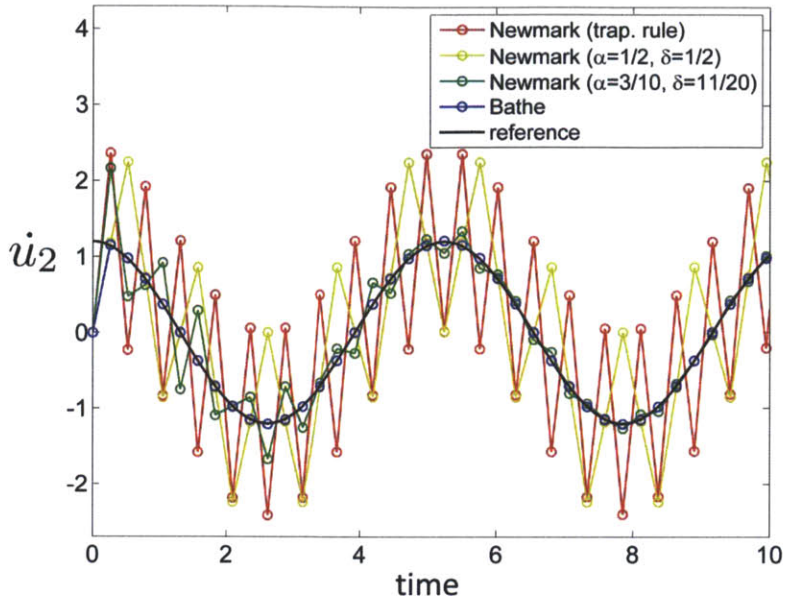

Figure 2-7 **Velocity of node 2 for various methods (the static correction gives the nonzero velocity at time = 0.0)**

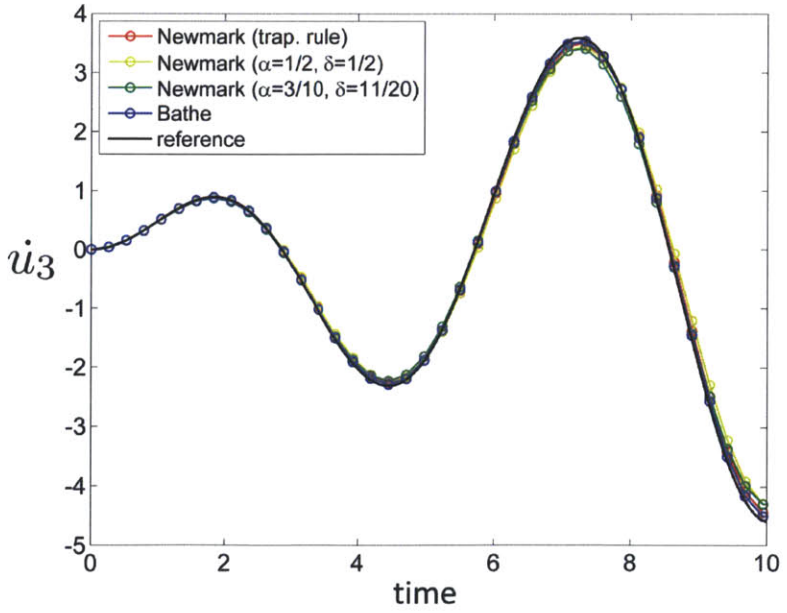

Figure 2-8 **Velocity of node 3 for various methods**

In addition, the time step used is $\Delta t = 0.2618$; therefore we have $\Delta t / T_p = 0.05$, $\Delta t / T_1 = 0.0417$, and $\Delta t / T_2 = 130.9$, where T_1, T_2 and T_p are the natural periods of the system in Eq. (2.17) and the period of the prescribed motion at node 1, respectively.

The calculated solutions are given in Figures 2-5 to 2-13. In these figures, we also give a "reference solution," which is obtained in a mode superposition solution, using only the lowest frequency mode plus the static correction as is typically done in a practical analysis for a many degrees-of-freedom model (of course, in practice, the number of low frequency modes used depends on the problem at hand) [1].

The calculated responses given in the figures indicate that the Bathe method performs very well while others provide inaccurate solutions, in particular for the acceleration at node 2 and the reaction. The trapezoidal rule shows "practically" instability in the calculation of the reactions and accelerations, (see Fig. 2-12). On the other hand, the Bathe method calculates the solutions very accurately without the adjustment of any parameter. Only for the first time step is there an "undershoot" as shown in Figs. 2-10 and 2-13 while, of course, this undershoot can also be removed by setting the initial conditions to excite only the physical mode. (See Appendix A2 for details). The important point to note is that the method performs as a mode superposition analysis is performed: it does not include the high frequency mode to the total responses, which is artificial due to modeling, so that the calculated response becomes accurate.

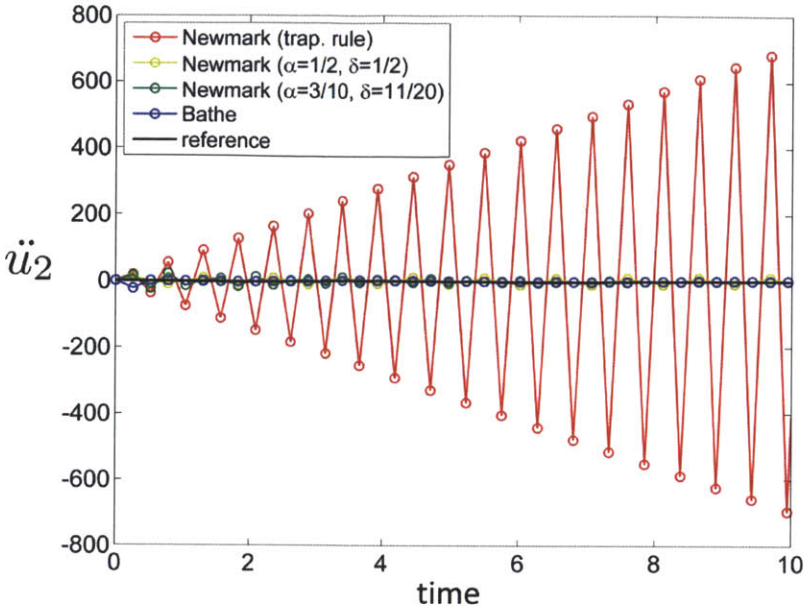

Figure 2-9 **Acceleration of node 2 for various methods**

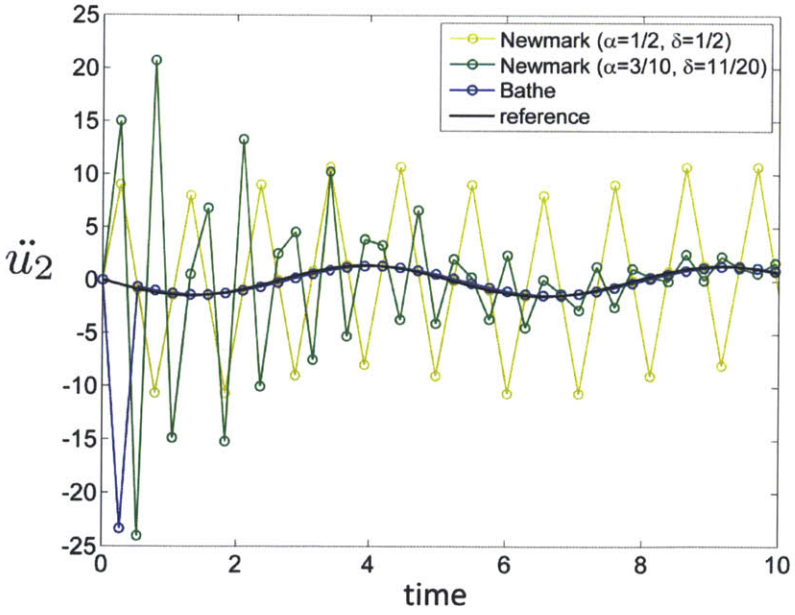

Figure 2-10 **Acceleration of node 2 for various methods**

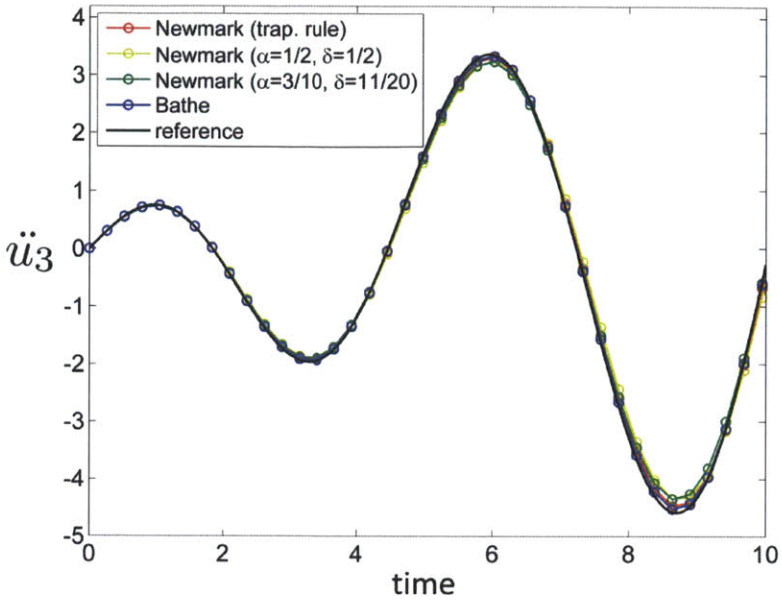

Figure 2-11 **Acceleration of node 3 for various methods**

This feature of the method is valuable for practical analyses, and valid for both linear and nonlinear analysis. Only a simple model problem was considered in order to focus on the essence of the characteristics of the method; however, the same conclusions can be applied solving a large finite element models in practical analysis.

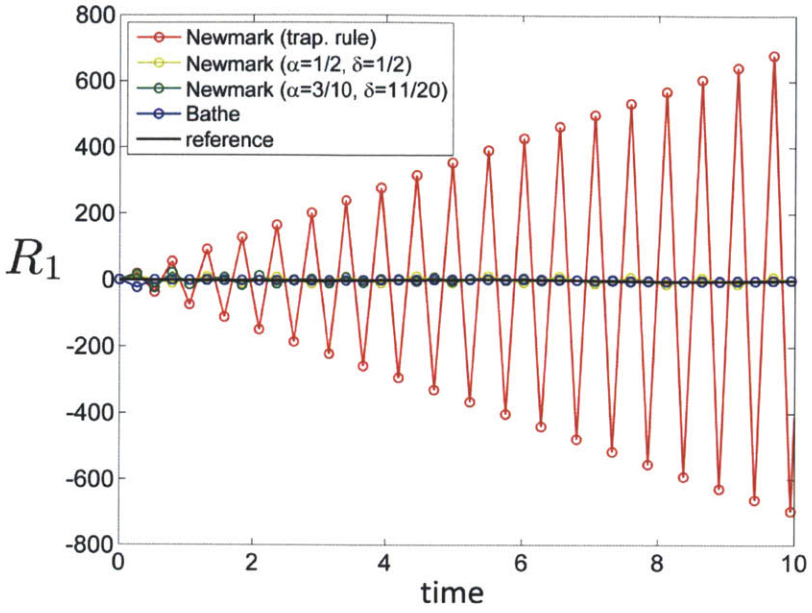

Figure 2-12 **Reaction force at node 1 for various methods**

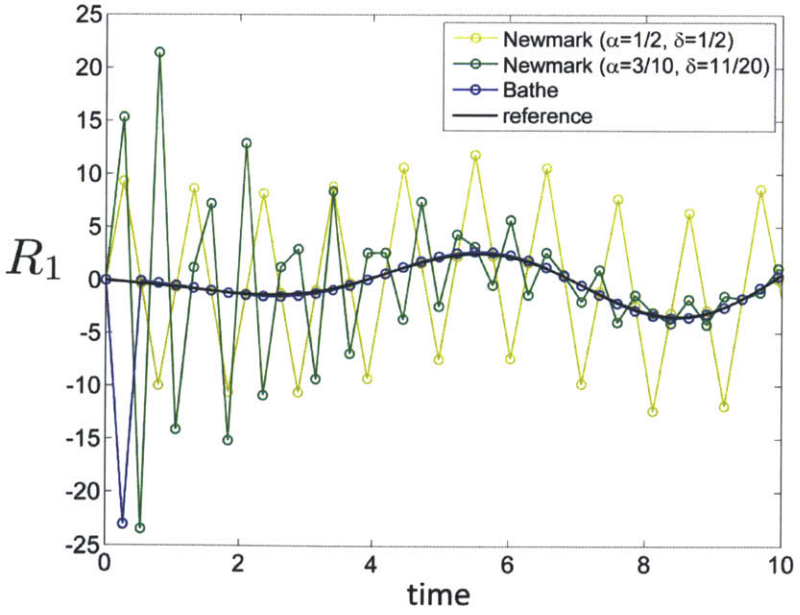

Figure 2-13 **Reaction force at node 1 for various methods**

2.4. Concluding remarks

Complex finite element systems with flexible and very stiff parts are frequently used in practice, where the stiff part may only model constraints. In solutions with appropriately chosen time step size, the direct time integration methods are used for all coupled degrees of freedom over the time domain.

In this Chapter, the performance of the Bathe method is studied for structural dynamics. In particular, to represent the essence of such complex flexible/stiff systems, we considered a simple two degree-of-freedom "model problem" to study the numerical solutions using the trapezoidal rule, two other direct time integration schemes from the Newmark family of methods, and the Bathe method.

The response from the Bathe method was obtained as in a mode superposition analysis. Numerical damping properties in the Bathe method damped out the artificial high frequency modes so that it is not included as errors in the solutions. As is desired in practice, only the physical mode that is excited is accurately included in the response together with the static correction in the solution of the Bathe method.

On the other hand, the other methods used, and in particular the trapezoidal rule, provided inaccurate solutions. Although numerical damping is included in one Newmark method, the solution errors are large.

Here, to focus on the essence of desired properties of time integration in structural dynamics, the study was deliberately limited to not include time integration techniques for which numerical parameters need to be chosen, such as the alpha-method [41]. We believe that the simple "model problem" considered in this Chapter would be valuable to analyze the other procedures for structural dynamics.

Chapter 3

On an implicit time integration scheme in the analysis of the wave propagations

In this Chapter, the Bathe method for wave propagation problems is discussed, and it is shown how the desired properties for structural dynamics can also be valuable for wave propagation problems. Dispersion properties of the Bathe method and the trapezoidal rule with linear spatial discretization for 1-D and 2-D cases are studied. Based on the dispersion analysis, it is demonstrated that the scheme's properties, which are valuable for structural dynamics, can be valuable for wave propagations; subsequently, the performances of the scheme, with the trapezoidal rule, are evaluated through numerical examples.

3.1. A dispersion analysis

This Section offers an analysis of dispersion errors resulting from spatial discretization coupled with temporal discretization of the Bathe method and the trapezoidal rule. These

dispersion errors can be analyzed by employing the scalar wave governed by

$$\frac{\partial^2 u}{\partial t^2} - c_0^2 \nabla^2 u = 0 \quad , \tag{3.1}$$

where u is the field variable and c_0 is the wave velocity. Here, the main consideration is the dispersion associated with the propagations of disturbances; therefore, body forces are not considered. The associated finite element approximation system gives

$$\mathbf{M}\ddot{\mathbf{U}} + c_0^2 \mathbf{K}\mathbf{U} = \mathbf{0}, \tag{3.2}$$

where **K** and **M** are the stiffness and mass matrices, and for element (m) with volume $V^{(m)}$,

$$\mathbf{M}^{(m)} = \int_{V^{(m)}} \mathbf{H}^{(m)T} \mathbf{H}^{(m)} \, dV^{(m)}, \tag{3.3}$$

$$\mathbf{K}^{(m)} = \int_{V^{(m)}} \left(\nabla \mathbf{H}^{(m)}\right)^T \left(\nabla \mathbf{H}^{(m)}\right) dV^{(m)}, \tag{3.4}$$

and $\mathbf{H}^{(m)}$ and **U** are the shape function matrix and the discretized field variable, respectively.

Eqs. (2.2)–(2.5) with Eq. (3.2) at time t, $t+\Delta t/2$ and $t+\Delta t$ can be rewritten in a linear multistep form representing the Bathe method as

$$\left(72\mathbf{M}+8c_0^2\Delta t^2\mathbf{K}\right)^{t+\Delta t}\mathbf{U}+\left(-144\mathbf{M}+5c_0^2\Delta t^2\mathbf{K}\right)^{t+\Delta t/2}\mathbf{U}$$
$$+\left(72\mathbf{M}+5c_0^2\Delta t^2\mathbf{K}\right)^{t}\mathbf{U}=\mathbf{0}. \tag{3.5}$$

Using the definition of the CFL number, $\mathrm{CFL}=\dfrac{c_0\Delta t}{h}$, where h is the "characteristic length" of a finite element (or fundamental length used) [1], Eq. (3.5) becomes

$$\left(72\mathbf{M}+8\gamma\mathbf{K}\right)^{t+\Delta t}\mathbf{U}+\left(-144\mathbf{M}+5\gamma\mathbf{K}\right)^{t+\Delta t/2}\mathbf{U}$$
$$+\left(72\mathbf{M}+5\gamma\mathbf{K}\right)^{t}\mathbf{U}=\mathbf{0}, \tag{3.6}$$

where $\gamma=\mathrm{CFL}^2h^2$.

For the Newmark method, using the equilibrium at time $t-\Delta t$, t and $t+\Delta t$, and Eqs. (2.14) and (2.15), and the same equations for the solution at time t, we get the linear multistep form of the Newmark method (for the case $\delta=1/2$) as

$$\left(\mathbf{M}+\alpha c_0^2\Delta t^2\mathbf{K}\right)^{t+\Delta t}\mathbf{U}+\left(-2\mathbf{M}+(1-2\alpha)c_0^2\Delta t^2\mathbf{K}\right)^{t}\mathbf{U}$$
$$+\left(\mathbf{M}+\alpha c_0^2\Delta t^2\mathbf{K}\right)^{t-\Delta t}\mathbf{U}=\mathbf{0} \tag{3.7}$$

or

$$\left(\mathbf{M}+\alpha\gamma\mathbf{K}\right)^{t+\Delta t}\mathbf{U}+\left(-2\mathbf{M}+(1-2\alpha)\gamma\mathbf{K}\right)^{t}\mathbf{U}$$
$$+\left(\mathbf{M}+\alpha\gamma\mathbf{K}\right)^{t-\Delta t}\mathbf{U}=\mathbf{0}. \tag{3.8}$$

With $\alpha=1/4$, the equations for the Newmark trapezoidal rule are obtained. The above equations may indicate that the computational cost in the Bathe method is twice that used in the Newmark method, since in the Bathe method, the solution at the half step is used; however, as demonstrated in Section 3.2, this is not the case when solutions of optimal accuracy are sought.

3.1.1. A dispersion error analysis in the 1D case

The general solutions of Eq. (3.1) have the form of $A\,e^{i(k_0x-\omega_0t)}$ in the 1-D case, where ω_0 is the frequency of a wave mode and $k_0=\omega_0/c_0$ is the corresponding wave number. A wave mode of an approximated system takes the form [30]

$$^{t}_{x}u=A_k\,e^{i(kx-\omega t)}, \tag{3.9}$$

where ω and $k = \omega / c$ are the approximated (numerical) frequency and the corresponding wave number, respectively. The approximated wave speed c is different from the exact wave speed c_0. In addition, the difference is a function of the wave number; therefore, this difference results in artificial dispersion. In addition, for unconditionally stable implicit methods, the amplitude of the numerically calculated wave typically decreases due to its numerical damping [1]. The Newmark trapezoidal rule is an exception since the scheme does not possess any numerical damping. In the following Sections, it is demonstrated that the damping properties in the Bathe method enable remarkably accurate solutions.

Considering a regular mesh with nodes equally spaced by Δx along the x axis, the solutions to the approximated system at time $t + n_t \Delta t$ and location $x + n_x \Delta x$ become

$$\begin{aligned} {}^{n_t \Delta t}_{n_x \Delta x} u &= A_k e^{i(k n_x \Delta x - \omega n_t \Delta t)} \\ &= A_k e^{ik\Delta x (n_x - n_t (\mathrm{CFL})(c/c_0))} \end{aligned}, \tag{3.10}$$

where the subscript and superscript denote the nodal value at $n_x \Delta x$ and time $n_t \Delta t$.

For the 2-node element, the corresponding mass matrix $\mathbf{M}$ and stiffness matrix $\mathbf{K}$ of the

finite element equations are

$$\mathbf{M} = \frac{\Delta x}{6}\begin{pmatrix} 2 & 1 & 0 & & \cdots & 0 \\ 1 & 4 & 1 & & \cdots & 0 \\ 0 & 1 & 4 & 1 & & \vdots \\ \vdots & & & \ddots & & \vdots \\ 0 & \cdots & \cdots & & 1 & 2 \end{pmatrix} \tag{3.11}$$

and

$$\mathbf{K} = \frac{1}{\Delta x}\begin{pmatrix} 1 & -1 & 0 & & \cdots & 0 \\ -1 & 2 & -1 & & \cdots & 0 \\ 0 & -1 & 2 & -1 & & \vdots \\ \vdots & & & \ddots & & \vdots \\ 0 & \cdots & \cdots & & -1 & 1 \end{pmatrix} . \tag{3.12}$$

An implicit relation can be obtained between CFL, c/c_0, wave number k, and the element size Δx of the Bathe method by substituting Eqs. (3.10)–(3.12) into Eq. (3.6) with $h = \Delta x$ and looking into an equation associated with a middle node. The dispersion error with respect to the wavelength λ and the element size used are given in Fig. 3-1. See Appendix A.3 for discussion of numerical wavelength and phase velocity with respect to the time step size.

An important point is that there is no CFL number that makes every wave mode have the same wave speed. This can be demonstrated as follows. After taking Taylor expansion on the explicit relation between CFL, c/c_0, k, and Δx with respect to $k\Delta x$, the

polynomial expression of the relative wave speed error is obtained as

$$\frac{c-c_0}{c_0} = -\frac{1}{1152}\left(41\mathrm{CFL}^2-48\right)(k\Delta x)^2+\frac{1}{13271040}\times \left(28363\mathrm{CFL}^4-59040\mathrm{CFL}^2+6912\right)(k\Delta x)^4+O\left((k\Delta x)^6\right) \quad . \tag{3.13}$$

From Eq. (3.13), wave modes with $k\Delta x<1$ can be rendered almost non-dispersive with $\mathrm{CFL}=\sqrt{48/41}$; otherwise, it is dispersive for these modes. However, since the shortest wave length is $2\Delta x$, there are wave modes with $k\Delta x>1$. For $\mathrm{CFL}=\sqrt{48/41}$, the wave modes with shorter wave lengths are dispersive (Fig. 3-1). Therefore, there is no CFL number which makes all modes non-dispersive.

However, in the Bathe method, the wave modes with $\Delta t/T>0.3$ are, in essence, discarded in the total solution (Fig. 2-1 and Chapter 2). Using the definition of the CFL number, $k\Delta x$ is rewritten as

$$\frac{k\Delta x}{\pi}=\frac{2c_0}{c}\frac{1}{\mathrm{CFL}}\frac{\Delta t}{T} \quad . \tag{3.14}$$

Therefore, for $\mathrm{CFL}\simeq 1$, since the ratio of numerical wave speed to the exact wave speed

becomes $c/c_0 \simeq 1$, it can be seen that wave modes with $k\Delta x \gtrsim 0.6\pi$ are not participating in the total solution (these discarded wave modes are presented in dashed lines in Fig. 3.1 for different CFL numbers). The important point to notice is that, with $\mathrm{CFL} = 1$, the Bathe method provides a numerical solution that is almost non-dispersive by calculating *every participating wave very accurately.*

For the Newmark method, using Eqs. (3.10)–(3.12) and (3.8), and looking into an equation associated with a middle node, the relation between CFL, c/c_0, wave number k, and the element size Δx is obtained (Fig. 3-2). After taking Taylor expansion on the relation with respect to $k\Delta x$, the following is obtained:

$$\frac{c-c_0}{c_0} = \frac{1}{24}\left(1+(1-12\alpha)\mathrm{CFL}^2\right)(k\Delta x)^2 + \frac{1}{1920}(1+(-120\alpha+10)\mathrm{CFL}^2 + \left(-120\alpha+9+720\alpha^2\right)\mathrm{CFL}^4)(k\Delta x)^4 + O\left((k\Delta x)^6\right) \quad . \quad (3.15)$$

For $\alpha = 1/4$, wave modes with $k\Delta x < 1$ become almost non-dispersive with $\mathrm{CFL} = \sqrt{1/2}$. However, wave modes with $k\Delta x > 1$ are dispersive (Fig. 3-2). Therefore, as in the Bathe method, there is no CFL number that makes the solution from all participating wave modes non-dispersive; however, unlike the Bathe method, the trapezoidal rule does not eliminate the dispersive modes from the solution. Hence the solution will generally show a significant dispersion error, as shown for specific examples in Section 3.2.

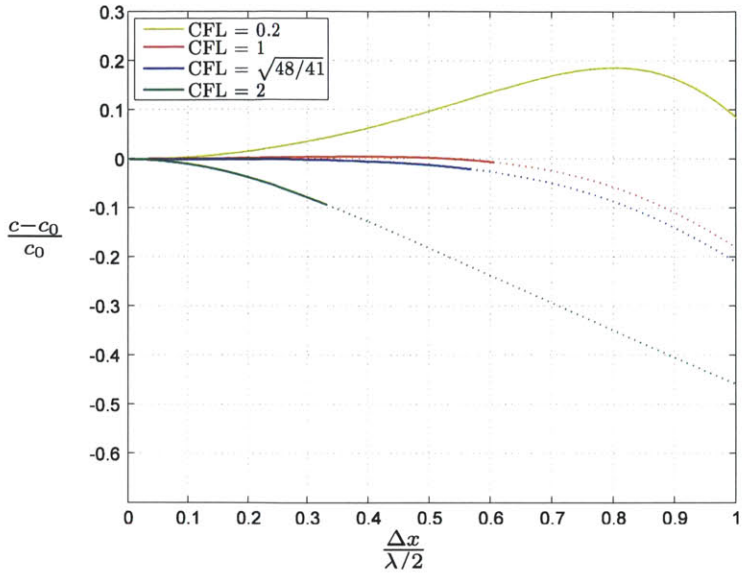

Figure 3-1 **Relative wave speed errors of the Bathe method for various CFL numbers; Discarded wave modes are presented in dashed lines**

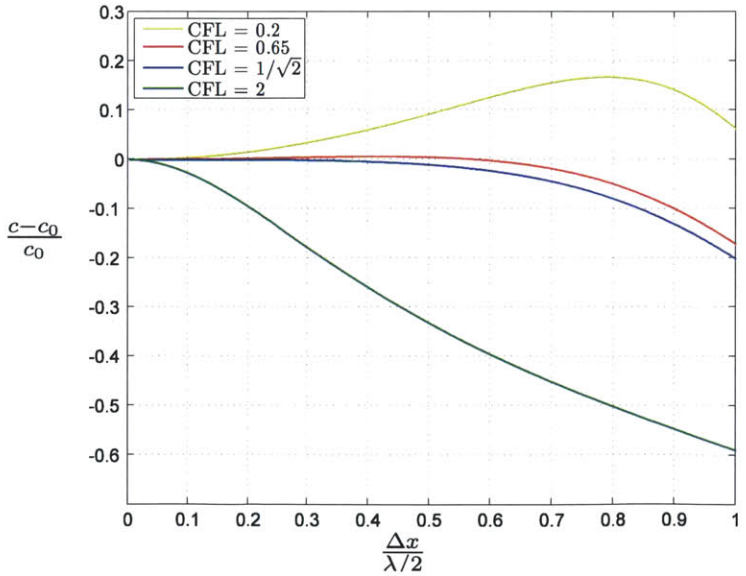

Figure 3-2 **Relative wave speed errors of the trapezoidal rule for various CFL numbers**

3.1.2. A dispersion error analysis in the 2D case

The general solution of Eq. (3.1) in 2-D analyses for a plane wave is given by $u = Ae^{i(k_0 x\cos(\theta)+k_0 y\sin(\theta)-\omega_0 t)}$, and the corresponding numerical solution is

$$ {}^{t}_{x,y}u = A_k e^{i(kx\cos(\theta)+ky\sin(\theta)-\omega t)}. \tag{3.16} $$

Considering a mesh with nodes equally spaced at distance h along both x and y axes ($\Delta x = \Delta y = h$), the solution of the finite element system at time $n_t \Delta t$ and location $n_x h$, $n_y h$ becomes

$$ \begin{aligned} {}^{n_t\Delta t}_{n_x h, n_y h}u &= A_k e^{i(k n_x h\cos(\theta)+k n_y h\sin(\theta)-\omega n_t \Delta t)} \\ &= A_k e^{ikh\left(n_x\cos(\theta)+n_y\sin(\theta)-n_t(\mathrm{CFL})(c/c_0)\right)} \end{aligned}, \tag{3.17} $$

where θ is the angle from the x-axis at which the wave is propagating.

Similar to the 1-D case, after substituting the above expression of approximated solution into the linear multistep formula, and looking into the equation associated with a middle node, the implicit relation between $\mathrm{CFL} = c_0 \Delta t / h$, c / c_0, wave number k, and the element size h is obtained.

For the four-node element, the row of the global mass matrix corresponding to the middle node at (x,y) is

$$\frac{h^2}{36}\,[0\ldots0\ 1\ 4\ 1\ 4\ 16\ 4\ 1\ 4\ 1\ 0\ldots0] \tag{3.18}$$

Therefore, the $\mathbf{M}^t\mathbf{U}$ term for the node at (x,y) is

$$\begin{aligned}\frac{h^2}{36}\ \ &[16\,{}^{t}u_{x,y} + 4\left({}^{t}u_{x-h,y} + {}^{t}u_{x+h,y} + {}^{t}u_{x,y-h} + {}^{t}u_{x,y+h}\right)\\ &+\left({}^{t}u_{x-h,y-h} + {}^{t}u_{x+h,y-h} + {}^{t}u_{x-h,y+h} + {}^{t}u_{x+h,y+h}\right)]\end{aligned} \tag{3.19}$$

Also, the corresponding row of the global stiffness matrix $\mathbf{K}$ is

$$\frac{1}{3}\,[0\ldots0\ -1\ -1\ -1\ -1\ 8\ -1\ -1\ -1\ -1\ 0\ldots0] \tag{3.20}$$

Therefore, the $\mathbf{K}^t\mathbf{U}$ term for the node is

$$\begin{aligned}\frac{1}{3}\ \ &[8\,{}^{t}u_{x,y} - ({}^{t}u_{x-h,y} + {}^{t}u_{x+h,y} + {}^{t}u_{x,y-h} + {}^{t}u_{x,y+h}\\ &+ {}^{t}u_{x-h,y-h} + {}^{t}u_{x+h,y-h} + {}^{t}u_{x-h,y+h} + {}^{t}u_{x+h,y+h})]\end{aligned} \tag{3.21}$$

Using Eqs. (3.17), (3.19), (3.21) and (3.6), we get an implicit relation between $\mathrm{CFL} = c_0 \Delta t / h$, c / c_0, wave number k, and the element size h for the Bathe method, and the results of various propagating angles with CFL = 1 are shown in Fig. (3-a). As in the 1-D case, no CFL number exists which makes every wave mode have the same wave speed. After taking Taylor expansion on the explicit relation, we get the following polynomial expression.

$$\begin{aligned}\frac{c-c_0}{c_0} = &-\frac{1}{1152}\left(96(\cos^2\theta - \cos^4\theta) + 41\mathrm{CFL}^2 - 48\right)(kh)^2 \\ &+ \frac{1}{13271040}(-46080\cos^8\theta + 92160\cos^6\theta \\ &+ (-3686 - 118080\ \mathrm{CFL}^2)\cos^4\theta + (118080\,\mathrm{CFL}^2 - 9216)\cos^2\theta \\ &+ 6912 - 59040\,\mathrm{CFL}^2 + 28363\,\mathrm{CFL}^4)(kh)^4 + O\left((kh)^6\right)\end{aligned} \tag{3.22}$$

Note that for $\theta = 0$, Eqs. (3.13) and (3.22) are equivalent. Also, the dispersion error depends on the propagating angle, and this is due to the spatial discretization. However, the Bathe method cuts the highly dispersive parts off effectively with $\mathrm{CFL} = 1$ case, where the largest dispersion error becomes less than 6 % (Fig. 3-3.a).

Interestingly, it was observed that the larger the propagating angle, the lower the dispersion characteristic curve. A similar trend in 1-D analysis is observed: the bigger the CFL number,

the lower the dispersion characteristic curve (Figs. 3-1 and 3-2). Therefore, this trend can be understood as the waves propagating with non-zero propagating angles behaving as if they have larger CFL numbers for the given $c_0\Delta t$; in other words, waves propagating with non-zero propagating angles have *shorter* effective fundamental length than the element size h.

This understanding can also be found from Eq. (3.22). For waves with propagating angle θ, the CFL number that makes the least dispersion error can be estimated from the first term of Eq. (3.22) as $\mathrm{CFL} \simeq \sqrt{1-2\cos^2\theta(1-\cos^2\theta)}$. This result indicates that, for a given mesh, to optimize the performance of the wave propagating in the direction θ, the time step size Δt is calculated by holding CFL =1 and by considering the *effective* fundamental length as $h \times (\sqrt{1-2\cos^2\theta(1-\cos^2\theta)})$. For example, to obtain the best results when the wave is propagating at the angle $\pi/4$, the effective fundamental length is considered to be $h/\sqrt{2}$ and not $\sqrt{2}h$.

The dispersion characteristic curves of the Bathe method, with CFL = 1 for various propagating angles and for various fundamental lengths calculated from various propagating angles, are given in Fig. 3-3. For each case, the performance of the wave with the propagating angle that is used for calculation of fundamental length is optimized, and the difference between the maximum error and the minimum error is about 6%. The

absolute error is minimized at about 3% when the fundamental length is calculated for a propagating angle around $\theta = \pi / 7$.

For the Newmark method ($\delta = 1/2$),the dispersion relation is obtained from Eqs. (3.17), (3.19), (3.21), and (3.6), and the results for the $\alpha = 1/4$ (trapezoidal rule), CFL = 0.65 case with various propagating angles are shown in Fig. 3-4. The trapezoidal rule also has no CFL number that can make every wave mode have the same propagating speed. The polynomial expression from Taylor expansion is

$$\begin{aligned}\frac{c - c_0}{c_0} = & \frac{1}{24}\left(2(\cos^4\theta - \cos^2\theta) + 1 + (1 - 12\alpha)\mathrm{CFL}^2\right)(kh)^2 \\ & + \frac{1}{5760}(-20\cos^8\theta + 40\cos^6\theta + \left(-16 + (60 - 720\alpha)\mathrm{CFL}^2\right)\cos^4\theta \\ & + \left(-4 + (720\alpha - 60)\mathrm{CFL}^2\right)\cos^2\theta + 3 + \left(27 + 2160\alpha^2 - 360\alpha\right)\mathrm{CFL}^4 \\ & + (30 - 360\alpha)\mathrm{CFL}^2)(kh)^4 + O\left((kh)^6\right)\end{aligned} \tag{3.23}$$

The propagating angle also affects the dispersion error in the Newmark method since this effect comes from the spatial discretization. However, unlike in the Bathe method, the dispersion errors of shorter wave length wave modes, which can only be poorly calculated, are participating in the total solution.

In addition, the effective fundamental length is reduced to about $h \times (\sqrt{1-2\cos^2\theta(1-\cos^2\theta)})$ for the propagating angle θ, as in the Bathe method. The dispersion characteristic curves of the trapezoidal rule with CFL = 0.65 for various propagating angles and for various fundamental lengths calculated from various propagating angles are shown in Fig. 3-3. For each case, the performance of the wave with the propagating angle calculated for the fundamental length is optimized, and the difference between the maximum error and the minimum error is about 17%. The absolute error is minimized at about 8% when the fundamental length is calculated for a propagating angle around $\theta = \pi / 7$.

This Section focused on the dispersion properties of time integration methods. However, it should be noted that it is also necessary to have good solution accuracy in the calculation of the participating wave modes for an accurate solution of wave propagation problems. Hence, time integration methods possessing good spectral radii curves might produce good dispersion characteristics, although they might not be effective due to the large errors in the calculation of the low frequency modes, Chapter 2. [3, 4, 58-60].

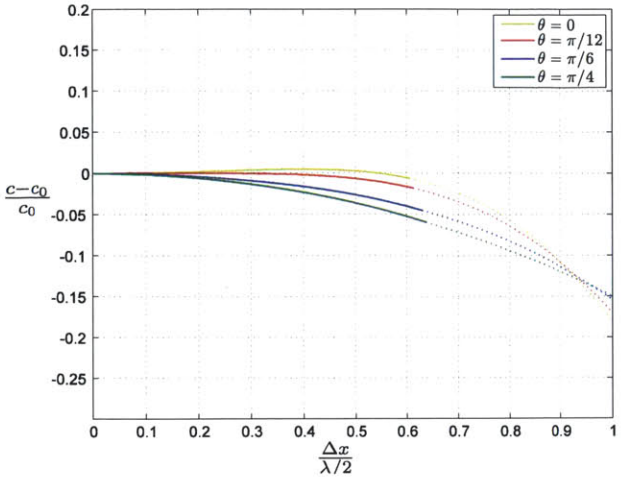

(a) $L = h$

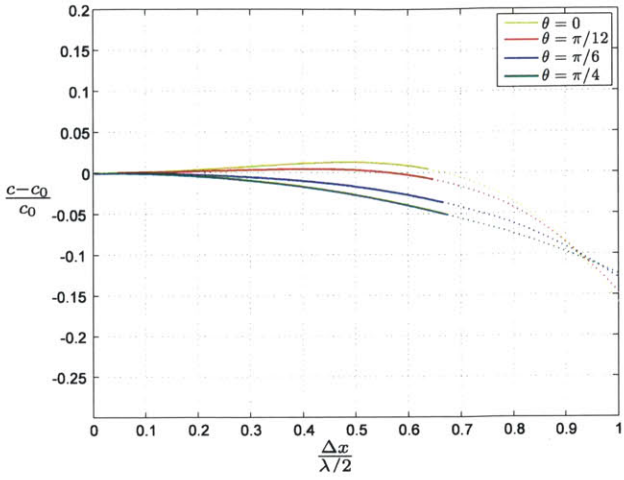

(b) $L = h\,[1-\cos^2(\frac{\pi}{12})\times(1-\cos^2(\frac{\pi}{12}))]$

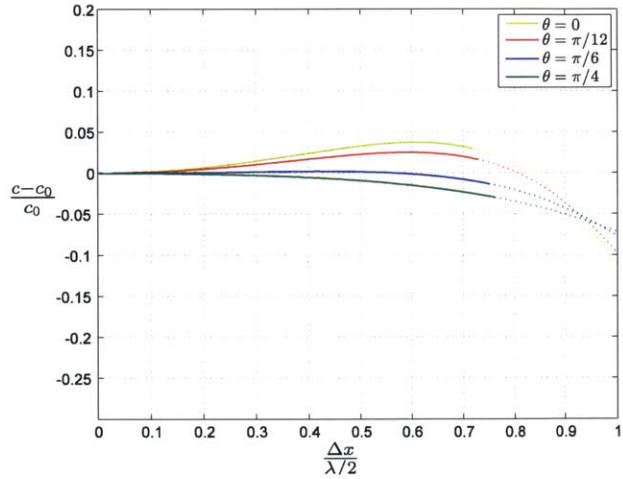

(c) $L = h\,[1-\cos^2(\frac{\pi}{6})\times(1-\cos^2(\frac{\pi}{6}))]$

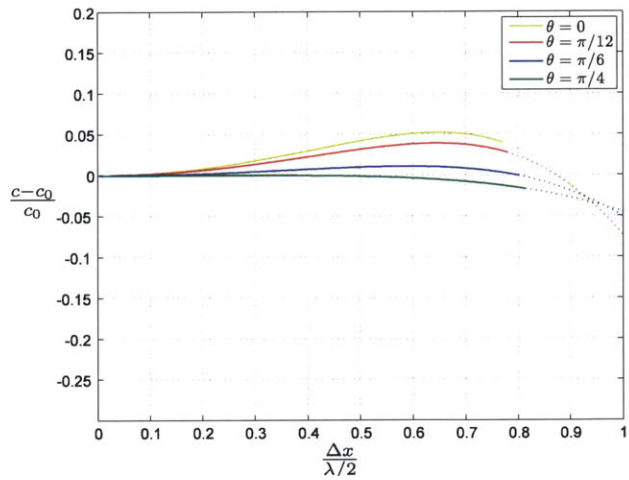

(d) $L = h\,[1-\cos^2(\frac{\pi}{4})\times(1-\cos^2(\frac{\pi}{4}))]$

Figure 3-3 **Relative wave speed errors of the Bathe method for various propagating angles; for** $\mathrm{CFL} = 1$ **calculated from various effective fundamental length, L; Disscarded wave modes are dashed;**

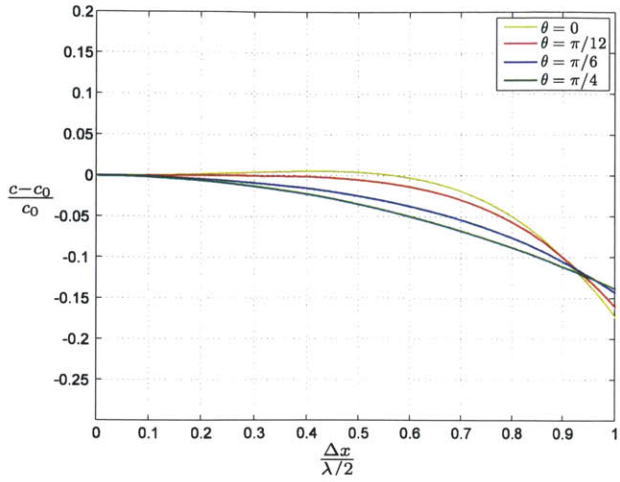

(a) $L = h$

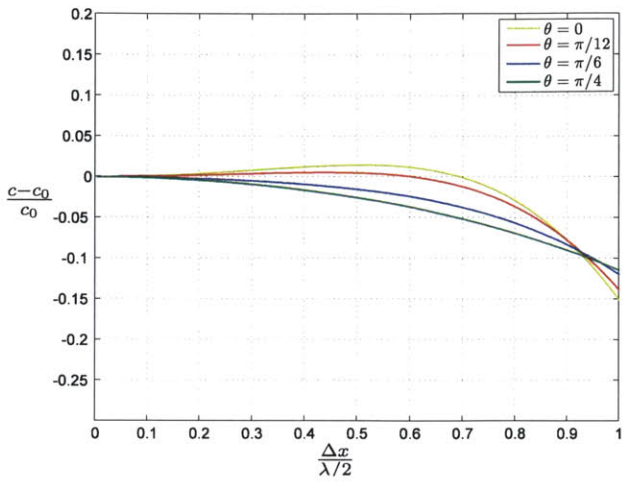

(b) $L = h\,[1-\cos^2(\frac{\pi}{12})\times(1-\cos^2(\frac{\pi}{12}))]$

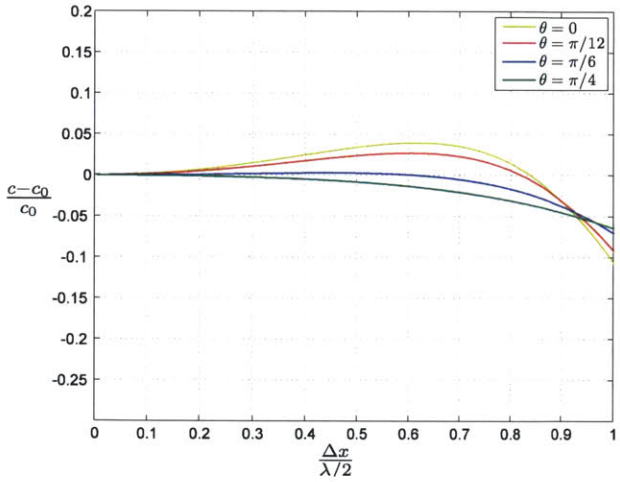

(c) $L = h\,[1-\cos^2(\frac{\pi}{6})\times(1-\cos^2(\frac{\pi}{6}))]$

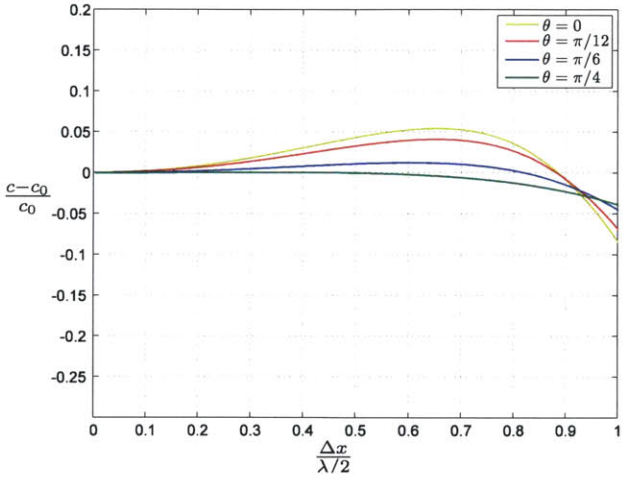

(d) $L = h\,[1-\cos^2(\frac{\pi}{4})\times(1-\cos^2(\frac{\pi}{4}))]$

Figure 3-4 **Relative wave speed errors of the trapezoidal rule for various propagating angles, for** $\mathrm{CFL} = 0.65$ **calculated from various effective fundamental length, L;**

3.2. Wave propagation solutions

In this Section, the performance of the Bathe method for wave propagation problems is presented with the help of several numerical examples. First, a one-dimensional impact problem is solved, and the effect of the CFL numbers on numerical dispersion properties and the resulting spurious oscillations are discussed. Then a 2-D transient scalar wave problem is solved and how propagation direction affects the dispersion properties is analyzed. Finally, the Lamb's problem is solved using the Bathe method and the trapezoidal rule, and the numerically calculated results are compared with the analytical solution.

3.2.1. 1-D bar impact

Considering the impact of an elastic bar on a rigid wall problem (Fig. 3-5) where the governing wave equation is

$$\frac{\partial^2 u}{\partial x^2} = \frac{1}{c_0^2}\frac{\partial^2 u}{\partial t^2}, \tag{3.24}$$

where the wave speed c_0 is 5000, the 1-D 2-node elements of size $\Delta x = 0.05$ are used to idealize the elastic bar.

For the solution, the Bathe method and the trapezoidal rule are used. The CFL numbers used for the Bathe method are 0.2, 1, $\sqrt{48/41}$, and 2. For the trapezoidal rule, CFL numbers 0.65, $1/\sqrt{2}$, and 2 are used. The corresponding time step sizes are the CFL numbers multiplied by 10^{-5} for each scheme.

Figure 3-5 **1D bar impact problem, $c_0 = 5000$; applied velocity at left end is 1for time $t > 0$; initial displacement and velocity are zero**

The calculated responses of the case of the bar with a length of 10 and having 200 elements are given in Figs. 3-6 to 3-9. As in Figs. 3-1 and 3-2, shorter wave modes in the solution of both methods move faster than that of the exact wave for CFL = 0.2. Hence, oscillations mainly occur ahead of the wave front (they also occur behind the wave front) for both methods with this CFL number. On the other hand, for CFL = 2, shorter wave modes have slower wave speeds for both schemes; therefore, oscillations occur behind the wave front, and the slope of the wave front is decreased.

Both methods perform very differently for CFL = 2, while they give very similar solutions for CFL = 0.2. This difference can be explained by the amount of discarded wave modes in the Bathe method. For CFL = 2, the range of discarded wave modes in the Bathe method is

obtained as $k\Delta x/\pi \gtrsim 2(\sim 1.1)(1/2)(\sim 0.3) \simeq 0.33$. For CFL = 0.2, no wave modes are discarded. Therefore, for CFL= 0.2, the dispersion property for both methods is very similar since they have a similar trend in the dispersion relation (Figs. 3-1 and 3-2). Hence, the total solutions from each method are also significantly different, since the participating wave modes are significantly different, although the overall trend of wave speed over the wave modes is very similar.

An important point to notice is that, for CFL = 1, in the Bathe method only the modes with almost no wave speed error participate in the total solution; therefore, the solution becomes almost non-dispersive. Of course, due to the loss of some high frequency modes, the Fourier truncation error is inevitably increased. However, it is observed that the effect of this increased truncation error is not significant (e.g., the slope of the wave front is slightly decreased compared to the results from the trapezoidal rule).

In the case CFL=1, the solution is very accurate for relatively long time simulation, since the solution in the Bathe method is not dispersive for CFL = 1. The solutions for the bar of length 100 with 2000 elements of the same size as the previous case are shown in Figs. 3-10 and 3-11, which show the results from the Bathe method with CFL = 1 and the trapezoidal rule with CFL = 0.65, respectively. While the solutions from the Bathe method are very accurate, the results from the trapezoidal rule with CFL = 0.65 show that the accuracy of the solution becomes decreased as the wave propagates due to its accumulation of the dispersion error.

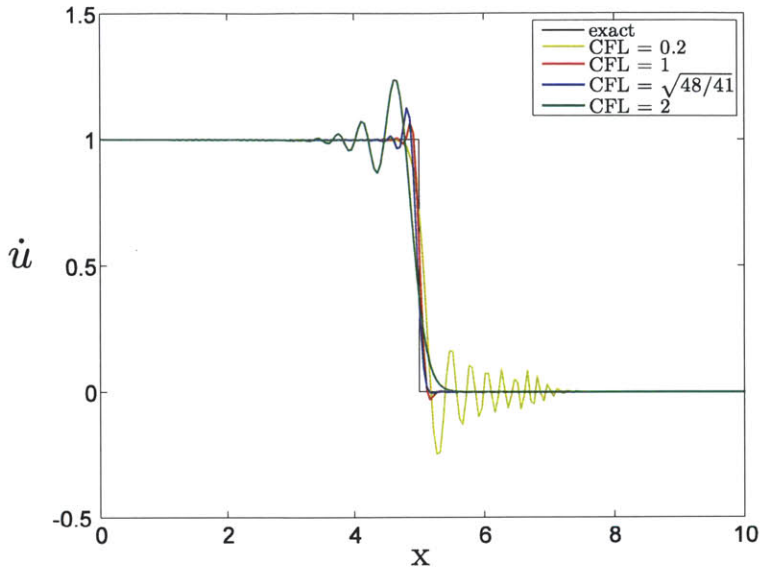

Figure 3-6 **Velocity distributions from the Bathe method for various CFL numbers**

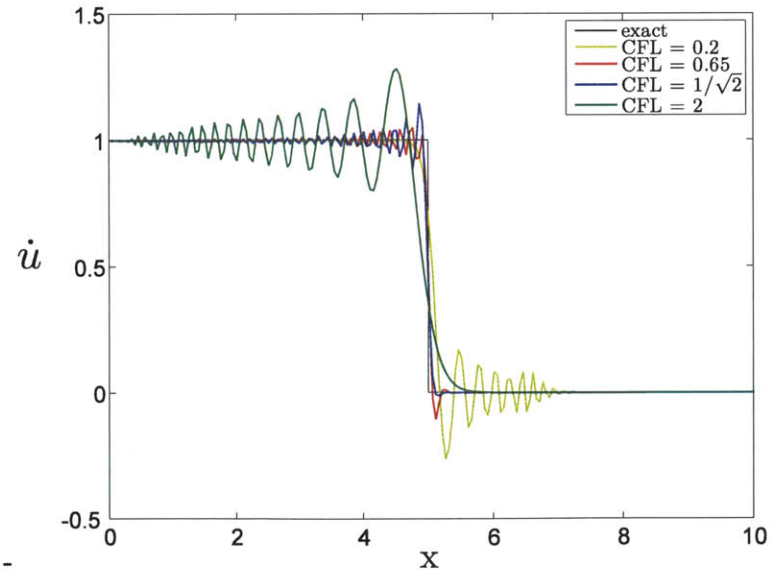

Figure 3-7 **Velocity distributions from the trapezoidal rule for various CFL numbers**

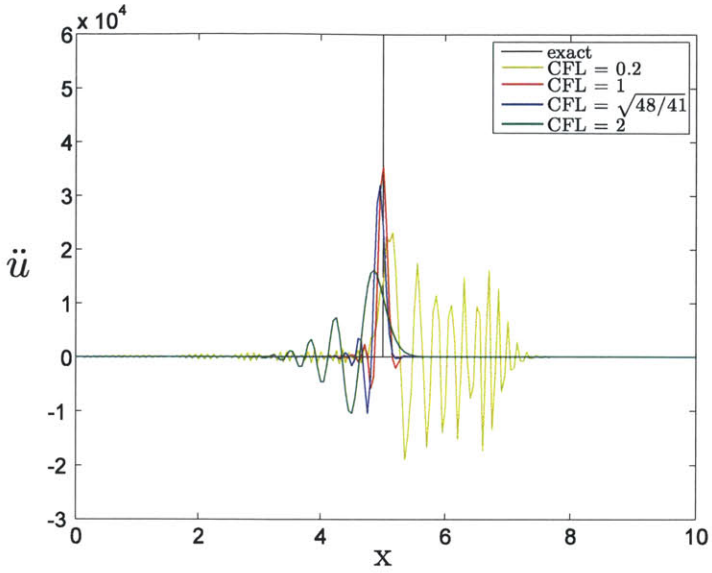

Figure 3-8 **Acceleration distributions from the Bathe method for various CFL numbers**

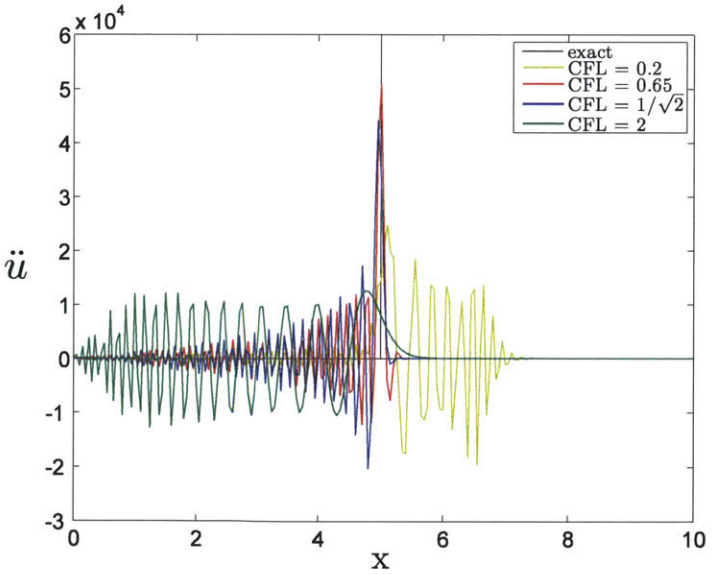

Figure 3-9 **Acceleration distributions from the trapezoidal rule for various CFL numbers**

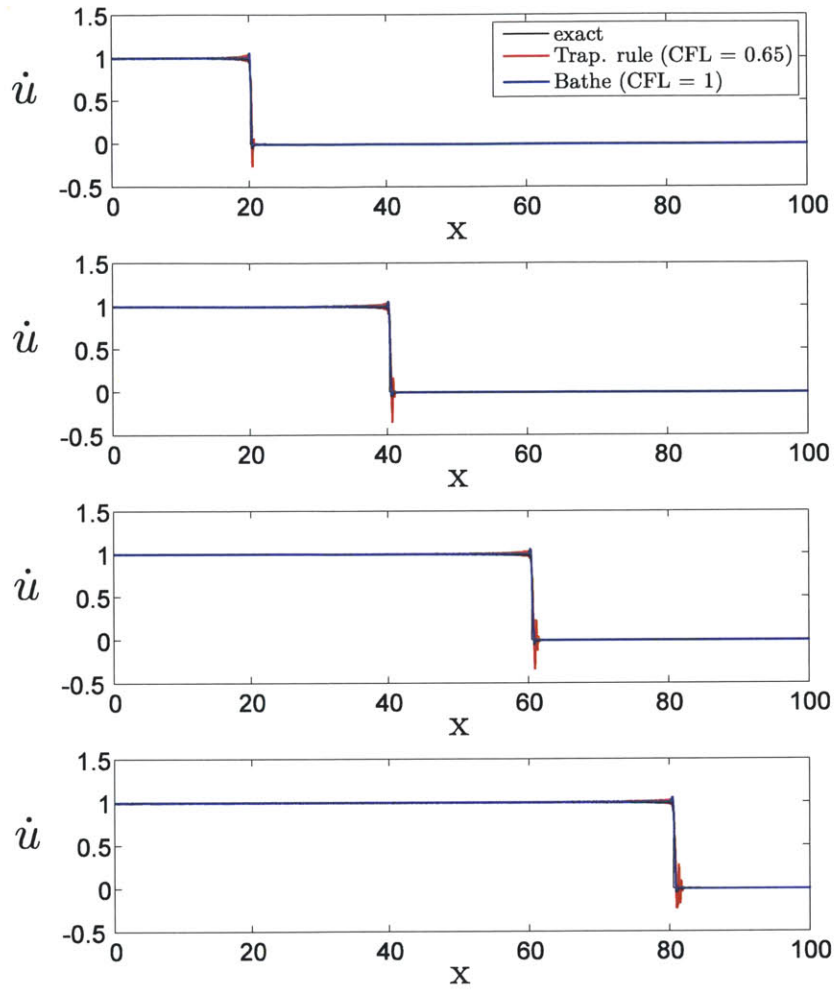

Figure 3-10 **Velocity distributions; blue line – Bathe method (CFL = 1) ; red line – Trapezoidal rule (CFL =0.65); for various observation times**

Note that the CFL numbers 1 and 0.65 are also reported as the ones that give the least global error norm at a certain observation time for each method [61]. CFL = 1 for the Bathe method is estimated from Fig. 3-1 in this study to yield the least dispersion error in the total solution. Since, for CFL = 1, the Bathe method gives almost non-dispersive solutions, it could be expected that the global error measure analysis at any observation

time gives a very similar optimal CFL number for the Bathe method for the same spatial discretization strategy.

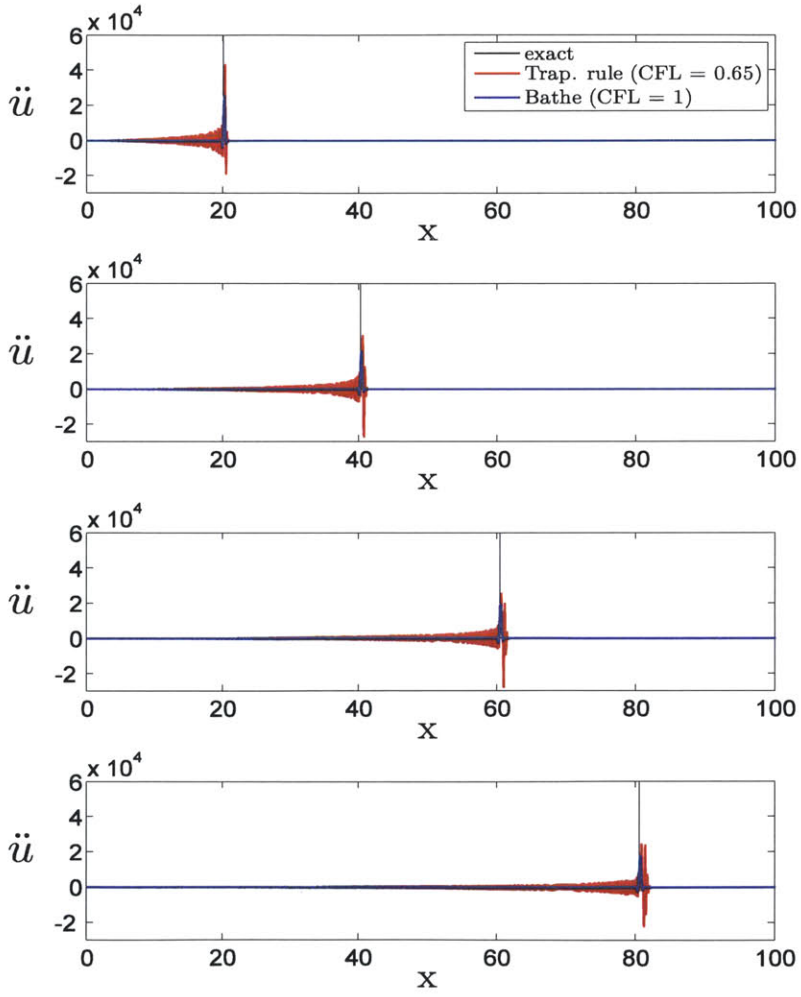

Figure 3-11 **Acceleration distributions; blue line – Bathe method (CFL = 1) ; red line – Trapezoidal rule (CFL =0.65); for various observation times**

3.2.2. 2-D scalar wave propagation

Considering the problem where the field variable u is governed by

$$\frac{\partial^2 u}{\partial x^2}+\frac{\partial^2 u}{\partial y^2}+F(0,0,t)=\frac{1}{c^2}\frac{\partial^2 u}{\partial t^2} \quad , \tag{3.25}$$

where c is the wave velocity which is set to 1 (Fig. 3-12), the load is given as

$$F(0,0,t)=4\left(1-(2-t)^2\right)H(1-t) \quad , \quad t>0 \quad , \tag{3.26}$$

and H is the Heaviside step function. Only the domain [0,15] × [0,15] is considered due to symmetry. In addition, since the wave does not propagate to the boundary for the time considered 13 s, no absorbing boundary conditions are used. Six different meshes with four-node elements are used to idealize the computational domain. For the solutions, the Bathe method and the trapezoidal rule are used with CFL numbers 1 and 0.65, respectively. In the calculations of the CFL numbers, the length of the side of the element is used as the fundamental length.

The snapshots of u from the Bathe method and the trapezoidal rule at $t = 13$ for various meshes are given in Figs. 3-13 and 3-14, respectively. The results show that, for low spatial discretization density, both methods give spurious oscillations, which are not only from the dispersion curve of one propagating angle but also from the difference between the curves of different propagating angles (Figs. 3-3 and 3-4). From the 75 by 75 mesh, however, accurate solutions are obtained using the Bathe method. On the other hand, in particular for propagating angles around $\pi/4$, the trapezoidal rule gives noticeable spurious oscillations until the 165 by 165 mesh.

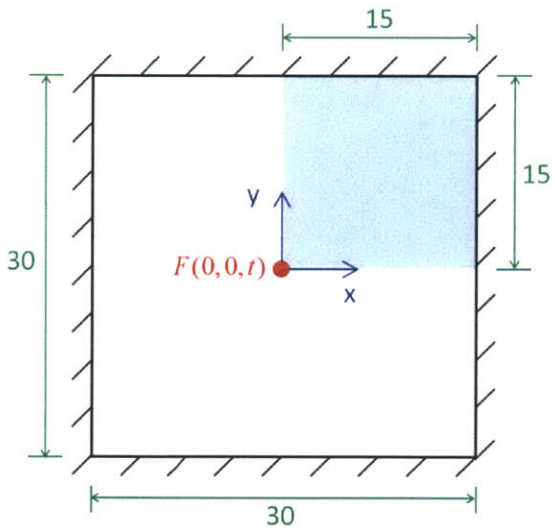

Figure 3-12 **Pre-stressed membrane problem, $c_0 = 1$, initial displacement and velocity are zero, computational domain is shaded**

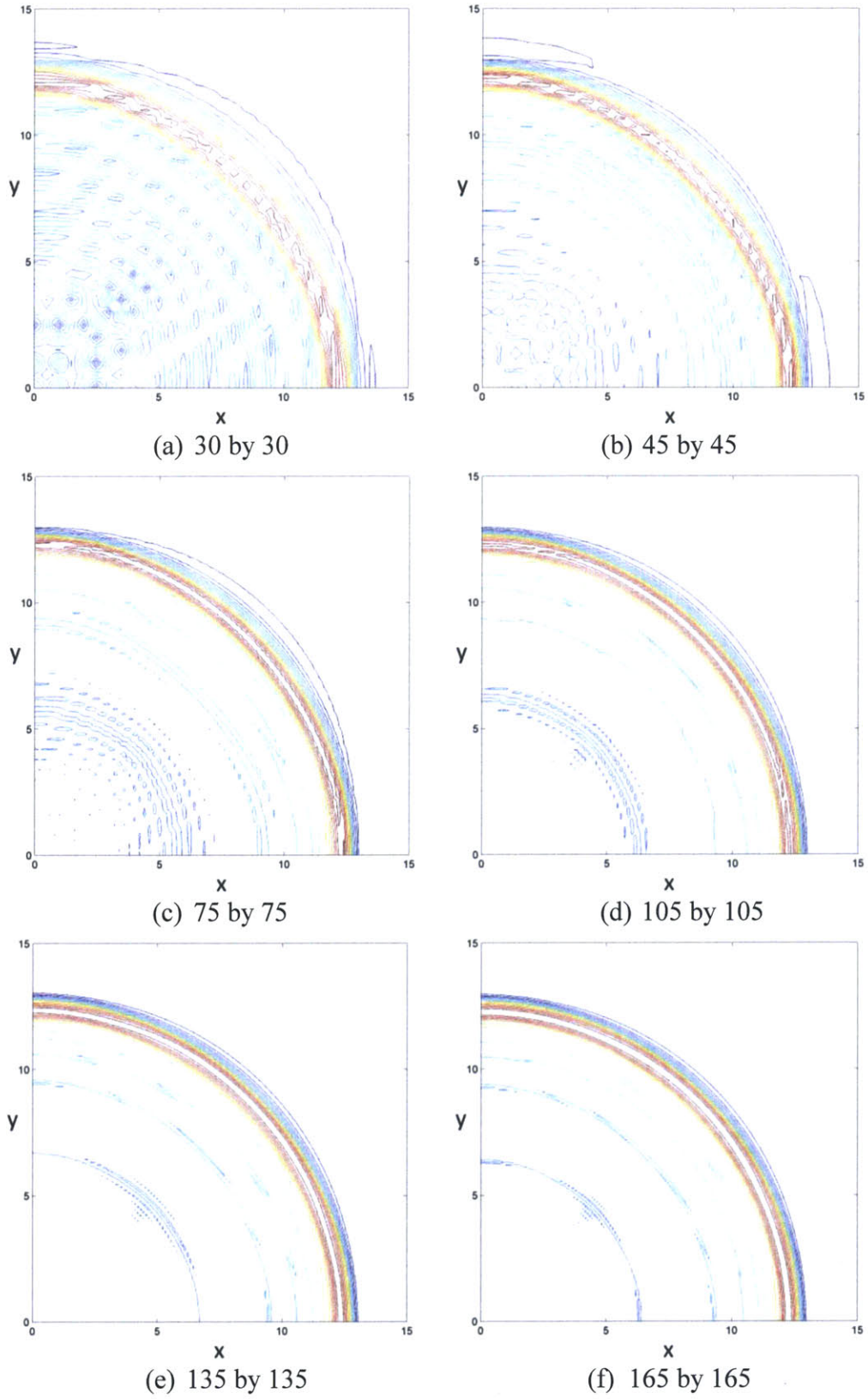

Figure 3-13 **Snapshots of displacements at $t = 13$, Trapezoidal rule, CFL = 0.65**

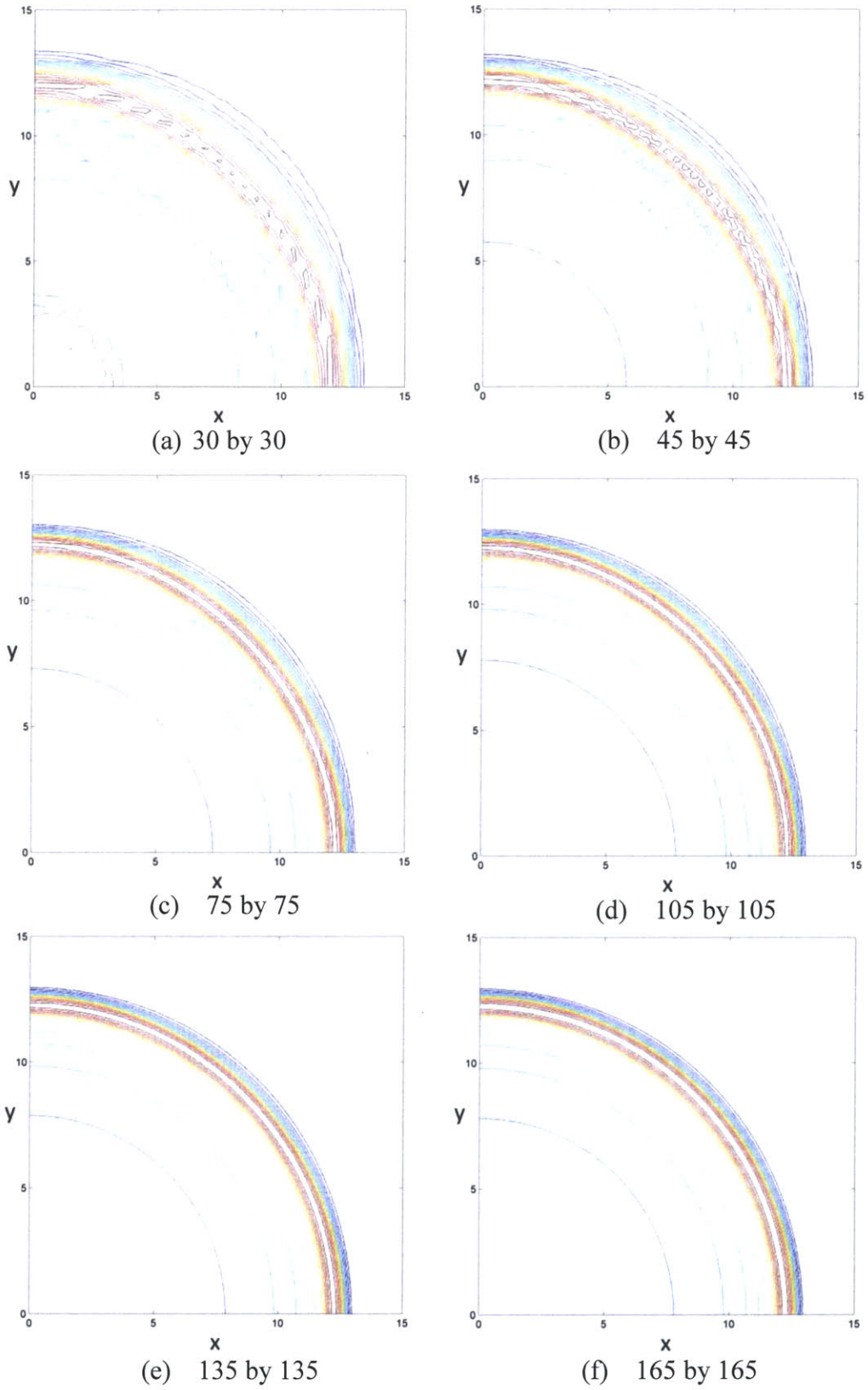

Figure 3-14 **Snapshots of displacements at $t = 13$, Bathe method, CFL = 1**

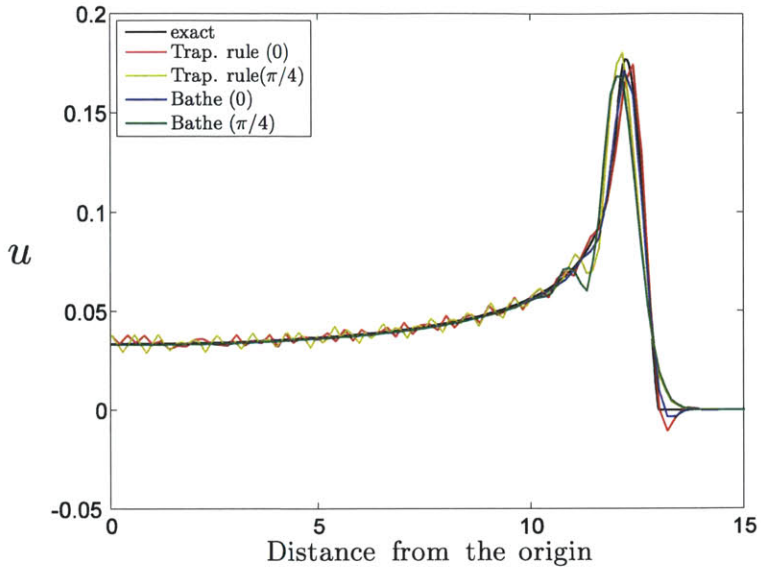

Figure 3-15 **Displacement variations along the various propagating angles, at time $t = 13$; 75 by 75 mesh**

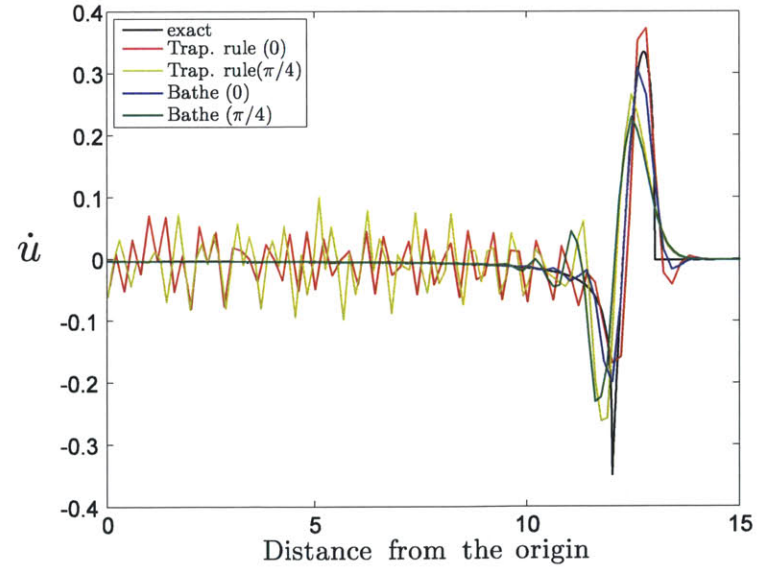

Figure 3-16 **Velocity variations along the various propagating angles, at time $t = 13$; 75 by 75 mesh**

The numerical results at propagating angle 0 and $\pi/4$ at time $t=13$ of the 75 by 75 mesh from the both methods are compared with the analytical solution in Figs. 3-15 and 3-16. The solution at propagating angle zero from the Bathe method is very accurate and almost non-dispersive; however, it also fails to catch the peak, especially for $\dot{u}$. The trapezoidal rule gives spurious oscillations in both the displacements and the velocities, for both 0 and $\pi/4$, though the solution at angle $\pi/4$ gives a less accurate solution. This is because although the Bathe method cuts the inaccurate wave modes for non-zero propagating angles, the remaining wave modes are also dispersive (Fig. 3-3). For angle $\pi/4$, the maximum wave velocity error in the Bathe method is about 6%.

The dispersion curves and the results of this example indicate that, although the Bathe method significantly improves the solution, $\Delta x/(\lambda/2) \leq 0.2$ is required for the waves propagating at nonzero angles to the element sides for sufficient accuracy.

3.2.3. 2-D elastic wave propagation

So far, scalar wave propagations problems with a single wave speed have been considered. The appropriate time step sizes are obtained for each time integration method using the CFL numbers to minimize the numerical dispersion of the waves with the same phase velocity. However, many physical problems are characterized by multiple wave speeds. In

this Section, a Lamb problem is considered, as an example, in which waves are propagating in a semi-infinite elastic domain in plane strain conditions [23].

Fig. 3-17 describes the problem at hand. The following material properties are used: P-wave velocity = 3200 m/s, S-wave velocity = 1848 m/s, and Rayleigh wave velocity = 1671 m/s. The time duration for computing the waves is 0.999 s. Since the P-wave does not reach the outer boundaries, it is not necessary to incorporate absorbing boundary conditions. Since the Rayleigh wave profile is the main interest, the time step sizes are calculated based on the speed of the Rayleigh wave. For the solutions, the Bathe method and the trapezoidal rule with the CFL numbers 1 and 0.65, respectively, are used.

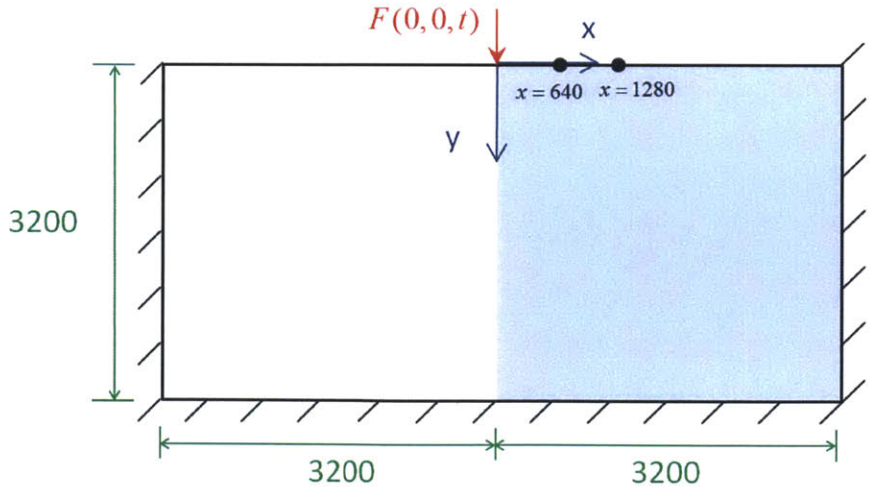

Figure 3-17 **A Lamb problem.** $V_P = 3200$, $V_S = 1848$, $V_{\text{Rayleigh}} = 1671$. **Two receivers are placed at** $x = 640$ **and** $x = 1280$, **computational domain is shaded.**

Two types of load are considered as the external force. First, a Ricker wavelet is used, which is defined as

$$F(0,0,t) = -2\times10^3 \times\left(1-2\pi^2\hat{f}^2(t-t_0)^2\right)\exp(-\pi^2\hat{f}^2(t-t_0)^2), \quad t>0, \tag{3.27}$$

where the central frequency $\hat{f} = 12.5\,\text{Hz}$ and $t_0 = 0.1\,\text{s}$. The solution uses symmetry and a domain with a mesh of 640×640 four-node elements of side lengths $\Delta x = \Delta y = 5\,m$. Fig. 3-18 shows the calculated displacements at two receivers that are located at $x = 640\,m$ and $x = 1280\,m$ from the source. The numerical solutions using the Bathe method and the trapezoidal rule, and the analytical solution, are displayed. The numerical solutions using both methods are in good agreement with the analytical solution.

There are a limited number of wave modes that are excited, since this load type can be well approximated with only a few harmonic functions. Hence, if a fine mesh is used, so that all excited wave modes are within $\Delta x/(\lambda/2) \le 0.2$ as done here, both the Bathe method and the trapezoidal rule give very accurate solutions. The calculated stress field at time $t = 0.9196$ is shown in Fig. 3-19. Color bars in Fig. 3-19 indicate the magnitudes of the von Mises stress.

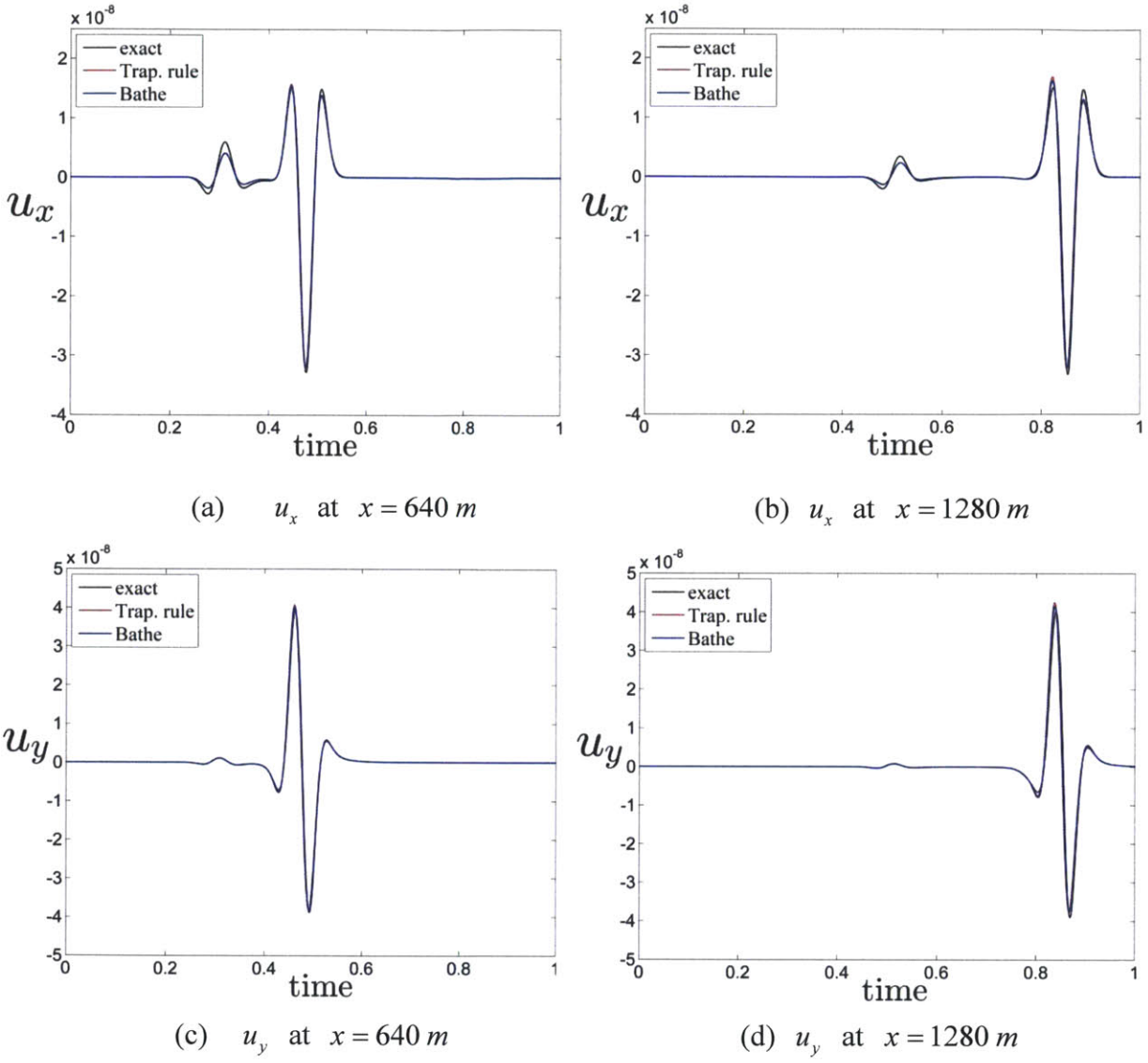

Figure 3-18 **Time history of displacement variations in x-direction and y-direction at the two receivers on the surface; Ricker wavelet line load**

The the line force is considered next, defined as

$$F(0,0,t) = 2\times10^{3}\times\left[H(0.15-t)-3H(0.1-t)+3H(0.05-t)\right] \quad , \quad t>0, \tag{3.28}$$

where H is the Heaviside step function. Three step functions are used in the load, and this renders the problem more difficult to solve numerically. The computational domain is now idealized using a mesh of 1600×1600 4-node elements of side lengths $\Delta x = \Delta y = 2\ m$.

The displacement results at the receivers as a function of time are shown in Fig. 3-20. These displacements are due to the P- and S- waves and the Rayleigh wave propagating along the surface, as in the previous load type case. While, as expected, similar errors in the solution of the P-wave using both the Bathe method and the trapezoidal rule are obtained, larger spurious oscillations are presented in the solution of the Rayleigh wave predicted using the trapezoidal rule.

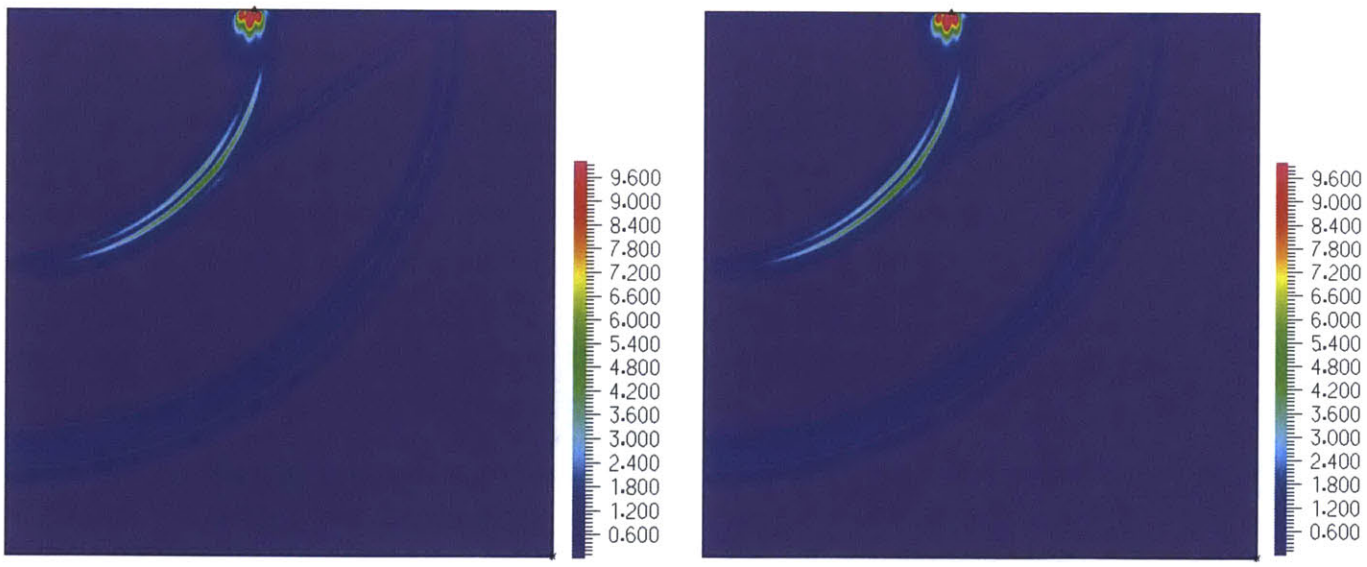

(a) Bathe method (b) Trapezoidal rule

Figure 3-19 **Snapshots of von Mises stress at $t = 0.9196\ s$; Ricker wavelet line load**

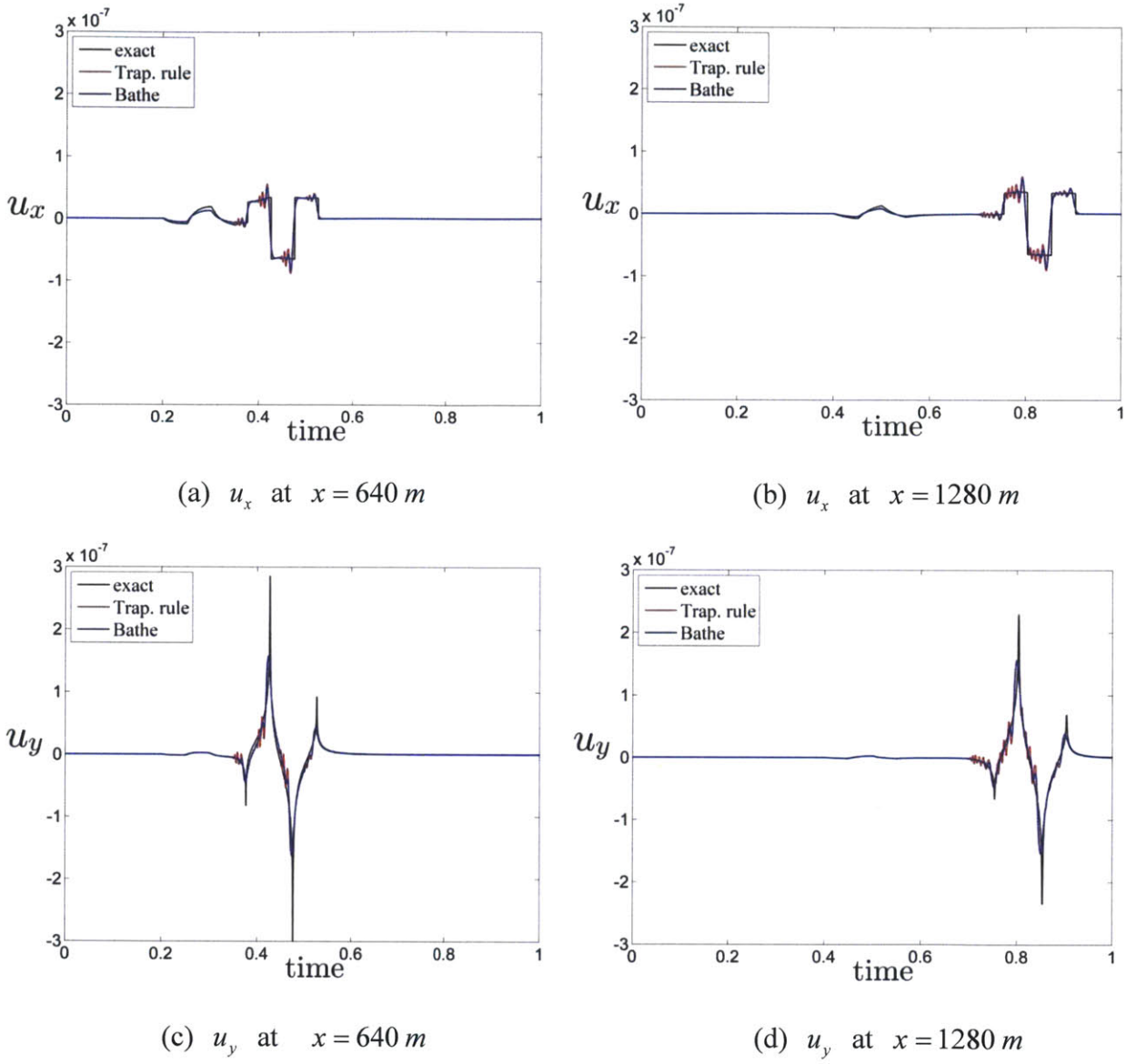

(a) u_x at $x = 640\ m$

(b) u_x at $x = 1280\ m$

(c) u_y at $x = 640\ m$

(d) u_y at $x = 1280\ m$

Figure 3-20 **Time history of displacement variations in the x- and y-directions at the two receivers on the surface; step functions line load**

The difference in the solution accuracy is also shown when considering the predicted stress wave fields, as shown in Fig. 3-21. The stress waves using the Bathe method are clearly

identified, while the solution using the trapezoidal rule shows undesirable spurious oscillations in various areas.

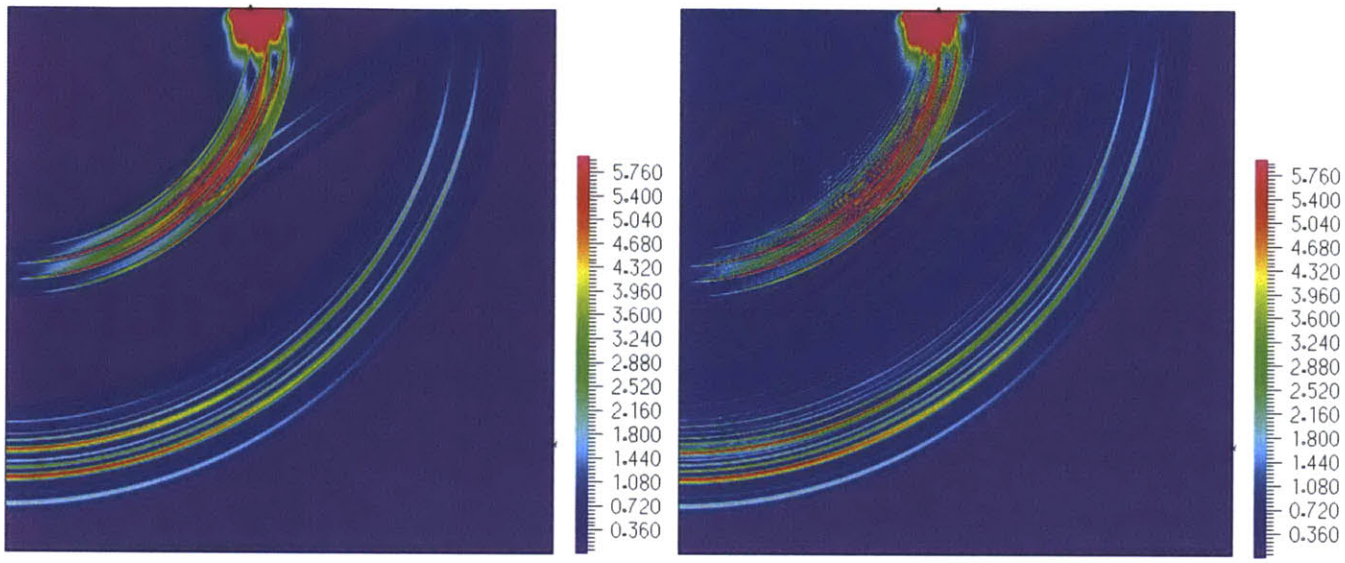

(a) Bathe method (b) Trapezoidal rule

Figure 3-21 **Snapshots of von Mises stress at $t = 0.9196\ s$; step functions line load**

3.3. Concluding remarks

The present Chapter analysed dispersion properties and performance of the Bathe method. First, it was showed that with an appropriate time step size for a given mesh, the scheme makes every participating wave accurate that the total solution is almost non-dispersive. The scheme considerably improves the solution by maintaining accuracy for the wave modes, which can be captured accurately from spatial discretization, and in essence

discarding the wave modes, which cannot be captured accurately and therefore result in spurious oscillations. Since the scheme does not require any additional treatment for wave propagation problems, it can be used for effective solutions in structural dynamics and wave propagation in a uniform manner.

While the solutions were significantly improved by considering the usage of time integration for a given spatial discretization, there was no attempt at improving solutions by enhancing spatial discretization, in particular for multidimensional problems and problems with multiple wave speeds. For more reliable solutions in the analysis of wave propagations in such problems, further research on enhanced spatial discretizations with the Bathe method would be of value.

Chapter 4

A new explicit time integration scheme for wave propagations

This Chapter presents a new explicit time integration scheme for wave propagation analysis. First, the method is formulated based on its stability and accuracy characteristics; then, the dispersion properties of the method using 4-node elements in two dimensions are analyzed. Finally, the solutions of various problems using the central difference method and the proposed scheme are provided to demonstrate the performance of the scheme in the analyses of wave propagation problems.

4.1. An explicit time integration scheme

The governing finite element equations in linear analysis take the form of

$$\mathbf{M}\ddot{\mathbf{U}}+\mathbf{C}\dot{\mathbf{U}}+\mathbf{K}\mathbf{U}=\mathbf{R}, \tag{4.1}$$

with initial conditions where $\mathbf{U}$ and $\mathbf{R}$ are the nodal values of the solution and the vector

of externally applied nodal forces, respectively, and $\mathbf{M}$, $\mathbf{C}$, $\mathbf{K}$ are the mass, damping, and stiffness matrices, respectively. The time integration scheme calculates the solutions at time $t+\Delta t$, with the predetermined time step size Δt, and some solution variables obtained up to time t.

In the proposed explicit scheme, the time step Δt is considered, consisting of two sub-steps, as inspired by the Bathe method, to calculate the unknown displacements, velocities, and accelerations. The time step sizes are $p\Delta t$ and $(1-p)\Delta t$ for the first and the second sub-step, respectively, where $p \in (0,1)$.

The first sub-step uses

$$\mathbf{M}^{t+p\Delta t}\ddot{\mathbf{U}}+\mathbf{C}^{t+p\Delta t}\dot{\mathbf{U}}+\mathbf{K}^{t+p\Delta t}\mathbf{U}={}^{t+p\Delta t}\mathbf{R}, \tag{4.2}$$

$${}^{t+p\Delta t}\mathbf{U}={}^{t}\mathbf{U}+\left[p\Delta t\right]{}^{t}\dot{\mathbf{U}}+\frac{1}{2}[p\Delta t]^2\,{}^{t}\ddot{\mathbf{U}}, \tag{4.3}$$

$${}^{t+p\Delta t}\dot{\mathbf{U}}={}^{t}\dot{\mathbf{U}}+\frac{1}{2}\left[p\Delta t\right]{}^{t}\ddot{\mathbf{U}}, \tag{4.4}$$

and

$${}^{t+p\Delta t}\dot{\mathbf{U}}={}^{t+p\Delta t}\dot{\mathbf{U}}+\frac{1}{2}\left[p\Delta t\right]{}^{t+p\Delta t}\ddot{\mathbf{U}}, \tag{4.5}$$

and in the second step

$$\mathbf{M}^{t+\Delta t}\ddot{\mathbf{U}}+\mathbf{C}^{t+\Delta t}\dot{\mathbf{U}}+\mathbf{K}^{t+\Delta t}\mathbf{U}={}^{t+\Delta t}\mathbf{R}, \tag{4.6}$$

$${}^{t+\Delta t}\mathbf{U}={}^{t+p\Delta t}\mathbf{U}+\left[(1-p)\Delta t\right]{}^{t+p\Delta t}\dot{\mathbf{U}}+\frac{1}{2}[(1-p)\Delta t]^2\,{}^{t+p\Delta t}\ddot{\mathbf{U}}, \tag{4.7}$$

$${}^{t+\Delta t}\dot{\mathbf{U}}={}^{t+p\Delta t}\dot{\mathbf{U}}+\frac{1}{2}\left[(1-p)\Delta t\right]{}^{t+p\Delta t}\ddot{\mathbf{U}}, \tag{4.8}$$

and

$${}^{t+\Delta t}\dot{\mathbf{U}}={}^{t+\Delta t}\dot{\mathbf{U}}+\left[(1-p)\Delta t\right](q_0{}^{t}\ddot{\mathbf{U}}+q_1{}^{t+p\Delta t}\ddot{\mathbf{U}}+q_2{}^{t+\Delta t}\ddot{\mathbf{U}}), \tag{4.9}$$

where

$${}^{t+p\Delta t}\dot{\mathbf{U}}=(1-s){}^{t+p\Delta t}\hat{\dot{\mathbf{U}}}+s{}^{t}\dot{\mathbf{U}} \tag{4.10}$$

and

$${}^{t+\Delta t}\dot{\mathbf{U}}=(1-s){}^{t+\Delta t}\hat{\dot{\mathbf{U}}}+s{}^{t+p\Delta t}\dot{\mathbf{U}}, \tag{4.11}$$

and p, q_0, q_1, q_2, and s are parameters to be determined, and the stability and accuracy characteristics of the method depend on these parameters. The load at the sub-step ${}^{t+p\Delta t}\mathbf{R}$, which should be determined based on the given external forces, will be addressed in Section 4.1.3. The first sub-step can be seen as a central difference method in a predictor-corrector form, with a balance equation where only velocity is allocated differently. The

second sub-step can be seen as a predictor-corrector form of a method with the same predictor and corrector for the displacement as in the first sub-step and the same predictor but with a different corrector, which uses three accelerations for velocity, and with the same balance equation. The proposed form is inherently explicit with a lumped mass matrix and a non-diagonal damping matrix. Note that the $\mathbf{K}^{t+p\Delta t}\mathbf{U}$ and $\mathbf{K}^{t+\Delta t}\mathbf{U}$ terms can be evaluated by summing over element force vectors rather than calculating stiffness matrices [1], and the same holds for the damping matrix terms.

4.1.1. Stability and accuracy characteristics

To have second order accuracy, the required relations are

$$q_0 + q_1 + q_2 = \frac{1}{2}, \quad q_2 = \frac{1}{2} - pq_1, \quad s = -1 \tag{4.12}$$

for undamped/damped cases. Note that $s = -1$ is not required for the undamped case, which is clear from Eqs. (4.2) and (4.6).

With modal decomposition, the method may be expressed as [1]

$$\begin{bmatrix} {}^{t+\Delta t}\ddot{x} \\ {}^{t+\Delta t}\dot{x} \\ {}^{t+\Delta t}x \end{bmatrix} = \mathbf{A} \begin{bmatrix} {}^{t}\ddot{x} \\ {}^{t}\dot{x} \\ {}^{t}x \end{bmatrix} + \mathbf{L}_{\mathbf{a}}\,{}^{t+p\Delta t}r + \mathbf{L}_{\mathbf{b}}\,{}^{t+\Delta t}r\,, \tag{4.13}$$

where $\mathbf{A}$ is the integration approximation, and $\mathbf{L}_{\mathbf{a}}$ and $\mathbf{L}_{\mathbf{b}}$ are the load operators. Some of the stability and accuracy characteristics of the method may be analyzed using the integration approximation matrix.

With relations in Eq. (4.12) and considering an undamped case, the characteristic polynomial of the integration approximation matrix becomes

$$\lambda^3 - 2A_1\lambda^2 + A_2\lambda - A_3 = 0\,, \tag{4.14}$$

where

$$A_1 = 1 - \frac{1}{2}\omega^2\Delta t^2 + \frac{1}{4}\,p(1-p)\left(p^2 q_1 - pq_1 + \frac{1}{2}\right)\omega^4\Delta t^4$$

$$A_2 = 1 + \frac{1}{2}\,pq_1(1-p)^3\,\omega^4\Delta t^4 \tag{4.15}$$

$$A_3 = 0\,,$$

and ω is modal natural frequency. Applying the Routh-Hurwitz stability criteria on Eq. (4.14), the expression for the possible maximum stability limit and the corresponding condition is obtained as

$$\Omega_s^2 = \frac{1}{\gamma p(1-p)} \tag{4.16}$$

and

$$-\frac{1}{4(1-p)} \leq q_1 \leq \frac{4p(1-p)-1}{8(1-p)^2 p}, \tag{4.17}$$

where

$$\gamma = \frac{1}{4} - \frac{1}{2}(1-p)q_1 \;; \qquad \Omega = \omega \Delta t \,. \tag{4.18}$$

It can be seen that if $p = 0.5$ and $q_1 = 0$, then the stability limit $\Omega_s = 4$; the method has the same stability limit as the central difference method for the same computational effort.

The principal eigenvalues of $\mathbf{A}$ should remain in the complex domain to represent oscillatory solutions. Since $A_3 = 0$, there are one zero spurious eigenvalue and two principal eigenvalues of $\mathbf{A}$ as

$$\lambda_{1,2} = A_1 \pm \sqrt{A_1^2 - A_2} \,. \tag{4.19}$$

The bifurcation points, Ω_b, where the eigenvalues become real, are obtained through

$$\Omega_{b1}^2 = \frac{2}{\alpha(1-p)}; \quad \Omega_{b2,3}^2 = \frac{2-p\pm\sqrt{\beta}}{\alpha(1-p)p}, \tag{4.20}$$

where

$$\alpha = \frac{1}{2} - (1-p)pq_1; \quad \beta = 8p(p-1)^2 q_1 + p^2. \tag{4.21}$$

From Eq. (4.17), $\alpha > 0$; hence, there is always a positive real bifurcation point from Ω_{b1}. To maximize the critical time step size, Ω_{b1} must be equal to the smaller value of $\Omega_{b2,3}$ so that the effective bifurcation point becomes the larger value of $\Omega_{b2,3}$ with the condition $\beta > 0$. This constraint results in

$$q_1 = \frac{1-2p}{2p(1-p)}. \tag{4.22}$$

Using Eq. (4.22), the bifurcation point and the stability limit are maximized as

$$\Omega_b = \frac{2}{p}; \quad \Omega_s = \frac{2}{\sqrt{(1-p)(3p-1)}}, \tag{4.23}$$

where $1/2 \le p < 2/3$ is the required condition, so that the eigenvalues always bifurcate first. The resulting integration approximation $\mathbf{A}$ and the load operators $\mathbf{L}_a$ and $\mathbf{L}_b$ are summarized in Appendix A4.

The value p is expressed using the spectral radius at the bifurcation point, which is denoted as ρ_b, as

$$p = \frac{2 - \sqrt{2 + 2\rho_b}}{1 - \rho_b}; \qquad p = 0.5 \text{ if } \rho_b = 1. \tag{4.24}$$

Hence the value of p can be determined based on ρ_b, which represents the amount of numerical dissipation in the high frequency domain. At this point, the proposed method can be treated as a one parameter (p or ρ_b) method. Eq. (4.24) gives the range of p for $0 \le \rho_b \le 1$ as $0.5 \le p \le 2 - \sqrt{2}$, while $p = 0.5$ gives $\rho_b = 1$, resulting in no numerical dissipation, and $p = 2 - \sqrt{2}$ results in the maximum numerical dissipation the minimum period error in the proposed method. It is interesting to note that in the Bathe method, the splitting ratio γ which provides the maximum dissipation and minimum period elongation is also $2 - \sqrt{2}$ (see ref. [44] and Appendix A1).

The spectral radii of the method for various ρ_b are given in Fig. 4-1. The results show that for all ρ_b, the spectral radii of $\mathbf{A}$ equals about 1 until $\Omega \sim 1$ $(\Delta t / T \sim 0.16)$. This property is desirable since it may result in high accuracy for the low frequency domain. Fig. 4-2 shows the period elongation and amplitude decays for various ρ_b [58–60]. The figures show the accuracy characteristics of the proposed scheme in the low frequency domain. The proposed scheme shows very small amplitude decay and (negative) period elongation for all ρ_b.

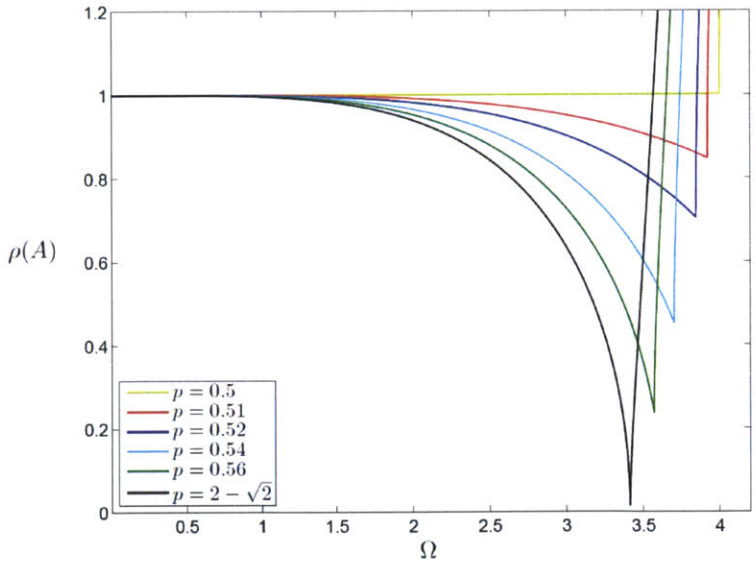

Figure 4-1 **Spectral radii of approximation operator, case $\xi = 0$, of the proposed explicit method for various values of p; $p = 0.5$ gives the stability limit $\Omega_s = 4$ which is twice the stability limit of the central difference method**

For an explicit method, it is also crucial to maintain the available frequency range as much as possible while attaining numerical dissipation in the high frequency domain. The bifurcation limit of the scheme also decreases as ρ_b decreases, as in other dissipative explicit methods (Fig. 4-1). This may also be observed in Eqs. (4.23) and (4.24). However, the relative amount of the decrease of available frequency domain in the proposed explicit method is significantly smaller than those of other methods. For example, the bifurcation limit Ω_b of the proposed method changes from 4 to 3.414 when ρ_b changes from one to zero (from minimum dissipation to maximum dissipation), while Ω_b of the Tchamwa-Wielgosz explicit scheme [54] and the method presented by Hulbert and Chung [4] change from 2 to 1 and from 2 to 1.414, respectively.

The proposed explicit method can be used as a method with one controllable parameter (p or ρ_b) that determines the amount of numerical dissipation for the high frequency modes and has improved range of available frequency. However, in practice it may not be possible to determine the best controllable parameter in general. Therefore, it is desirable to have a good suggestion for this parameter for general usage of the method. $p = 0.54$ is suggested here for this purpose. With $p = 0.54$, the proposed scheme possesses very good accuracy for low frequency responses, which may be seen from the very small period elongation (-1.08%) and amplitude decay (2.62%) at $\Delta t / T$=0.2. In addition, it has been shown that the Bathe method eradicates nearly all frequencies in $\Delta t / T > 0.3$, maintaining high accuracy for the low frequency domain so that surprisingly accurate solutions are obtained in

preceding Chapters. The proposed explicit method, with $p = 0.54$, has practically the same spectral radii as those of the Bathe method until $\Delta t / T \sim 0.3$ and has smaller spectral radii from $\Delta t / T \sim 0.3$ until it bifurcates, where $\rho_b = 0.451$ and $\Omega_b = 3.704$ (Fig. 4-3). Hence, with $p = 0.54$, similar results can be expected from the proposed explicit method and the Bathe method.

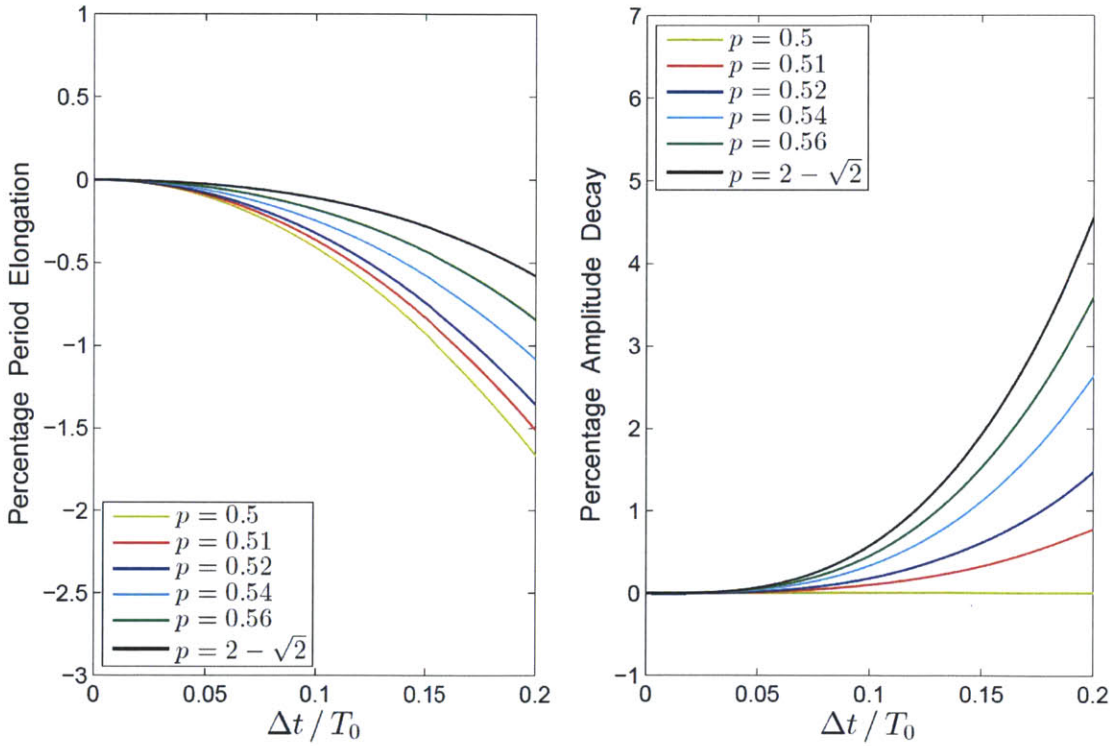

Figure 4-2 **Percentage period elongation and percentage amplitude decay of the proposed method for various values of** p

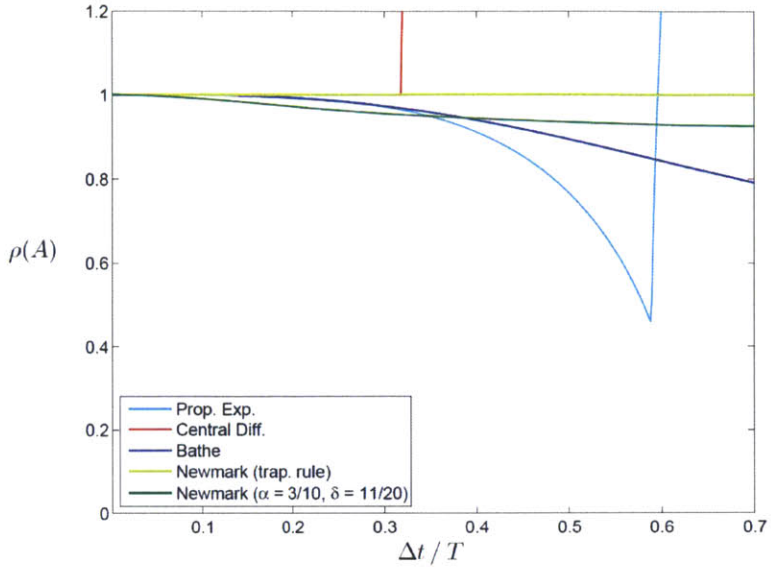

Figure 4-3 **Spectral radii of approximation operators, case $\xi = 0$, for various methods; for the proposed explicit scheme, $p = 0.54$ is used**

4.1.2. A dispersion error analysis for 2D case

The present Section analyses the dispersion errors resulting from the spatial discretization coupled with the temporal discretizations from the proposed explicit method and the central difference method. For spatial discretization, a mesh of four-node elements is considered.

To analyze the dispersion properties, solutions for the scalar wave propagation governed by

$$\frac{\partial^2 u}{\partial t^2} - c_0^2 \nabla^2 u = 0 \tag{4.25}$$

are used, where u is the field variable and c_0 is the exact wave velocity. The corresponding finite element system may become [1, 45]

$$\mathbf{M}_{lump}\ddot{\mathbf{U}}+c_0^2\mathbf{K}\mathbf{U}=\mathbf{0}, \tag{4.26}$$

where

$$\mathbf{M}^{(m)}=\frac{1}{4}\int_{V^{(m)}} dV^{(m)}\cdot\begin{bmatrix}1&0&0&0\\0&1&0&0\\0&0&1&0\\0&0&0&1\end{bmatrix} \tag{4.27}$$

and

$$\mathbf{K}^{(m)}=\int_{V^{(m)}}\left(\nabla\mathbf{H}^{(m)}\right)^T\left(\nabla\mathbf{H}^{(m)}\right)dV^{(m)}, \tag{4.28}$$

and $\mathbf{H}^{(m)}$ and $\mathbf{U}$ are the element displacement interpolation matrix and the nodal displacement values of the solution, respectively, and $\mathbf{K}^{(m)}$ and $\mathbf{M}^{(m)}$ are the stiffness and lumped mass matrices for element (m) with volume $V^{(m)}$. In the actual evaluation, a unit thickness in accordance with Eq. (4.25) is used.

From Eqs. (4.13)–(4.15), a linear multistep form of the proposed scheme in modal basis is obtained as

$${}^{t+\Delta t}x+\left(-2+\Delta t^2\omega^2+\alpha_1\Delta t^4\omega^4\right){}^{t}x+\left(1+\beta_1\Delta t^4\omega^4\right){}^{t-\Delta t}x=0 \tag{4.29}$$

or

$$^{t+\Delta t}\mathbf{X}+\left(-2\mathbf{I}+\Delta t^2\mathbf{\Lambda}+\alpha_1\Delta t^4\mathbf{\Lambda}^2\right)^{t}\mathbf{X}+\left(\mathbf{I}+\beta_1\Delta t^4\mathbf{\Lambda}^2\right)^{t-\Delta t}\mathbf{X}=0, \tag{4.30}$$

where

$$\alpha_1=\frac{1}{2}p^2(p-1);\quad \beta_1=-\frac{1}{2}p^3+\frac{5}{4}p^2-p+\frac{1}{4}. \tag{4.31}$$

Here, x is a modal degree of freedom, $\mathbf{X}$ is the corresponding modal degrees of freedom vector, ω is the natural frequency of a mode, and $\mathbf{\Lambda}$ is the corresponding diagonal matrix listing all ω_i^2.

Modal analysis is considered in Eq. (4.26), and the resulting eigenproblem becomes

$$c_o^2\mathbf{M}_{lump}^{-1}\mathbf{K}\mathbf{\Phi}=\mathbf{\Phi}\mathbf{\Lambda}, \tag{4.32}$$

where the columns in $\mathbf{\Phi}$ are the eigenvectors of corresponding eigenvalues in $\mathbf{\Lambda}$ and the nodal values of the solution $\mathbf{U}$ equals $\mathbf{\Phi X}$. In addition, from Cayley-Hamilton theorem, the eigenvectors of $\mathbf{M}_{lump}^{-1}\mathbf{K}$ are the same as those of $(\mathbf{M}_{lump}^{-1}\mathbf{K})^2$, and the eigenvalues of $(\mathbf{M}_{lump}^{-1}\mathbf{K})^2$ are the square of those of $\mathbf{M}_{lump}^{-1}\mathbf{K}$. Consider a mesh with nodes equally spaced at distance h along both x- and y-axes ($\Delta x=\Delta y=h$), and using the definition of

$\mathrm{CFL} = \frac{c_0 \Delta t}{h}$, the linear multistep from of the proposed scheme in Eq. (4.30) can be rewritten in the physical domain as

$$^{t+\Delta t}\mathbf{U} + \left(-2\mathbf{I} + \mathrm{CFL}^2\mathbf{K} + \alpha_1 \mathrm{CFL}^4 \mathbf{K}^2\right)^t\mathbf{U} + \left(\mathbf{I} + \beta_1 \mathrm{CFL}^4 \mathbf{K}^2\right)^{t-\Delta t}\mathbf{U} = 0. \qquad (4.33)$$

For the central difference method [1], the linear multistep form in modal basis is obtained as

$$^{t+\Delta t}x + \left(-2 + \Delta t^2 \omega^2\right)^t x + ^{t-\Delta t}x = 0 \qquad (4.34)$$

or, equivalently in the physical domain the linear multistep form, becomes

$$^{t+\Delta t}\mathbf{U} + \left(-2\mathbf{I} + \mathrm{CFL}^2\mathbf{K}\right)^t\mathbf{U} + ^{t-\Delta t}\mathbf{U} = 0. \qquad (4.35)$$

From Eqs. (4.33) and (4.35), the added feature in the proposed method can be seen as the use of the second order term, $(\mathbf{M}_{lump}^{-1}\mathbf{K})^2$ in linear multistep form.

The general solution of Eq. (4.25) for a plane wave in 2-D analyses has the form $u = Ae^{i(k_0 x\cos(\theta)+k_0 y\sin(\theta)-\omega_0 t)}$, where ω_0 is the exact frequency of the wave mode and $k_0 = \omega_0 / c_0$ is the corresponding exact wave number. The numerical solution takes a general form

$$ {}^{t}_{x,y}u = A_k e^{i(kx\cos(\theta)+ky\sin(\theta)-\omega t)} , \tag{4.36} $$

where ω, $k = \omega / c$, and θ are the numerical frequency, the corresponding wave number, and the propagating angle from the x-axis, respectively. Since the numerical wave speed c is different from the exact wave c_0 and it is a function of the wave number, this difference results in the numerical dispersion error. In addition, the amplitude decay in time integration schemes results in the decrease of the amplitude of the calculated wave.

Considering a regular mesh with nodes equally spaced at distance h along both x- and y-axes ($\Delta x = \Delta y = h$), the solution of the finite element system at time $n_t \Delta t$ and location $n_x h$, $n_y h$ is

$$ \begin{aligned} {}^{n_t\Delta t}_{n_x h,\, n_y h}u &= A_k e^{i(k n_x h\cos(\theta)+k n_y h\sin(\theta)-\omega n_t \Delta t)} \\ &= A_k e^{ikh\left(n_x\cos(\theta)+n_y\sin(\theta)-n_t(\mathrm{CFL})(c/c_0)\right)} . \end{aligned} \tag{4.37} $$

After substituting the above expression into the linear multistep formulae in Eqs. (4.33) and (4.35) , and looking at the equation corresponding to the middle node of a patch of elements, which consists of sixteen square finite elements for Eq. (4.33) and of four finite elements for Eq. (4.35), a relation is obtained between $\mathrm{CFL} = c_0 \Delta t / h$, c / c_0, the wave number k, and the element size h for the proposed method and for the central difference method.

Note that the corresponding $\mathbf{K}^t\mathbf{U}$ term for the middle node at (x,y) is

$$\frac{1}{3}[8\,{}^{t}_{x,y}u - ({}^{t}_{x\pm h,y}u + {}^{t}_{x,y\pm h}u + {}^{t}_{x\pm h,y\pm h}u)] \tag{4.38}$$

and the corresponding term from $\mathbf{K}^2\,{}^t\mathbf{U}$ is

$$\begin{aligned}\frac{1}{9}[\,&72\,{}^{t}_{x,y}u - 12\,({}^{t}_{x\pm h,y}u + {}^{t}_{x,y\pm h}u) - 14\,{}^{t}_{x\pm h,y\pm h}u \\ &+ 3({}^{t}_{x\pm 2h,y}u + {}^{t}_{x,y\pm 2h}u) + 2({}^{t}_{x\pm 2h,y\pm h}u + {}^{t}_{x\pm h,y\pm 2h}u) + {}^{t}_{x\pm 2h,y\pm 2h}u\,]\end{aligned} \tag{4.39}$$

To analyze the effect of the CFL number on numerical dispersion error, the case for zero propagating angle is first considered. Figs. 4-4 and 4-5 show that as the CFL number increases (i.e., as the time step size become close to the critical time step size), the

dispersion error is minimized for both the proposed method and the central difference method. As is well known, for CFL =1, the central difference method provides no dispersion error for all wave modes.

For the proposed method, the wave modes in $\Delta t / T > 0.3$ are effectively discarded in the numerical solution by the numerical damping, as in the Bathe method (see Section 2.1 and [1]). Therefore, for CFL = 1.85, the wave modes with $k\Delta x \gtrsim 2$ are, in essence, not participating in the total solution. As a result, with CFL = 1.85, the dispersion error in the total solution is reasonably small.

However, we should note that, in actual practical analyses, the wave will travel in all directions across elements, and it is crucial to have good dispersion accuracy for all propagating angles. Fig. 4-6 and 4-7 show the dispersion error curves for various propagating angles of the proposed method with CFL = 1.85 and of the central difference method with CFL =1. The dispersion errors in both methods increase as the propagating angle is increased.

The important point is that the characteristics of the proposed method also hold for the multidimensional case. Due to its damping properties, the dispersion error in the proposed scheme is well limited, as in the 1-D case, while the errors in the central difference method become notably increased. Hence, the solution from the central difference method will generally show a significant

dispersion error due to its large errors in the high frequency wave modes for multidimensional analysis.

It is interesting to note that the effect of the increasing propagating angle on the dispersion error curves in Figs. 4-6 and 4-7 is similar to those of the decreasing CFL number in Figs. 4-4 and 4-5. Hence larger angles of propagation result in the errors in the same way that smaller CFL numbers do. This is the opposite of the results in implicit methods with the consistent mass matrix. The difference can be explained by the opposite dispersion characteristics of the lumped mass matrix and the consistent matrix, and period elongations in implicit methods and period shortening in explicit methods. An important point is that larger angles of propagation have the same effect as using a smaller time step size for the time integration method in usage of explicit time integration methods with the lumped mass matrix. Therefore, if the time step size is set based on the zero propagating angle, then the stability condition is satisfied for the all propagating angles.

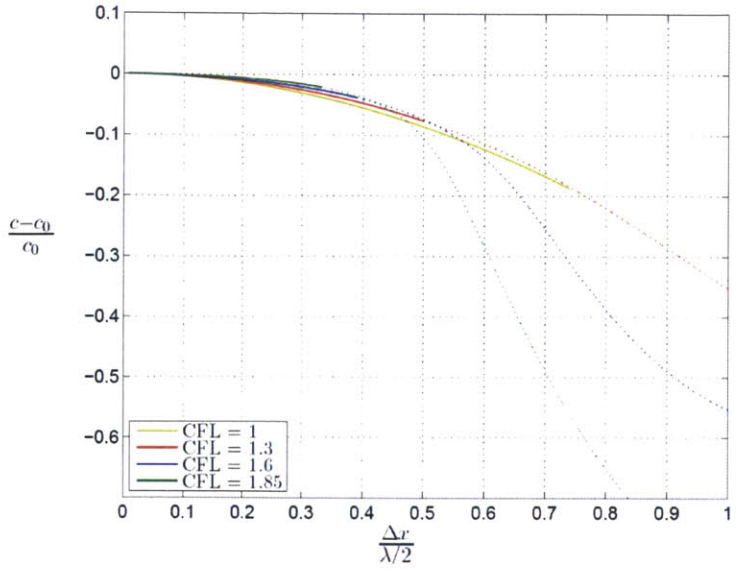

Figure 4-4 **Relative wave speed errors of the proposed method for various CFL numbers; using $p = 0.54$; results for discarded wave modes are given by dotted lines**

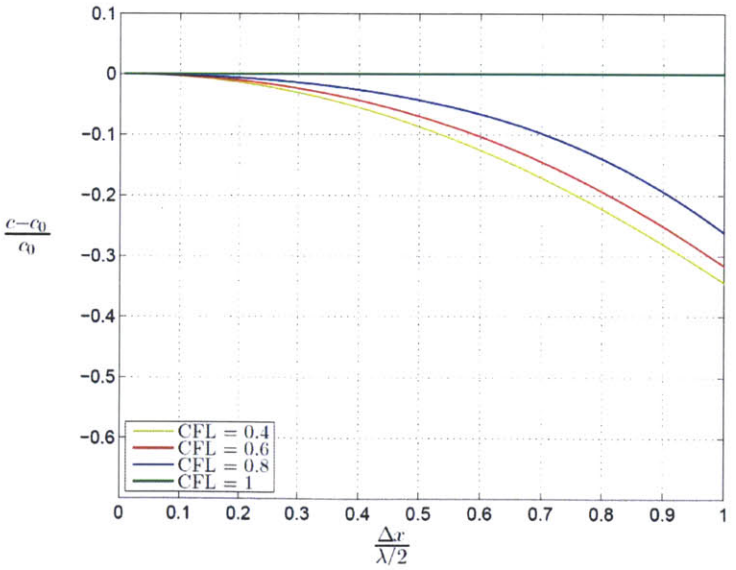

Figure 4-5 **Relative wave speed errors of the central difference method for various CFL numbers**

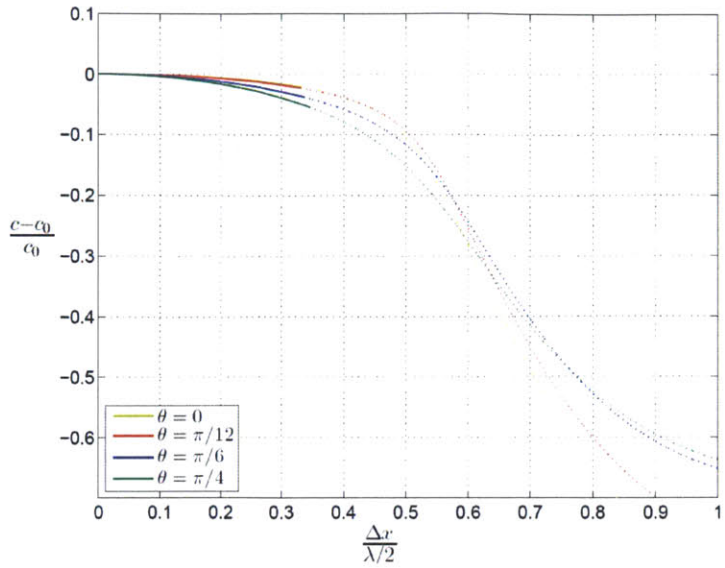

Figure 4-6 **Relative wave speed errors of the proposed method for various propagating angles, using** $\mathrm{CFL} = 1.85$ **and** $p = 0.54$ **; results for discarded wave modes are shown by dotted lines**

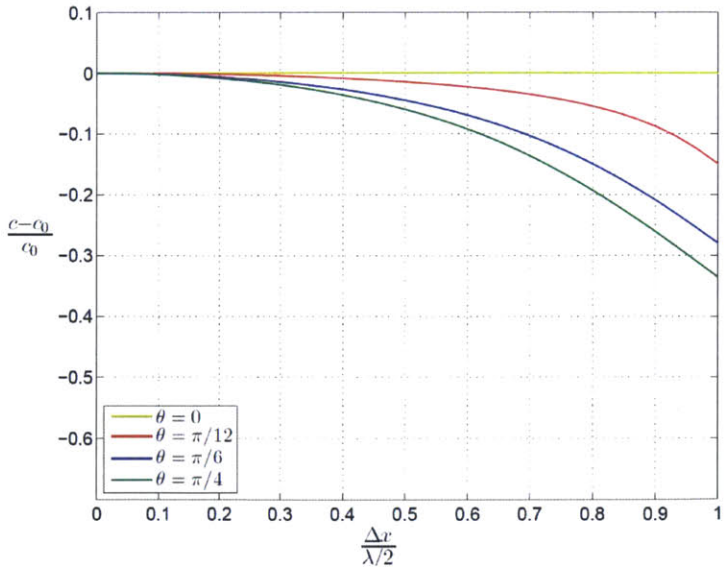

Figure 4-7 **Relative wave speed errors of the central difference method for various propagating angles, using** $\mathrm{CFL} = 1$

4.1.3. Selection of load magnitude at substep

This Section analyses how the proposed time integration scheme interprets external forces defined at discrete time points. For this purpose, Eq. (4.26) is considered, which can be expressed as n (the number of degree of freedom) decoupled equations in the modal basis as

$$\ddot{x} + \omega^2 x = r \,. \tag{4.40}$$

Since the time integration of a coupled system and of the corresponding decoupled system with the same time integration yield the same solution, instead of the time integration on Eq. (4.26), the time integration is considered in n decoupled equations, Eq. (4.40).

After rearranging and taking an integral over the time domain from t_1 to t_2 in Eq. (4.40), we obtain

$$\int_{t_1}^{t_2} \left(r - \omega^2 x \right) dt = \int_{t_1}^{t_2} \ddot{x} \; dt \tag{4.41}$$

or

$$\int_{t_1}^{t_2} \left(r - \omega^2 x \right) dt = \int_{t_1}^{t_2} d\dot{x} \,. \tag{4.42}$$

In the first sub-step, considering the time step from t to $t+p\Delta t$, Eq. (4.42) is approximated, using Eqs. (4.4) and (4.5), as

$$\int_t^{t+p\Delta t}\left(r-\omega^2 x\right)dt\Big|_{\text{1st substep}}=\frac{1}{2}p\Delta t\left({}^t\ddot{x}+{}^{t+p\Delta t}\ddot{x}\right). \tag{4.43}$$

Note that here the integral sign indicates the numerically approximated integration by the time integration scheme. Using the equilibrium, Eq (4.40) at time point t and $t+p\Delta t$, and from the fact that the Eq. (4.42) holds for general loading and trajectory, the approximated numerical impulse is obtained as

$$\int_t^{t+p\Delta t} r\,dt\Big|_{\text{1st substep}}=\frac{1}{2}p\Delta t\left({}^t r+{}^{t+p\Delta t}\hat{r}\right), \tag{4.44}$$

where $\hat{r}$ is the modal load at time $t+p\Delta t$ corresponding to the load $\mathbf{R}$ in Eq. (4.2).

Similarly, the numerically approximated impulse in the second sub-step is obtained as

$$\int_{t+p\Delta t}^{t+\Delta t} r\,dt\Big|_{\text{2nd substep}}=(1-p)\Delta t\left(q_0{}^t r+(q_1+\frac{1}{2})\,{}^{t+p\Delta t}\hat{r}+q_2\,{}^{t+\Delta t}r\right). \tag{4.45}$$

Therefore, from Eqs. (4.44) and (4.45), and using the relations in Eqs. (4.12) and (4.22), the proposed scheme approximates the impulse as

$$\int_t^{t+\Delta t} r\,dt\Big|_{\text{prop. scheme}} = \frac{\Delta t}{2}\left(\frac{-p^2+3p-1}{p}\,{}^{t}r + \frac{1-p}{p}\,{}^{t+p\Delta t}\hat{r} + p\,{}^{t+\Delta t}r\right). \tag{4.46}$$

In general, external loads can be defined/sampled at discrete time points only, and these values can be used for the external forces at the end of each time step in direct time integration methods. If external loads are given at time t and $t+\Delta t$ as ${}^{t}r$ and ${}^{t+\Delta t}r$, then the numerical impulse approximated by the trapezoidal rule gives the most accurate approximation in general. This numerical impulse is accomplished with the proposed method by setting the sub-step load as

$${}^{t+p\Delta t}\hat{r} = (1-p)\,{}^{t}r + p\,{}^{t+\Delta t}r, \tag{4.47}$$

which corresponds to the mean value and integrates the load by the trapezoidal rule over the time step. For smooth loads, the actual value of the load at time $t+p\Delta t$ can also be used. Note that a similar analysis for the Bathe implicit method shows that for rapidly varying loads the mean value of the loads at times t and $t+\Delta t$ is also best used.

Table 4-1 *Step-by-step solution using the proposed method for linear analysis with general loading*

A. *Initial calculation*

6. Form stiffness matrix $\mathbf{K}$, lumped mass matrix $\mathbf{M}$, and damping matrix $\mathbf{C}$
7. Initialize ${}^{0}\mathbf{U}$, ${}^{0}\dot{\mathbf{U}}$ and ${}^{0}\ddot{\mathbf{U}}$.
8. Select time step Δt and p (= 0.54) and calculate integration constants a_n :

$$q_1 = \frac{1-2p}{2p(1-p)};\quad q_2 = \frac{1}{2} - pq_1;\quad q_0 = -q_1 - q_2 + \frac{1}{2};\quad a_0 = p\Delta t;$$

$$a_1 = \frac{1}{2}(p\Delta t)^2;\quad a_2 = \frac{a_0}{2};\quad a_3 = (1-p)\Delta t;\quad a_4 = \frac{1}{2}\left((1-p)\Delta t\right)^2;$$

$$a_5 = q_0 a_3;\quad a_6 = (\frac{1}{2} + q_1)a_3;\quad a_7 = q_2 a_3;$$

B. *For each time step:*

<First sub-step>

5. Calculate displacements and effective loads at time $t + p\Delta t$:

$$ {}^{t+p\Delta t}\mathbf{U} = {}^{t}\mathbf{U} + a_0\,{}^{t}\dot{\mathbf{U}} + a_1\,{}^{t}\ddot{\mathbf{U}} $$

$$ {}^{t+p\Delta t}\hat{\mathbf{R}} = (1-p)\,{}^{t}\mathbf{R} + p\,{}^{t+\Delta t}\mathbf{R} $$

$$ {}^{t+p\Delta t}\hat{\mathbf{R}} = {}^{t+p\Delta t}\hat{\mathbf{R}} - \mathbf{K}\,{}^{t+p\Delta t}\mathbf{U} - \mathbf{C}\left({}^{t}\dot{\mathbf{U}} + a_0\,{}^{t}\ddot{\mathbf{U}}\right) $$

6. Solve for accelerations at time $t + p\Delta t$:

$$ \mathbf{M}\,{}^{t+p\Delta t}\ddot{\mathbf{U}} = {}^{t+p\Delta t}\hat{\mathbf{R}} $$

7. Calculate velocities at time $t + p\Delta t$:

$$ {}^{t+p\Delta t}\dot{\mathbf{U}} = {}^{t}\dot{\mathbf{U}} + a_2\left({}^{t}\ddot{\mathbf{U}} + {}^{t+p\Delta t}\ddot{\mathbf{U}}\right) $$

<Second sub-step>

4. Calculate displacements and effective loads at time $t + \Delta t$:

$$ {}^{t+\Delta t}\mathbf{U} = {}^{t+p\Delta t}\mathbf{U} + a_3\,{}^{t+p\Delta t}\dot{\mathbf{U}} + a_4\,{}^{t+p\Delta t}\ddot{\mathbf{U}} $$

$$ {}^{t+\Delta t}\hat{\mathbf{R}} = {}^{t+\Delta t}\mathbf{R} - \mathbf{K}\,{}^{t+\Delta t}\mathbf{U} - \mathbf{C}\left({}^{t+p\Delta t}\dot{\mathbf{U}} + a_3\,{}^{t+p\Delta t}\ddot{\mathbf{U}}\right) $$

5. Solve for accelerations at time $t + \Delta t$:

$$ \mathbf{M}\,{}^{t+\Delta t}\ddot{\mathbf{U}} = {}^{t+\Delta t}\hat{\mathbf{R}} $$

6. Calculate velocities at time $t + \Delta t$:

$$ {}^{t+\Delta t}\dot{\mathbf{U}} = {}^{t+p\Delta t}\dot{\mathbf{U}} + a_5\,{}^{t}\ddot{\mathbf{U}} + a_6\,{}^{t+p\Delta t}\ddot{\mathbf{U}} + a_7\,{}^{t+\Delta t}\ddot{\mathbf{U}} $$

The resulting procedure of the proposed explicit method for linear systems is summarized in Table 4-1. Note that comparing the number of operations needed per step when damping is neglected, that in using the proposed scheme, as in the central difference method, evaluation of the elastic nodal forces corresponding to given displacements requires the largest proportion of the computational cost. Hence, using the CFL number = 1.85 for the proposed scheme, the computational effort is near that of using the central difference method.

4.2. Wave propagation solutions

In this Section, the solutions of some wave propagation problems using the proposed scheme are presented. A 2-D transient scalar wave propagation and then a Lamb problem with two types of external loadings are considered.

4.2.1. 2D scalar wave propagation

Considering a pre-stressed membrane for which the governing equation is

$$\frac{\partial^2 u}{\partial x^2} + \frac{\partial^2 u}{\partial y^2} + F(0,0,t) = \frac{1}{c_0^2}\frac{\partial^2 u}{\partial t^2}, \tag{4.47}$$

where u is the transverse displacement and c_0 is the wave velocity, here set to 1.0, the load is given as

$$F(0,0,t) = 4\left(1-(2t-1)^2\right)H(1-t) \quad , \quad t>0\,, \tag{4.48}$$

where H is the Heaviside step function. Only the domain $[0,11] \times [0,11]$ is discretized due to symmetry, and no absorbing boundary conditions are employed since the wave does not propagate to the boundary for the solution time considered (Fig. 4-8).

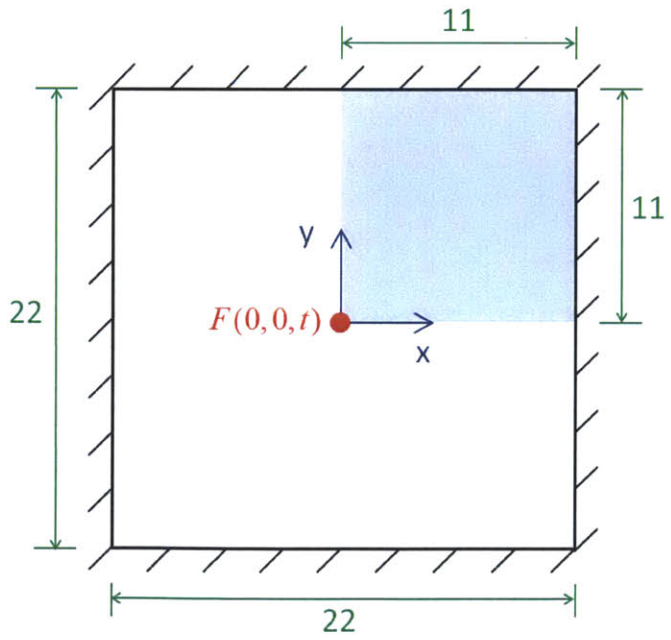

Figure 4-8 **Pre-stressed membrane problem, $c_0 = 1$, initial displacement and velocity are zero, computational domain is shaded**

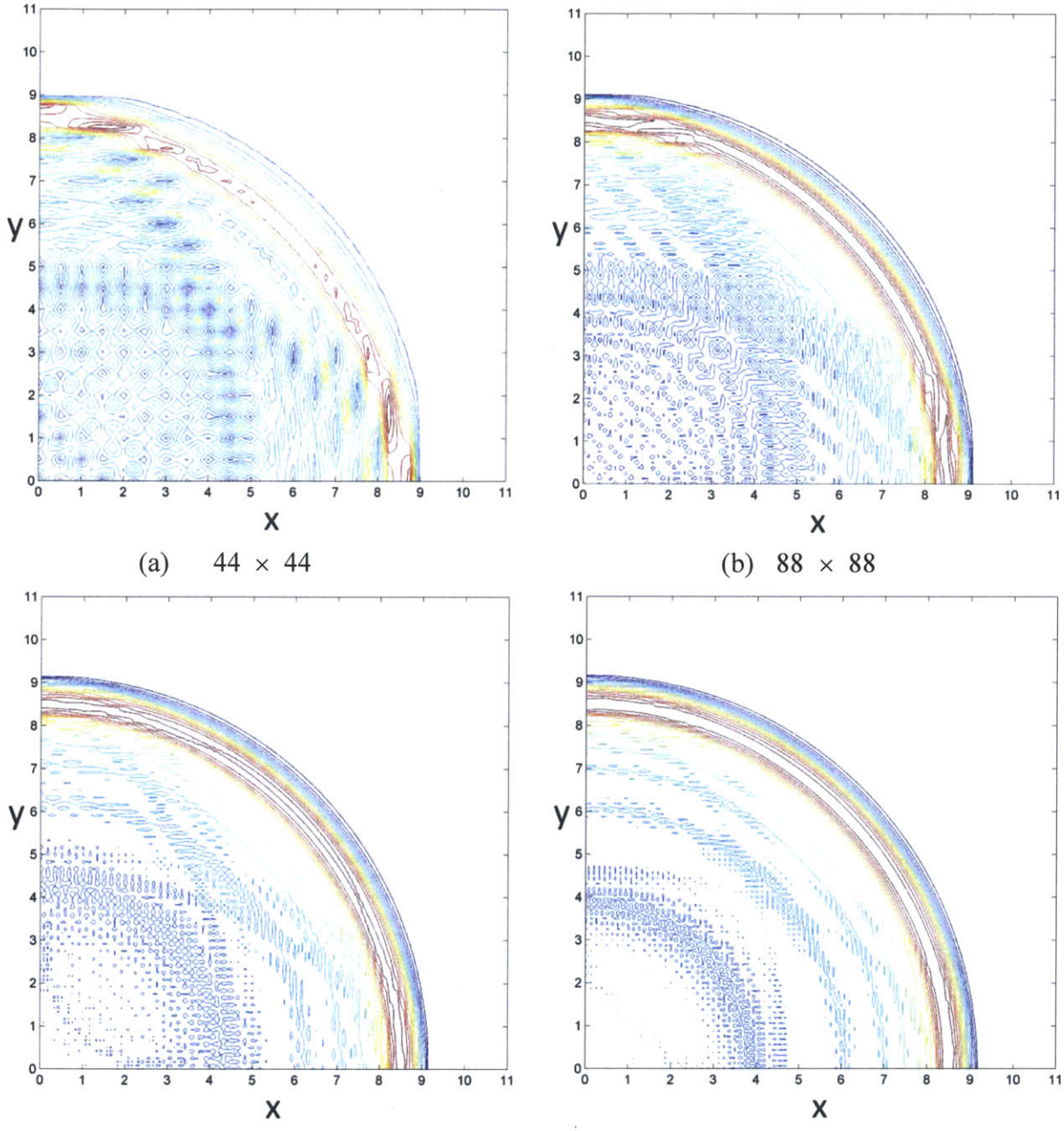

(a) 44 × 44

(b) 88 × 88

(c) 132 × 132

(d) 176 × 176

Figure 4-9 **Snapshots of displacements at $t = 9.25$, Central Difference method, CFL = 1**

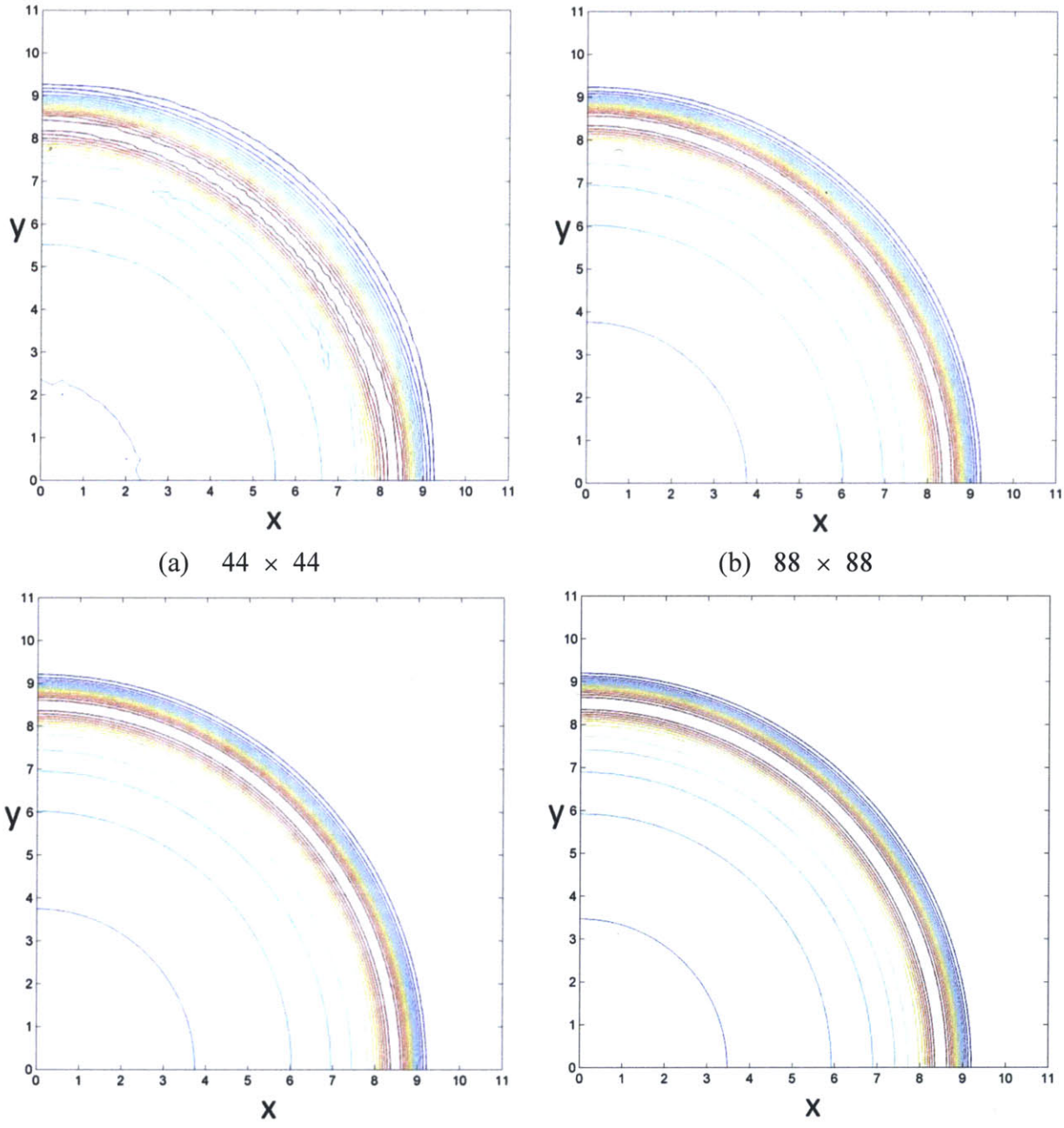

(a) 44 × 44

(b) 88 × 88

(c) 132 × 132

(d) 176 × 176

Figure 4-10 **Snapshots of displacements at** $t = 9.25$**, Proposed method, CFL = 1.85,** $p = 0.54$

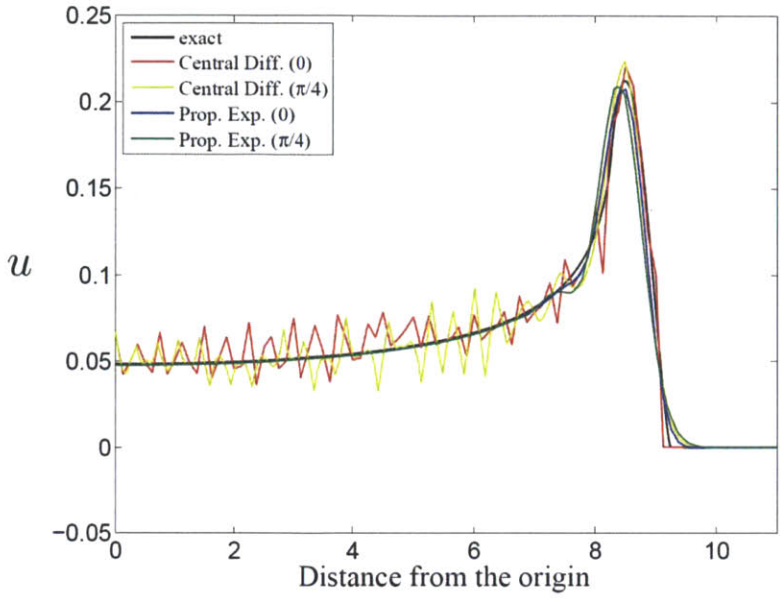

Figure 4-11 **Displacement variations along the various propagating angles, at time** $t = 9.25$, **88 × 88 element mesh**

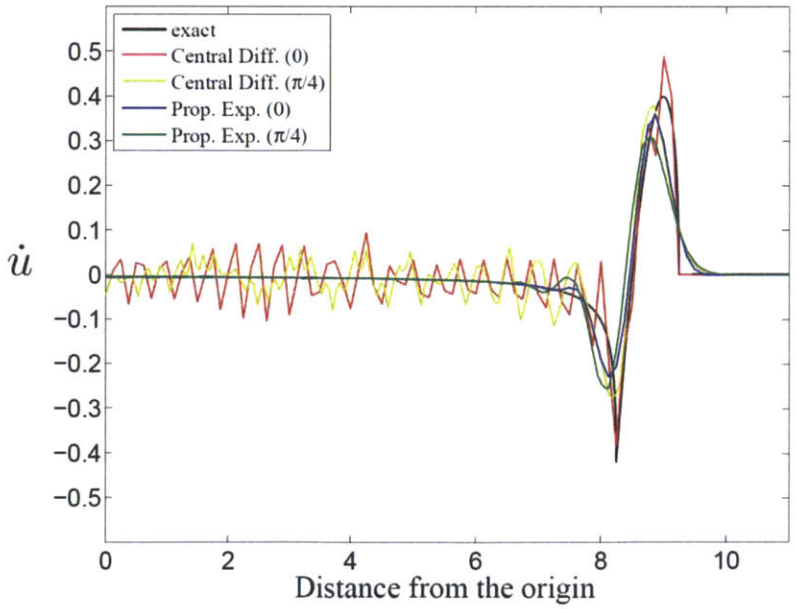

Figure 4-12 **Velocity variations along the various propagating angles, at time** $t = 9.25$, **88 × 88 element mesh**

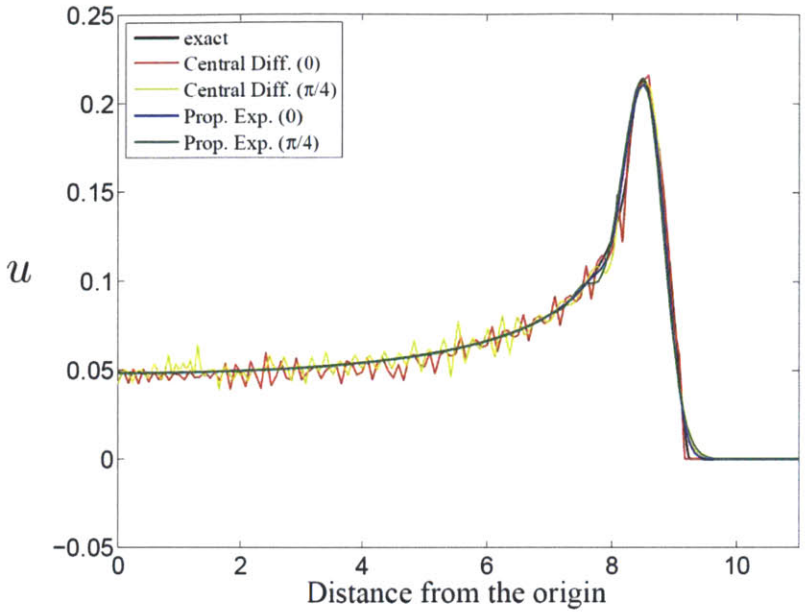

Figure 4-13 **Displacement variations along the various propagating angles, at time** $t = 9.25$, **132** $\times$ **132 element mesh**

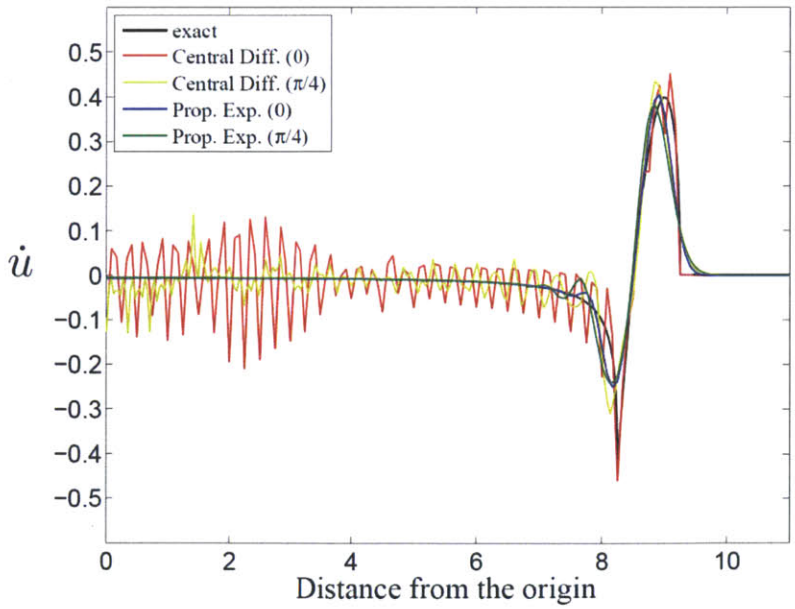

Figure 4-14 **Velocity variations along the various propagating angles, at time** $t = 9.25$, **132** $\times$ **132 element mesh**

The CFL numbers used for the proposed explicit method and the central difference method are 1.85 and 1, respectively. In the calculation of the CFL numbers, to satisfy the stability criteria in each case, the length of the sides of the elements is used as the fundamental length.

Snapshots of the solution variable u, calculated using the central difference method and the proposed scheme at $t = 9.25$ for various meshes are shown in Figs. 4-9 and 4-10. It is observed that, using a coarse mesh, both methods give spurious oscillations. The solution accuracy of the central difference method is still not good with the 176×176 element mesh; however, the proposed method gives a reasonably accurate solution using the 88×88 element mesh.

The numerical results at angles 0 and $\pi/4$ at time $t = 9.25$ using the 88×88 and 132×132 meshes are compared with the corresponding analytical solution in Figs. 4-11 to 4-14. Noticeable spurious oscillations are presented in the solution of the central difference method. The solution for u using the proposed method is reasonably accurate using either mesh; however, a significant solution error is seen in the peak value of $\dot{u}$ when using the 88×88 mesh. Also, at the angle $\pi/4$, solution errors for the response are large, and these are well explained given Figs. 4-6 and 4-7.

Numerical results indicate that, while the proposed method significantly improves the

solution, a high accuracy in the prediction of the velocity requires $\Delta x/(\lambda/2) \leq 0.2$. In fact, the proposed explicit method behaves quite similar to the Bathe implicit method, while the central difference method behaves similar to the trapezoidal rule [45].

4.2.2. Wave propagations in a semi-infinite elastic domain

This Section considers a Lamb problem, where waves are propagating in a semi-infinite elastic domain in plane strain conditions, as described in Fig. 4-15. Here, the P-wave velocity = 3200 m/s, S-wave velocity = 1848 m/s, and the Rayleigh wave velocity = 1671 m/s. No absorbing boundary conditions are employed since the time duration for computing the waves is 0.999 s so that the P-wave does not reach the outer boundaries.

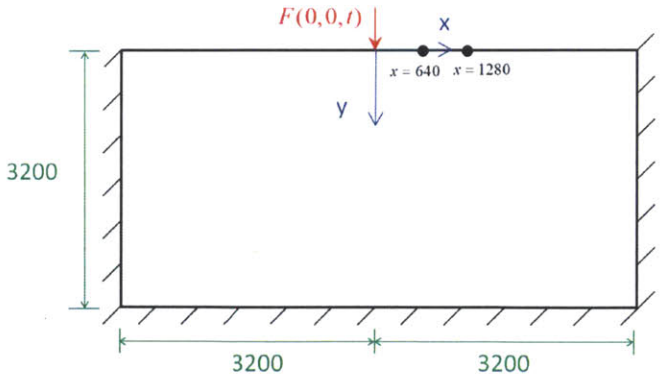

Figure 4-15 **A Lamb problem.** $V_P = 3200$, $V_S = 1848$, $V_{\text{Rayleigh}} = 1671$; **two receivers are placed at** $x = 640$ **and** $x = 1280$; **using symmetry only the right side of the domain is modeled**

The CFL numbers used for the proposed explicit method and the central difference method are 1.85 and 1, respectively. In the calculation of the CFL numbers, the length of the sides of the elements is used as the fundamental length, and the fastest wave, the P-wave, is used to satisfy the stability condition.

First, a Ricker wavelet line force is considered which is defined as

$$F(0,0,t) = -10^6 \times \left(1 - 2\pi^2 \hat{f}^2 (t - t_0)^2\right) \exp(-\pi^2 \hat{f}^2 (t - t_0)^2), \quad t > 0 \qquad (4.49)$$

with the frequency $\hat{f} = 12.5\,\text{Hz}$ and $t_0 = 0.1\,\text{s}$. Only the right side of the domain in Fig. 4-15 is meshed using 1280×640 4-node elements of side lengths $\Delta x = \Delta y = 5\,m$ due to the symmetry. Two observers at $x = 640\,m$ and $x = 1280\,m$ from the source measure the calculated displacements, and the results are shown in Fig. 4-16. The analytical solution and the numerical solutions using either the proposed method or the central difference method are in good agreement, as expected.

Next, the line force is considered, defined as

$$F(0,0,t) = 10^6 \times \left[H(0.15 - t) - 3H(0.1 - t) + 3H(0.05 - t)\right] \quad , \quad t > 0. \qquad (4.50)$$

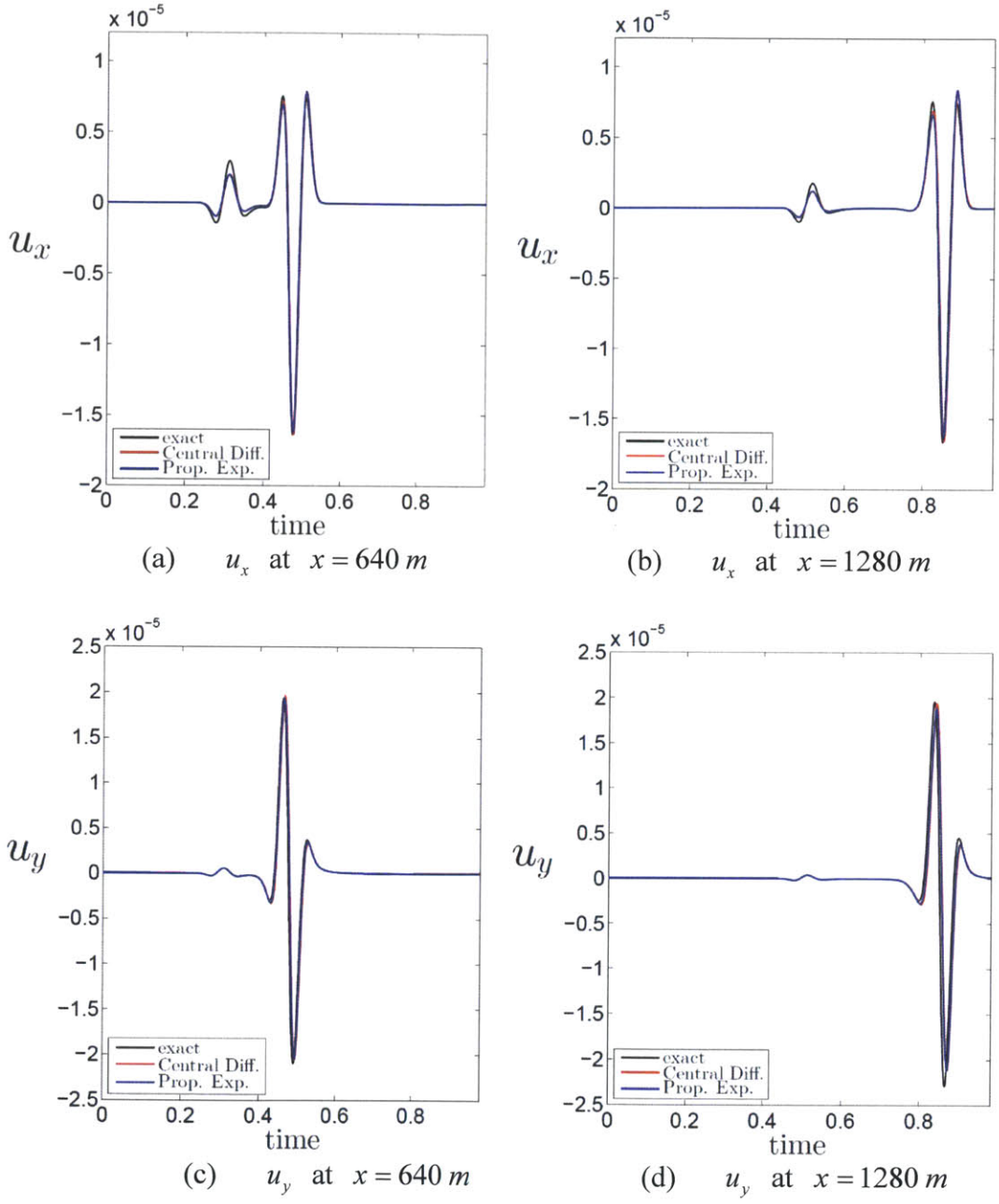

Figure 4-16 **Time history of displacement variations in x-direction and y-direction at the two receivers on the surface; Ricker wavelet line load**

The applied line load consists of three step functions; hence, many wave modes are excited, which renders the problem more difficult to solve. The computational domain is now meshed with 3200×1600 4-node elements of side lengths $\Delta x = \Delta y = 2\,m$. The displacements at the two receivers are shown in Fig. 4-18. While both time integration methods show spurious oscillations, the predicted response using the proposed method is remarkably more accurate.

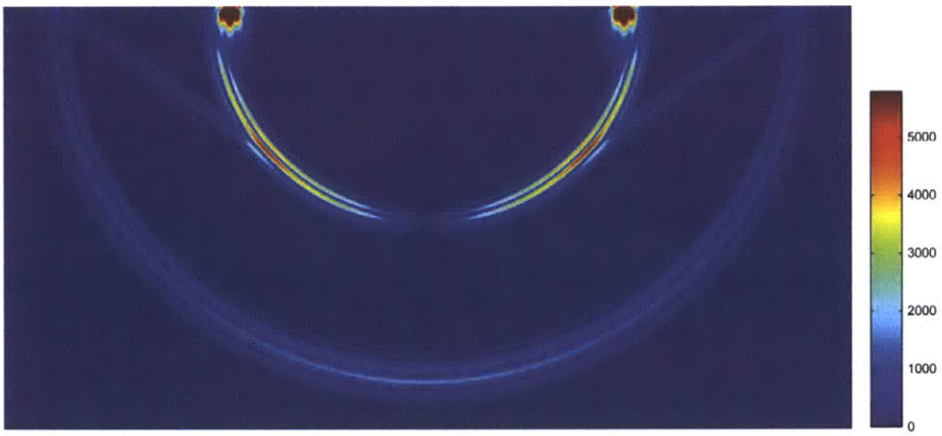

(a) Central difference method

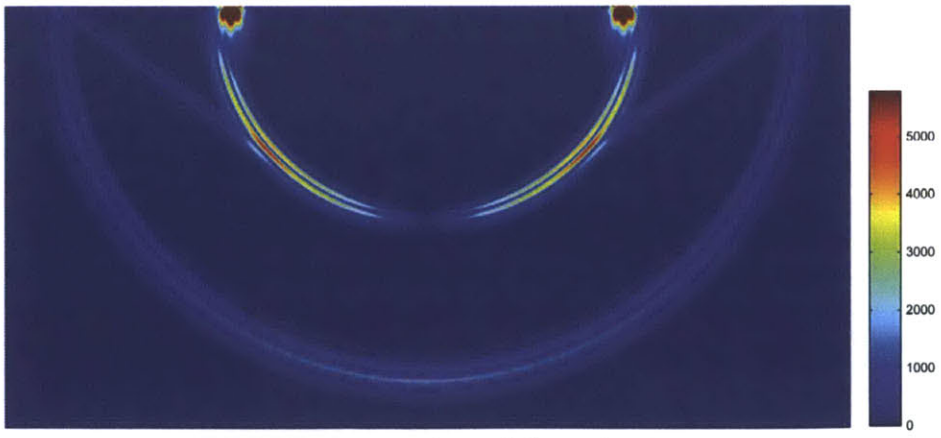

b) Proposed explicit method

Figure 4-17 **Snapshots of von Mises stress at $t = 0.9828\,s$; Ricker wavelet line load**

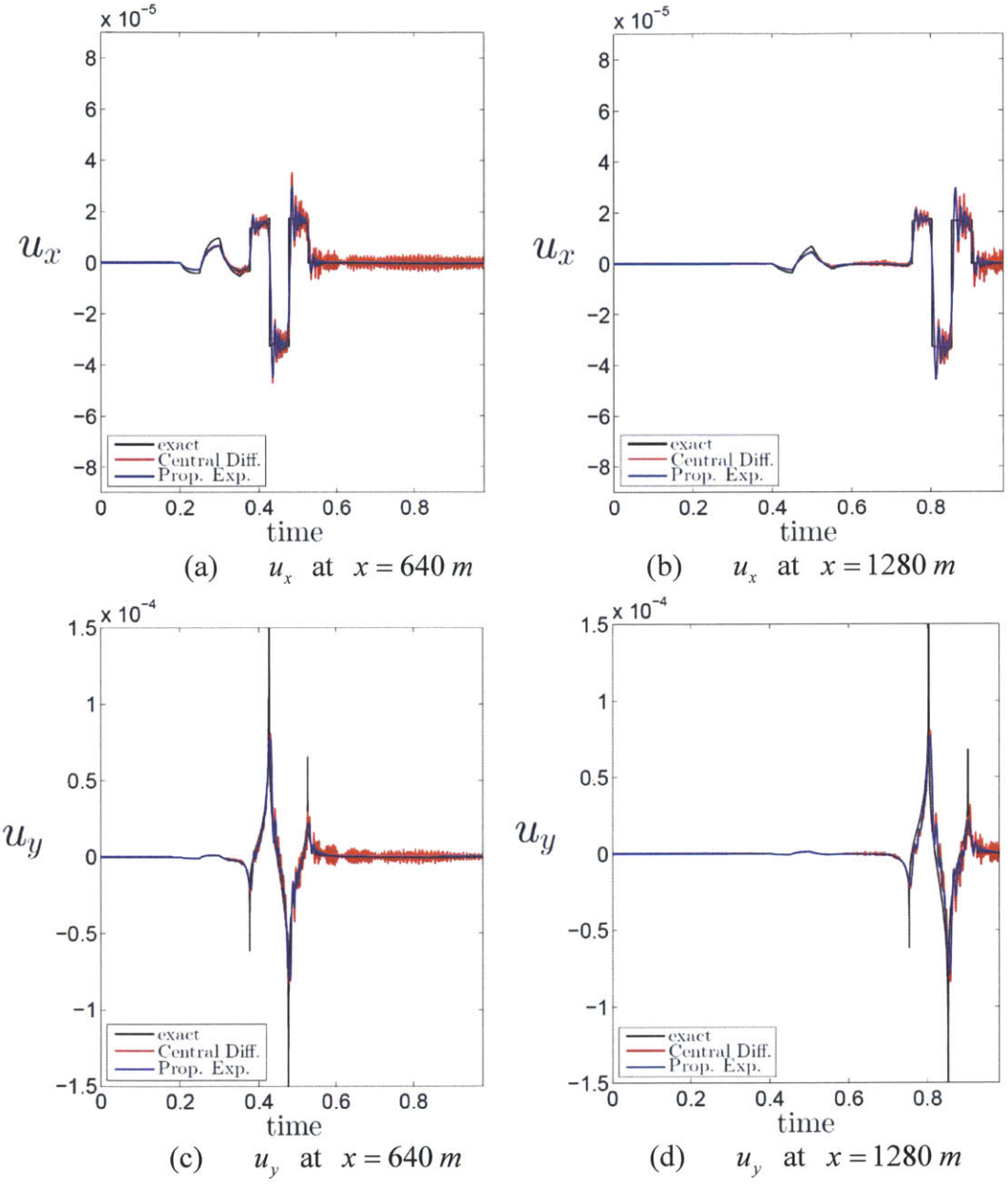

Figure 4-18 **Time history of displacement variations in x-direction and y-direction at the two receivers on the surface; line load of step functions**

The predicted stress wave fields show the difference in the solution accuracy more clearly, as shown in Fig. 4-19. The proposed method provides the predicted stress waves very accurately, while the solution using the central difference method shows undesirable spurious oscillations in various areas.

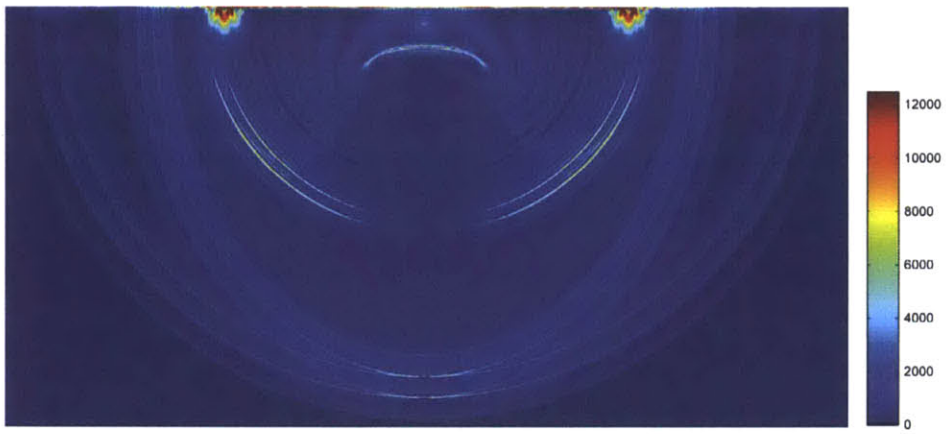

(a) Central difference m-ethod

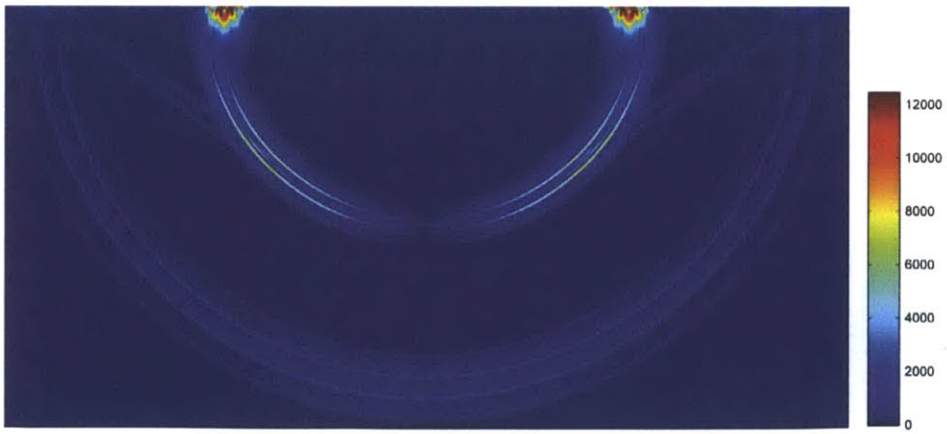

b) Proposed explicit method

Figure 4-19 **Snapshots of von Mises stress at** $t = 0.9828\ s$ **; line load of step functions**

4.3. Concluding Remarks

In this Chapter, an explicit time integration method for the analysis of wave propagations was proposed. We first focused on formulating the method to significantly improve the solution using its property of suppressing undesirable spurious oscillations while maintaining high accuracy for low frequency responses. In addition, to minimize the additional computational cost, the maximization of the bifurcation limit has been considered as a critical design requirement. The characteristics of the proposed explicit method were analysed, with emphasis on the selection of the CFL number for optimal accuracy.

The performance of the proposed method in solving wave propagation problems was demonstrated relative to the widely used central difference method by solving numerical examples. The proposed explicit method provides significantly more accurate solutions than the central difference method by calculating the participating wave modes accurately, so that the dispersion errors in the total solution are reasonably small. As in the Bathe method, the wave modes that cannot be spatially represented are effectively discarded and, therefore, do not result in the spurious oscillations that are found when using the central difference method and the trapezoidal rule. In addition, the load at the sub-step is used in such a way that the numerical impulse from the external load is well approximated and, thus, the solution accuracy is further improved.

To solve a wave propagation problem, a good spatial discretization is also important. In this Chapter, only the linear element in uniform meshes is considered in order to focus on the basic characteristics of the time integration scheme. Theoretical and numerical studies of the behavior of the proposed method when using higher-order element discretizations and distorted meshes would be of value.

Chapter 5

Conclusions

The present thesis first presented the capabilities of the Bathe method with some insight into the use of the time integration method for effective solutions in structural dynamics and wave propagations.

The Bathe method has resulted in remarkably accurate solutions by giving responses similar to a mode superposition analysis in both structural dynamics and wave propagation problems. In particular, the ability of this scheme to practically eliminate high frequency modes that cannot be spatially resolved and to accurately integrate those modes that can be spatially resolved, results in relatively small dispersion error. This thesis focuses on the linear analysis of structural systems; nevertheless, the conclusions reached are also valid in nonlinear analysis.

With the experience and knowledge from the analysis of the Bathe method, a new explicit time integration method was proposed for the analysis of wave propagation problems. The scheme was formulated using a sub-step within a time step to achieve desired numerical damping to suppress undesirable spurious oscillations of high frequencies. The load at the sub-step is chosen for good accuracy. With the optimal CFL number of 1.85, the method uses about 10% more solution effort than the standard central difference scheme while

significantly improving the solution accuracy and allowing direct inclusion of a non-diagonal damping matrix.

Regarding future research, the possible usage of the Bathe method and the proposed explicit method with higher-order element discretizations and distorted meshes would be useful areas of study for achieving more effective solutions.

References

[1] K. J. Bathe, *Finite Element Procedures*, Prentice Hall, 1996.

[2] W. L. Wood, *Practical Time-Stepping Schemes*, Claredon Press, Oxford, 1990.

[3] J. Chung and J. M. Lee, A new family of explicit time integration methods for linear and non-linear structural dynamics, INT J NUMER METH ENG, 37, 3961-3976, 1994.

[4] G. M. Hulbert and J. Chung, Explicit time integration algorithms for structural dynamics with optimal numerical dissipation, COMPUT METHOD APPL M, 137, 175-188, 1996.

[5] S. Y. Chang and W.I. Liao, An unconditionally stable explicit method for structural dynamics, J EARTHQAUKE ENG, 9, 349-370, 2005.

[6] I. Babuska, F. Ihlenburg, T. Strouboulis and S. K. Gangaraj, A posteriori error estimation for finite element solutions of Helmholtz' equation .2. Estimation of the pollution error, INT J NUMER METH ENG , 40, 3883 – 3900, 1997.

[7] A. Deraemaeker, I. Babuska and P. Bouillard, Dispersion and pollution of the FEM solution for the Helmholtz equation in one, two and three dimensions, INT J NUMER METH ENG, 46, 471-499, 1999.

[8] I. M. Babuska and S. A. Sauter, Is the pollution effect of the FEM avoidable for the Helmholtz equation considering high wave numbers?, SIAM REV, 42, 451-484, 2000.

[9] G. Bao, G. W. Wei and S. Zhao, Numerical solution of the Helmholtz equation with high wavenumbers, INT J NUMER METH ENG, 59, 389-408, 2004.

[10] R. C. Y. Chin, Dispersion and Gibbs phenomenon associated with difference approximations to initial boundary-value problems for hyperbolic equations, J COMPUT PHYS, 18, 233-247, 1975.

[11] J. P. Boris and D. L. Book, Flux-corrected transport .3. Minimal-error FCT algorithms, J COMPUT PHYS, 20, 397-431, 1976.

[12] T. Belytschko and R. Mullen, On dispersive properties of finite element solutions, in: J. Miklowitz and J. D. Achenbach, eds., *Modern Problems in Elastic Wave Propagation*, John Wiley, 67-82, 1978.

[13] Y. C . Wang, V. Murti and S. Valliappan, Assessment of the accuracy of the Newmark method in transient analysis of wave-propagation problems, EARTHQUAKE ENG STRUCT, 21, 987-1004, 1992.

[14] D. Gottlieb and S. A. Orszag, *Numerical Analysis of Spectral Methods: Theory and Applications*, Capital City Press, 1993.

[15] G. Seriani and E. Priolo, Spectral element method for acoustic wave simulation in heterogeneous media, FINITE ELEM ANAL DES, 16, 337-348, 1994.

[16] E. Faccioli, F. Maggio, R. Paolucci and A. Quarteroni, 2D and 3D elastic wave propagation by a pseudo-spectral domain decomposition method, J SEISMOL, 1, 237-251, 1997.

[17] D. Komatitsch and J. Tromp, Introduction to the spectral element method for three-dimensional seismic wave propagation, GEOPHYS J INT, 139, 806-822, 1999.

[18] D. R. Mahapatra and S. Gopalakrishnan, A spectral finite element model for analysis of axial–flexural–shear coupled wave propagation in laminated composite beams, COMPOS STRUCT, 59, 67-88, 2003.

[19] G. E. Karniadakis and S. J. Sherwin, *Spectral/hp Element Methods for Computational Fluid Dynamics,* Oxford University Press, 2005.

[20] P. Gamallo and R. J. Astley, The partition of unity finite element method for short wave acoustic propagation on non-uniform potential flows, INT J NUMER METH ENG, 65, 425-444, 2006.

[21] T. Huttunen, P. Gamallo and R. J. Astley, Comparison of two wave element methods for the Helmholtz problem, COMMUN NUMER METH EN, 25, 35-52, 2009.

[22] H. Kohno, K. J. Bathe and J. C. Wright, A finite element procedure for multiscale wave equations with application to plasma waves, COMPUT STRUCT, 88, 87-94, 2010.

[23] S. Ham and K. J. Bathe, A finite element method enriched for wave propagation problems, COMPUT STRUCT, 94-95, 1-12, 2012.

[24] J. Kim and K.J. Bathe, The finite element method enriched by interpolation covers, COMPUT STRUCT, 116, 35-49, 2013.

[25] R. D. Krieg and S. W. Key, Transient shell response by numerical time integration, INT J NUMER METH ENG, 7, 273-286, 1973.

[26] R. Mullen and T. Belytschko, Dispersion analysis of finite element semidiscretizations of the two-dimensional wave equation, INT J NUMER METH ENG, 18, 11-29, 1982.

[27] M. G. G. Foreman, A two-dimensional dispersion analysis of selected methods for solving the linearized shallow-water equations, J COMPUT PHYS, 56, 287-323, 1984.

[28] L. Jiang and R. J. Rogers, Effects of spatial discretization on dispersion and spurious oscillations in elastic wave-propagation, INT J NUMER METH ENG, 29, 1205-1218, 1990.

[29] H. P. Cherukuri, Dispersion analysis of numerical approximations to plane wave motions in an isotropic elastic solid, COMPUT MECH, 25, 317-328, 2000.

[30] B. Yue and M. N. Guddati, Dispersion-reducing finite elements for transient acoustics, J ACOUST SOC AM, 118, 2132-2141, 2005.

[31] K. J. Marfurt, Accuracy of finite-difference and finite-element modeling of the scalar and elastic wave-equations, GEOPHYSICS, 49, 533-549, 1984.

[32] M. A. Christon, The influence of the mass matrix on the dispersive nature of the semi-discrete, second-order wave equation, COMPUT METHOD APPL M, 173, 147-166, 1999.

[33] S. Krenk, Dispersion-corrected explicit integration of the wave equation, COMPUT METHOD APPL M, 191, 975-987, 2001.

[34] G. Seriani and S. P. Oliveira, Optimal blended spectral-element operators for acoustic wave modeling, GEOPHYSICS, 72, 95-106, 2007.

[35] A. V. Idesman, M. Schmidt and J. R. Foley, Accurate finite element modeling of linear elastodynamics problems with the reduced dispersion error, COMPUT MECH, 47, 555-572, 2011.

[36] M. N. Guddati and B. Yue, Modified integration rules for reducing dispersion error in finite element methods, COMPUT METHOD APPL M, 193, 275-287, 2004.

[37] N. Holmes and T. Belytschko, Postprocessing of finite element transient response calculations by digital filters, COMPUT STRUCT, 6, 211-216, 1976.

[38] A. Idesman, H. Samajder, E. Aulisa and P. Seshaiyer, Benchmark problems for wave propagation in elastic materials, COMPUT MECH, 43, 797-814, 2009.

[39] D. Kuhl and M. A. Crisfield, Energy-conserving and decaying algorithms in non-linear structural dynamics, INT J NUMER METH ENG, 45, 569-599, 1999.

[40] T. C. Fung, Numerical dissipation in time-step integration algorithms for structural dynamic analysis, PROG STRUCT ENG MAT, 5, 167-180, 2003.

[41] J. Chung and G. M. Hulbert, A time integration algorithm for structural dynamics with improved numerical dissipation: the generalized alpha method, J APPL MECH TRANS ASME, 60, 371–5, 1993.

[42] K. J. Bathe and M. M. I. Baig, On a composite implicit time integration procedure for nonlinear dynamics, COMPUT STRUCT, 83, 2513 – 2524, 2005.

[43] K. J. Bathe, Conserving energy and momentum in nonlinear dynamics: A simple implicit time integration scheme, COMPUT STRUCT, 85, 437-445, 2007.

[44] K. J. Bathe and G. Noh, Insight into an implicit time integration scheme for structural dynamics, COMPUT STRUCT, 98-99, 1-6, 2012.

[45] G. Noh, S. Ham and K. J. Bathe, Performance of an implicit time integration scheme in the analysis of wave propagations, COMPUT STRUCT, 123, 93-105, 2013.

[46] Z. Kazanci and K. J. Bathe, Crushing and crashing of tubes with implicit time integration, INT J IMPACT ENG, 42, 80-88, 2012.

[47] G.Dahlquist, A special stability problem for linear multistep methods, BIT, 3, 27-43, 1963.

[48] R. D. Krieg, Unconditional stability in numerical time integration methods, J APPL MATH, 40, 417-421, 1973.

[49] G. B. Warburton, Some recent advances in structural vibration, VIBR ENG STRUCT, I. A. Brebbia and S. A. Orszag (eds.), Lecture Notes in Engineering, Springer, Berlin, 10, 215-224, 1963.

[50] G. D. Hahn, A modified Euler method for dynamic analyses, INT J NUMER METH ENG, 32, 943-955, 1991.

[51] L. Maheo, V. Grolleau and G. Rio, Numerical damping of spurious oscillations: a comparison between the bulk viscosity methods and the explicit dissipative Tchamwa-Wielgosz scheme, COMPUT MECH, 51, 109-128, 2013.

[52] N. Newmark, A method of computation for structural dynamics, J ENG MECH DIV ASCE, 85, 67-94, 1959.

[53] W. Zhai, Two simple fast integration methods for large scale dynamic problems in engineering, INT J NUMER METH ENG, 85, 67-94, 1959.

[54] B. Tchamwa, T. Conway and C. Wielgosz , An accurate explicit direct time integration method for computational structural dynamics, ASME-PUBLICATIONS-PVP, 398, 77-84, 1999.

[55] G. Rio, A. Soive and V. Grolleau, Comparative study of numerical explicit time integration algorithms, ADV ENG SOFTW, 35, 252-265, 2005.

[56] N. Nsiampa, J. Ponthot, L. Noels, Comparative study of numerical explicit schemes for impact problems., INT J IMPACT ENG, 35, 1688-1694, 2008.

[57] G. Noh and K. J. Bathe, An explicit time integration scheme for the analysis of wave propagations, COMPUT STRUCT, in press.

[58] E. L. Wilson, I. Farhoomand and K. J. Bathe, Nonlinear dynamic analysis of complex structures, EARTHQUAKE ENG STRUCT, 1, 241-252, 1973.

[59] K. J. Bathe and E. L. Wilson, Stability and accuracy analysis of direct integration methods, EARTHQUAKE ENG STRUCT, 1, 283-291, 1973.

[60] K. J. Bathe, On reliable finite element methods for extreme loading conditions. Chapter in *Extreme Man-made and Natural Hazards in Dynamics of Structures*, A. Ibrahimbegovic and I. Kozar, eds., Springer, 2007.

[61] D. J. Payen and K. J. Bathe, A stress improvement procedure, COMPUT STRUCT, 112-113, 311-326, 2012.

Appendix

A.1 Effect of splitting ratio, γ in the Bathe method

In this Section, to study the effect of splitting ratio, γ on the stability and accuracy characteristics, we obtain the spectral radii curves, and the period elongations and the amplitude decays for various γ. The Bathe method uses the following relations with equilibrium at time $t+\gamma\Delta t$ and at $t+\Delta t$.

$$ {}^{t+\gamma\Delta t}\underline{\dot{\mathrm{U}}} = {}^{t}\underline{\dot{\mathrm{U}}} + \frac{{}^{t}\underline{\ddot{\mathrm{U}}} + {}^{t+\gamma\Delta t}\underline{\ddot{\mathrm{U}}}}{2}\gamma\Delta t \tag{A1.1} $$

$$ {}^{t+\gamma\Delta t}\underline{\mathrm{U}} = {}^{t}\underline{\mathrm{U}} + \frac{{}^{t}\underline{\dot{\mathrm{U}}} + {}^{t+\gamma\Delta t}\underline{\dot{\mathrm{U}}}}{2}\gamma\Delta t \tag{A1.2} $$

$$ {}^{t+\Delta t}\underline{\dot{\mathrm{U}}} = c_1\,{}^{t}\underline{\mathrm{U}} + c_2\,{}^{t+\gamma\Delta t}\underline{\mathrm{U}} + c_3\,{}^{t+\Delta t}\underline{\mathrm{U}} \tag{A1.3} $$

$$ {}^{t+\Delta t}\underline{\ddot{\mathrm{U}}} = c_1\,{}^{t}\underline{\dot{\mathrm{U}}} + c_2\,{}^{t+\gamma\Delta t}\underline{\dot{\mathrm{U}}} + c_3\,{}^{t+\Delta t}\underline{\dot{\mathrm{U}}} \tag{A1.4} $$

where

$$ c_1 = \frac{1-\gamma}{\Delta t\,\gamma}, \quad c_2 = \frac{-1}{(1-\gamma)\,\gamma\,\Delta t}, \quad c_3 = \frac{2-\gamma}{(1-\gamma)\,\Delta t} \tag{A1.5} $$

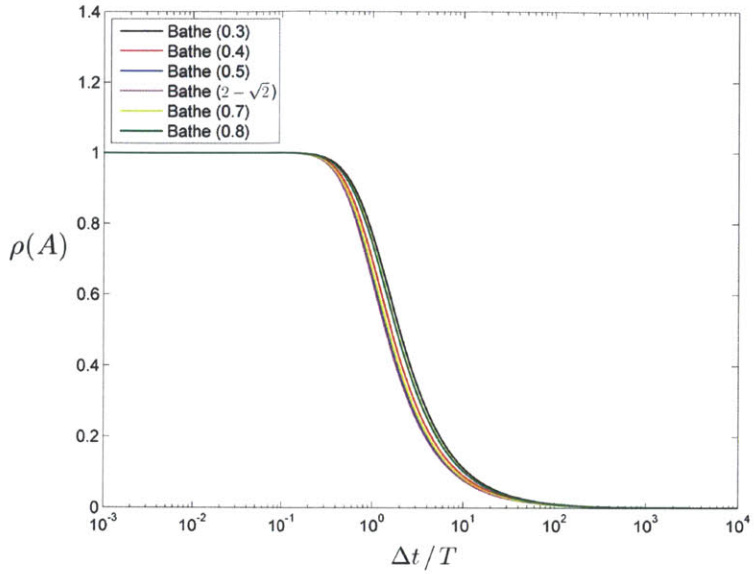

Figure A1-1 **Spectral radii of approximation operator of the Bathe methods. The fraction factor γ is given in the parentheses.**

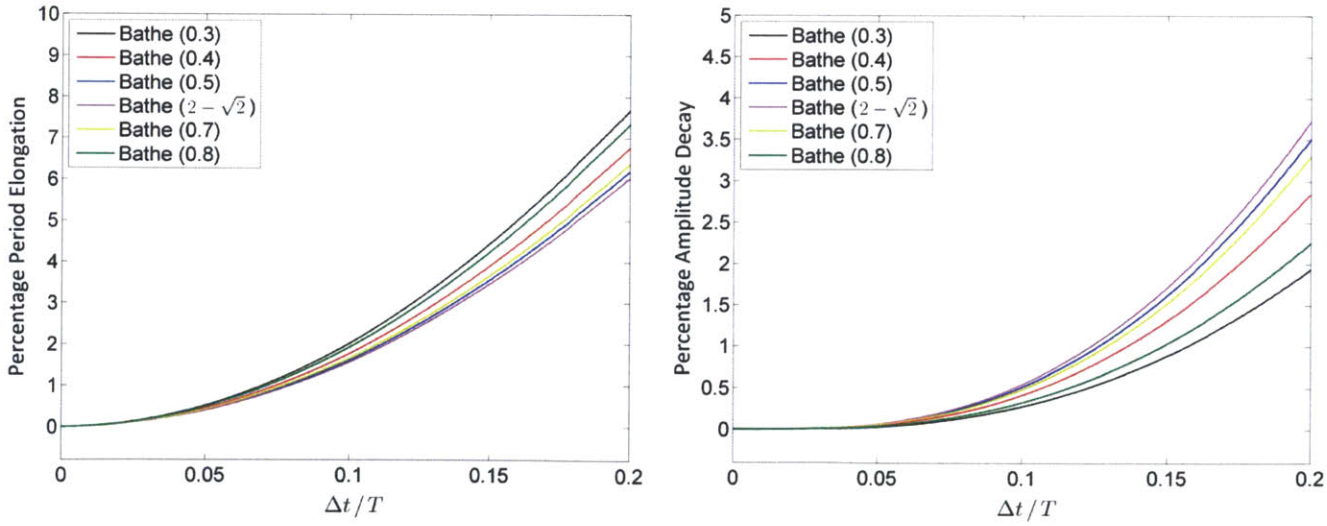

Figure A1-2 **Percentage period elongations and percentage amplitude decays of the Bathe methods. The fraction factor γ is given in the parentheses.**

With any given γ value, the Bathe method shows sufficiently good stability and accuracy characteristics. Interestingly, as γ goes to $2-\sqrt{2}$, the method maximizes the amplitude decays and minimizes the period elongation. In the spectral radii curves, we see that as γ goes to $2-\sqrt{2}$, the curve drops fast.

A.2 On the solution of the Bathe method for a model problem

A.2.1 Desired solution : mode 1 + static correction

The desired solution becomes

$$ {}_{d}u_2 = \frac{k_2}{k_1}\,(x_1 + {}_{S}x_1) + {}_{S}x_2 \tag{A2.1} $$

$$ {}_{d}u_3 = x_1 + {}_{S}x_1 - \frac{k_2}{k_1}\,{}_{S}x_2 \tag{A2.2} $$

where ${}^{S}x_2$ indicates the static correction and it can be obtained as

$$ \underline{K}\;{}_{S}\underline{U} = \Delta\underline{R} = \underline{R} - r_1\,\underline{M}\,\underline{\phi}_1 \tag{A2.3} $$

$$ \underline{\Phi}^T\,\underline{K}\,\underline{\Phi}\;{}_{S}\underline{X} = \underline{\Phi}^T\,\underline{R} - \underline{\Phi}^T\,(r_1\,\underline{M}\,\underline{\phi_1}) \tag{A2.4} $$

where $r_1 \simeq k_2\,\sin\omega_p t$. Eq. (2.16) gives

$$ \begin{bmatrix} \omega_1^2 & 0 \\ 0 & \omega_2^2 \end{bmatrix} \begin{bmatrix} {}_{S}x_1 \\ {}_{S}x_2 \end{bmatrix} \simeq \begin{bmatrix} -(k_2^3/k_1^2)\,\sin\omega_p t \\ k_1\,\sin\omega_p t \end{bmatrix} \simeq \begin{bmatrix} 0 \\ k_1\,\sin\omega_p t \end{bmatrix} \tag{A2.5} $$

Therefore,

$$ {}_{S}x_1 \simeq 0 \tag{A2.6} $$

$$ {}_{S}x_2 \simeq \sin \omega_p t \tag{A2.7} $$

$$ {}_{d}u_2 \simeq \frac{k_2}{k_1} x_1 + \sin \omega_p t \tag{A2.8} $$

$$ {}_{d}u_3 \simeq x_1 - \frac{k_2}{k_1} \sin \omega_p t \tag{A2.9} $$

and the velocities and the accelerations are obtained by taking time derivative of above equations.

A.2.2 Solution from the Bathe method

In modal basis, the relations in the Bathe method are

$$ {}^{t+\Delta t/2}\dot{x} = {}^{t}\dot{x} + \frac{\Delta t}{4} ({}^{t}\ddot{x} + {}^{t+\Delta t/2}\ddot{x}) \tag{A2.10} $$

$$ {}^{t+\Delta t/2}x = {}^{t}x + \frac{\Delta t}{4} ({}^{t}\dot{x} + {}^{t+\Delta t/2}\dot{x}) \tag{A2.11} $$

$$ {}^{t+\Delta t}\dot{x} = \frac{1}{\Delta t} {}^{t}x - \frac{4}{\Delta t} {}^{t+\Delta t/2}x + \frac{3}{\Delta t} {}^{t+\Delta t}x \tag{A2.12} $$

$$^{t+\Delta t}\ddot{x} = \frac{1}{\Delta t}\,{}^{t}\dot{x} - \frac{4}{\Delta t}\,{}^{t+\Delta t/2}\dot{x} + \frac{3}{\Delta t}\,{}^{t+\Delta t}\dot{x} \qquad \text{(A2.13)}$$

and for each mode shape, the structural dynamic equations at $t + \Delta t/2$ and $t + \Delta t$ are

$$^{t+\Delta t/2}\ddot{x} + \omega^2\,{}^{t+\Delta t/2}x = {}^{t+\Delta t/2}r \qquad \text{(A2.14)}$$

$$^{t+\Delta t}\ddot{x} + \omega^2\,{}^{t+\Delta t}x = {}^{t+\Delta t}r \qquad \text{(A2.15)}$$

Using Eqs. (A2.10) ~ (A2.15), we obtain the solutions of the Bathe method for i-th mode shape as

$$^{t+\Delta t}_{BM}x = \frac{1}{\left(16 + w^2\Delta t^2\right)\left(9 + w^2\Delta t^2\right)}\left({}^{t+\Delta t}r\Delta t^4 w^2 - 5\,{}^{t}\dot{x}\,\Delta t^3 w^2\left(16\,{}^{t+\Delta t}r + 28\left({}^{t+\Delta t/2}r + {}^{t}\ddot{x}\right) - 19\,{}^{t}x w^2\right)\right.$$

$$\left. + \Delta t^2 + 144\left(\Delta t\,{}^{t}\dot{x} + {}^{t}x\right)\right) \qquad \text{(A2.16)}$$

$$^{t+\Delta t}_{BM}\dot{x} = \frac{1}{\left(16 + w^2\Delta t^2\right)\left(9 + w^2\Delta t^2\right)}\left(w^2\left(3\,{}^{t+\Delta t}r + w^2\,{}^{t}x - 4\,{}^{t+\Delta t/2}r - 4\,{}^{t}\ddot{x}\right)\Delta t^3\right.$$

$$\left. - 47\,\Delta t^2 w^2\,{}^{t}\dot{x} + \left(48\,{}^{t+\Delta t}r + 48\,{}^{t+\Delta t/2}r - 96\,w^2\,{}^{t}x + 48\,{}^{t}\ddot{x}\right)\Delta t + 144\,{}^{t}\dot{x}\right) \qquad \text{(A2.17)}$$

$$
{}^{t+\Delta t}_{BM}\ddot{x} = \frac{1}{\left(16 + w^2\Delta t^2\right)\left(9 + w^2\Delta t^2\right)}\left(\left(5\,\Delta t^{3\,t}\dot{x} + 19\,\Delta t^{2\,t}x\right)w^4\right.
$$

$$
\left. + \left(\left(-28\,{}^{t+\Delta t/2}r - 28\,{}^{t}\ddot{x} + 9\,{}^{t+\Delta t}r\right)\Delta t^2 - 144\,\Delta t\,{}^{t}\dot{x} - 144\,{}^{t}x\right)w^2 + 144\,{}^{t+\Delta t}r\right) \quad \text{(A2.18)}
$$

where $x = x_i$, $\omega = \omega_i$ and $r = r_i$ for the i-th mode shape.

Therefore, the solutions become

$$
{}^{t+\Delta t}_{BM}u_2 = \frac{k_2}{k_1}\,{}^{t+\Delta t}_{BM}x_1 + {}^{t+\Delta t}_{BM}x_2 \quad \text{(A2.19)}
$$

$$
{}^{t+\Delta t}_{BM}u_3 = {}^{t+\Delta t}_{BM}x_1 - \frac{k_2}{k_1}\,{}^{t+\Delta t}_{BM}x_2 \quad \text{(A2.20)}
$$

$$
{}^{t+\Delta t}_{BM}\dot{u}_2 = \frac{k_2}{k_1}\,{}^{t+\Delta t}_{BM}\dot{x}_1 + {}^{t+\Delta t}_{BM}\dot{x}_2 \quad \text{(A2.21)}
$$

$$
{}^{t+\Delta t}_{BM}\dot{u}_3 = {}^{t+\Delta t}_{BM}\dot{x}_1 - \frac{k_2}{k_1}\,{}^{t+\Delta t}_{BM}\dot{x}_2 \quad \text{(A2.22)}
$$

$$
{}^{t+\Delta t}_{BM}\ddot{u}_2 = \frac{k_2}{k_1}\,{}^{t+\Delta t}_{BM}\ddot{x}_1 + {}^{t+\Delta t}_{BM}\ddot{x}_2 \quad \text{(A2.23)}
$$

$$
{}^{t+\Delta t}_{BM}\ddot{u}_3 = {}^{t+\Delta t}_{BM}\ddot{x}_1 - \frac{k_2}{k_1}\,{}^{t+\Delta t}_{BM}\ddot{x}_2 \quad \text{(A2.24)}
$$

A.2.3 Comparisons

In Chapters 2 and 3, the Bathe method gives the solutions like in a mode superposition analysis, includes only the physical modes together with the static correction resulted from

the artificial high frequency response. In other words, the Bathe method effectively treats the responses from high frequency mode as if it is from the static correction.

Also, we observed that the Bathe method immediately does this desired behavior in displacement and velocity (in acceleration, it needs one more step.) We show this characteristic by comparing the explicit expressions of the solutions from the Bathe method and of the desired solution (mode1 + SC). Here, we consider the solution from second mode of our model system at time Δt.

1) Displacement

The time step size, Δt is set to capture the physical modes, therefore, for the high frequency mode the ratio of Δt to the period of the high frequency mode is

$$\frac{\Delta t}{T_{high}} \gg 1 \tag{A2.25}$$

Or,

$$\omega_{high}\, \Delta t \gg 1 \tag{A2.26}$$

With Eq. (A2.26), the solution from the Bathe method, Eq. (A2.16), becomes

$${}^{t+\Delta t}_{BM}x_2 = \frac{{}^{t+\Delta t}r_2/\omega_2^2}{\frac{9}{\omega_2^2\,\Delta t^2}+1} + O(\frac{1}{\omega_2^2\,\Delta t^2}) \tag{A2.27}$$

Since $r_2 = k_1 \sin \omega_p t$, at time point Δt, Eq. (A2.27) becomes

$$ {}^{\Delta t}_{BM}x_2 \simeq \sin \omega_p \Delta t \tag{A2.28} $$

while the desired static correction solution at time Δt is

$$ {}^{\Delta t}_{S}x_2 \simeq \sin \omega_p \Delta t \tag{A2.29} $$

Therefore, the solution from the Bathe method for displacement is very close to the displacement of the static correction for the high frequency mode.

2) Velocity

Similarly, the solution from the Bathe method for velocity, Eq. (A2.17), becomes

$$ {}^{t+\Delta t}_{BM}\dot{x}_2 = \frac{3\,{}^{t+\Delta t}r_2\,\Delta t}{9+\omega_2^2\Delta t^2} + \frac{4\,{}^{t+\Delta t/2}r_2\,\omega_2^2\,\Delta t^3}{(9+\omega_2^2\,\Delta t^2)(16+\omega_2^2\,\Delta t^2)} + O(\frac{1}{\omega_2^2\,\Delta t^2}) \tag{A2.30} $$

Using $r_2 = k_1 \sin \omega_p t$, Eq. (A2.30) can be rewritten at time point Δt as

$$ {}^{\Delta t}_{BM}\dot{x}_2 \simeq \frac{3\,\sin(\omega_p\,\Delta t)}{\Delta t} - \frac{4\,\sin(1/2\,\omega_p\,\Delta t)}{\Delta t} \tag{A2.30} $$

$$ = \omega_p - \frac{5}{12}\,\omega_p^3\,\Delta t^2 + \frac{23}{960}\,\omega_p^5\,\Delta t^4 + O(\Delta t^5) \tag{A2.31} $$

The exact expression of the desired static correction solution at time Δt is

$$ {}^{\Delta t}_{S}\dot{x}_2 = \omega_p \cos \omega_p \Delta t \tag{A2.32} $$

and its Taylor expansion is

$$ {}^{\Delta t}_{S}\dot{x}_2 = \omega_p - \frac{1}{2}\omega_p^3 \Delta t^2 + \frac{1}{24}\omega_p^5 \Delta t^4 + O(\Delta t^6) \tag{A2.33} $$

Therefore, the solution from the Bathe method for velocity is very close to the velocity of the static correction for the high frequency mode.

3) Acceleration

Similarly, the solution from the Bathe method for acceleration, Eq. (A2.18), for the high frequency mode can be expressed as

$$ \begin{aligned} {}^{t+\Delta t}_{BM}\ddot{x}_2 = \frac{1}{(9+\omega_2^2\Delta t^2)(16+\omega_2^2\Delta t^2)} & (5\ {}_{BM}{}^{t}\dot{x}_2\omega_2^4\Delta t^3 + 19\ {}_{BM}{}^{t}x\,\omega_2^4\Delta t^2 \\ & +9\,{}^{\Delta t}r_2\,\omega_2^2\Delta t^2 - 28\,{}^{\Delta t/2}r_2\,\omega_2^2\Delta t^2) \end{aligned} \tag{A2.34} $$

And the desired static correction solution at time Δt is

$$ \begin{aligned} {}^{\Delta t}_{S}\ddot{x}_2 &= -\omega_p^2 \sin \omega_p \Delta t \\ &= -\omega_p^3 \Delta t + \frac{1}{6}\omega_5 \Delta t^3 - \frac{1}{120}\omega_p^7 \Delta t^5 + O(\Delta t^6) \end{aligned} \tag{A2.35} $$

At the time point Δt, since ${}^{0}_{BM}\dot{x}_2$ and ${}^{0}_{BM}\dot{x}_2$ are zero, Eq. (A2.35) becomes

$$ {}^{\Delta t}_{BM}\ddot{x}_2 = -\frac{5\,\omega_p}{\Delta t} - \frac{11}{12}\,\omega_p^3\,\Delta t + \frac{13}{192}\,\omega_p^5\,\Delta t^3 + O(\Delta t^4) \qquad \text{(A2.36)} $$

and it is not similar to the Eq. (A2.35) due to the first term; therefore, the solution at the first time point from the Bathe method is not accurate and the method provides the undershoot.

However, at the time point $2\,\Delta t$, since ${}^{\Delta t}_{BM}\dot{x}_2 \simeq \sin\omega_p\,\Delta t$ and ${}^{\Delta t}_{BM}\dot{x}_2 \simeq \omega_p \cos\omega_p\,\Delta t$, the solution at the second time step becomes

$$ {}^{2\,\Delta t}_{BM}\ddot{x}_2 = -\frac{23}{12}\,\omega_p^3\,\Delta t + \frac{191}{192}\,\omega_p^5\,\Delta t^3 - \frac{281}{161280}\,\omega_p^7\,\Delta t^5 + O(\Delta t^7) \qquad \text{(A2.37)} $$

while the static correction solution at time $2\,\Delta t$ is

$$ \begin{aligned} {}^{2\,\Delta t}_{S}\ddot{x}_2 &= -\omega_p^2\,\sin\omega_p\,2\,\Delta t \\ &= -2\,\omega_p^3\,\Delta t + \frac{4}{3}\,\omega_5\,\Delta t^3 - \frac{4}{15}\,\omega_p^7\,\Delta t^5 + O(\Delta t^6) \end{aligned} \qquad \text{(A2.38)} $$

Therefore, from the second time point, the solution from the Bathe method for acceleration is sufficiently close to the acceleration of the static correction for high frequency mode.

A.3 On numerical wavelength and phase speed with respect to the time step size

Recall our general form

$$ {}^{t}_{x}u = A_k \, e^{i(kx-\omega t)} \tag{A3.1} $$

We now consider a regular mesh with nodes equally spaced Δx apart along the x axis, then the solution to the finite element system at time $n_t \Delta t$ and location $n_x \Delta x$ can be rewritten as

$$ \begin{aligned} {}^{n_t\Delta t}_{n_x\Delta x}u &= A_k \, e^{i(k n_x \Delta x - \omega n_t \Delta t)} \\ &= A_k \, e^{i 2\pi \frac{\Delta t}{T_0}\left(n_x \frac{1}{\mathrm{CFL}} \frac{\lambda_0}{\lambda} - n_t \frac{T_0}{T} \right)} \end{aligned} \tag{A3.2} $$

All variables with 0 subscript indicate the exact value. For the 2-node element, with a similar procedure in Chapter 3, we obtain the relations between the values of the CFL number, $\Delta t / T_0$, λ / λ_0 and T_0 / T for the Bathe method and the Newmark method. Note that using the measured period elongation, which is function of $\Delta t / T_0$, we express the error in the wave length with respect to $\Delta t / T_0$ and CFL (Figs. A3-1 and A3-2).

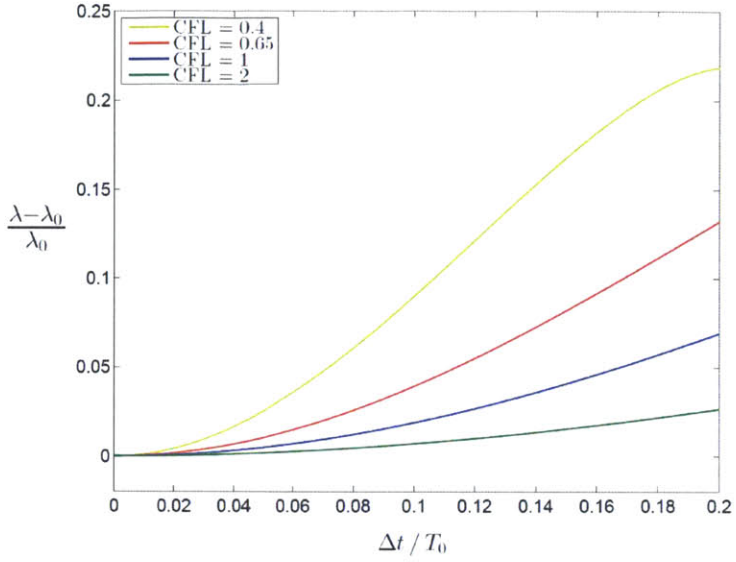

Figure A3-1 **Relative wavelength errors of the Bathe method for various CFL numbers;**

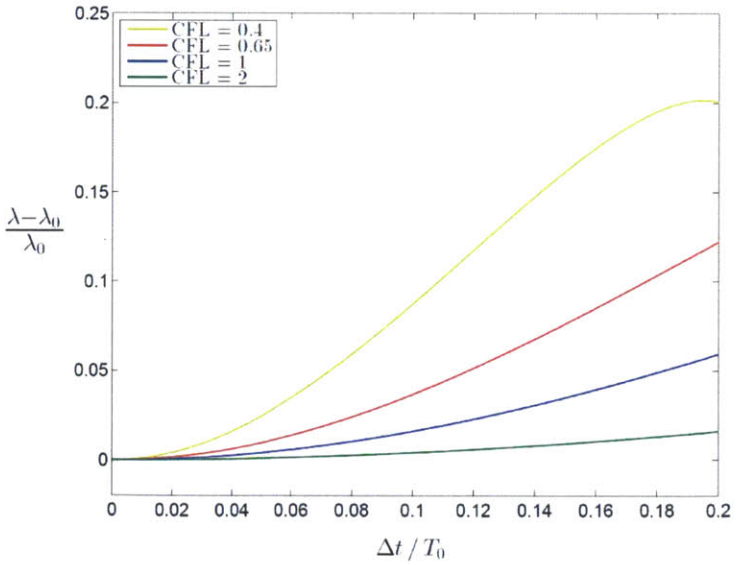

Figure A3-2 **Relative wavelength errors of the Trapezoidal rule for various CFL numbers;**

Note that, for the both methods, with the CFL number which makes the solution least dispersive, the curve of the wavelength error is almost the same with the period elongation curve. Since $\frac{c}{c_0} = \frac{\lambda}{\lambda_0}\frac{T_0}{T} = 1$, with these CFL numbers when $\Delta t / T_0 \ll 1$, the results are well understood.

We also can check the above observation from the approximated expression of wavelength error. For $\Delta t / T_0 \ll 1$, the wavelength error are estimated as

(Bathe method)

$$\frac{\lambda - \lambda_0}{\lambda_0} = \frac{T - T_0}{T_0} - \frac{\pi^2}{96}\left(13 - \frac{16}{\mathrm{CFL}^2}\right)\frac{T_0}{T}\left(\frac{\Delta t}{T_0}\right)^2 + O\left(\left(\frac{\Delta t}{T_0}\right)^4\right) \qquad \text{(A3.3)}$$

(Newmark method)

$$\frac{\lambda - \lambda_0}{\lambda_0} = \frac{T - T_0}{T_0} - \frac{\pi^2}{6}\left(2 - \frac{1}{\mathrm{CFL}^2}\right)\frac{T_0}{T}\left(\frac{\Delta t}{T_0}\right)^2 + O\left(\left(\frac{\Delta t}{T_0}\right)^4\right) \qquad \text{(A3.4)}$$

Also, the results show that with the given time step size, smaller finite element reduces the error in the wavelength.

We also can express Eq. (A3.2) as

$$
\begin{aligned}
{}^{n_t\Delta t}_{n_x\Delta x}u &= A_k e^{i(k n_x \Delta x - \omega n_t \Delta t)} \\
&= A_k e^{i2\pi \frac{\Delta t}{T_0}\left(n_x \frac{c_0}{c}\frac{T_0}{T}\frac{1}{\mathrm{CFL}} - n_t \frac{T_0}{T}\right)}
\end{aligned}
\tag{A3.5}
$$

Therefore, we obtain the dispersion error in terms of time step size Δt (Figs. A3-4 and A3-5). In particular, Fig. A3-4 may show accuracy characteristic of remained wave modes in the Bathe method.

The approximated expressions for dispersion error with respect to the time step size are obtained as

(Bathe method)

$$
\frac{c - c_0}{c_0} = -\frac{\pi^2}{96}\left(13 - \frac{16}{\mathrm{CFL}^2}\right)\left(\frac{T_0}{T}\right)^2\left(\frac{\Delta t}{T_0}\right)^2 + O\left(\left(\frac{\Delta t}{T_0}\right)^4\right) \tag{A3.6}
$$

(Newmark method)

$$
\frac{c - c_0}{c_0} = -\frac{\pi^2}{6}\left(2 - \frac{1}{\mathrm{CFL}^2}\right)\left(\frac{T_0}{T}\right)^2\left(\frac{\Delta t}{T_0}\right)^2 + O\left(\left(\frac{\Delta t}{T_0}\right)^4\right) \tag{A3.7}
$$

Note that Eqs. (A3.6) and (A3.7) can also be derived from Eqs. (A3.3) and (A3.4).

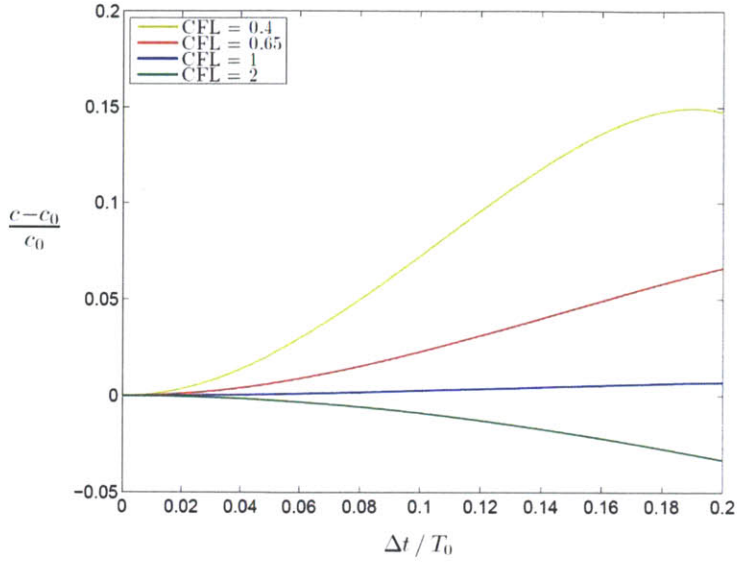

Figure A3-3 **Relative wave speed errors of the Bathe method for various CFL numbers;**

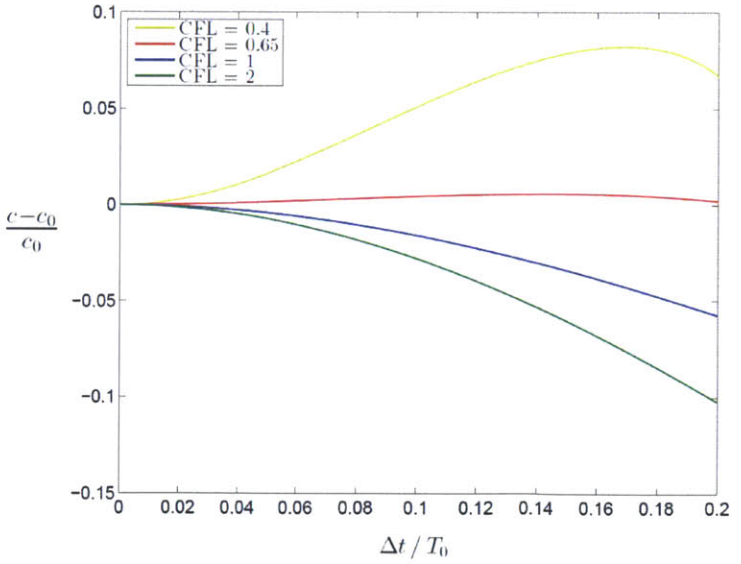

Figure A3-4 **Relative wave speed errors of the Trapezoidal rule for various CFL numbers;**

A.4 Integration approximation and load operators of the proposed method

Using the relations in Eqs. (4.12) and (4.22), we obtain an expression for the integration approximation $\mathbf{A}$ load operators $\mathbf{L}_a$ and $\mathbf{L}_b$ of the proposed explicit method as

$$\mathbf{A} = \begin{bmatrix} a_{11} & a_{12} & a_{13} \\ a_{21} & a_{22} & a_{23} \\ a_{31} & a_{32} & a_{33} \end{bmatrix} \tag{A4.1}$$

$$\mathbf{L}_a = \begin{bmatrix} \frac{1}{2}(p-1)\Omega_0{}^2 + \xi(-2+p)\Omega_0 \\ \frac{\Delta t}{2p}\left(\left(1+\Omega_0\left((1/2)\Omega_0+\xi\right)p^3 - 2\Omega_0\left((1/4)\Omega_0+\xi\right)p^2 - p\right)\right) \\ -\frac{\Delta t^2}{2}(p-1) \end{bmatrix} \tag{A4.2}$$

$$\mathbf{L}_b = \begin{bmatrix} 1 \\ \frac{p\Delta t}{2} \\ 0 \end{bmatrix} \tag{A4.3}$$

where

$$a_{11} = -\frac{p\Omega_0}{2}\left(\left(-(1/2)p + (1/2)p^2\right)\Omega_0{}^3 + \xi\left(p^2 - 2\right)\Omega_0{}^2 + \left(1 + \left(-8 + 4p\right)\xi^2\right)\Omega_0 + 2\xi\right) \quad \text{(A4.4)}$$

$$a_{12} = -\frac{\Omega_0}{\Delta t}\left(\left(-(1/2)p + (1/2)p^2\right)\Omega_0{}^3 + \xi\left(-1 + p^2 - p\right)\Omega_0{}^2 + \left(1 + \left(-4 + 2p\right)\xi^2\right)\Omega_0 + 2\xi\right) \quad \text{(A4.5)}$$

$$a_{13} = -\frac{\Omega_0{}^2}{\Delta t^2}\left(1 + \left((1/2)p - (1/2)\right)\Omega_0{}^2 + \xi\left(-2 + p\right)\Omega_0\right) \quad \text{(A4.6)}$$

$$a_{21} = -\frac{\Delta t}{8p}\left(\begin{array}{l} p^5\Omega_0{}^4 + 2p^5\xi\Omega_0{}^3 - p^4\Omega_0{}^4 + 8p^4\xi^2\Omega_0{}^2 - 4\xi\Omega_0{}^3p^3 \\ +4p^3\xi\Omega_0 - 16p^3\xi^2\Omega_0{}^2 - 8\xi\Omega_0p^2 + 4p^2 + 2\Omega_0{}^2p^2 + 8\xi\Omega_0p - 12p + 4 \end{array}\right) \quad \text{(A4.7)}$$

$$a_{22} = \frac{1}{4p}\left(\begin{array}{l} \left(-p^4 + p^3\right)\Omega_0{}^4 - 2\xi p^2\left(-1 + p^2 - p\right)\Omega_0{}^3 \\ +\left(8\xi^2p^2 - 4p^3\xi^2 - 2p\right)\Omega_0{}^2 - 4\xi\left(-p + p^2 + 1\right)\Omega_0 + 4p \end{array}\right) \quad \text{(A4.8)}$$

$$a_{23} = -\frac{\Omega_0{}^2}{2p\Delta t}\left(1 + \Omega_0\left((1/2)\Omega_0 + \xi\right)p^3 + \left(1 - (1/2)\Omega_0{}^2 - 2\xi\Omega_0\right)p^2 - p\right) \quad \text{(A4.9)}$$

$$a_{31} = \frac{1}{4}\left(2 + \left(p^2 - p\right)\Omega_0{}^2 + 4\xi\left(p - 1\right)\Omega_0\right)\Delta t^2 p \quad \text{(A4.10)}$$

$$a_{32} = \frac{\Delta t}{2}\left(2 + \left(p^2 - p\right)\Omega_0{}^2 + 2\xi\left(p - 1\right)\Omega_0\right) \quad \text{(A4.11)}$$

$$a_{33} = 1 + \frac{1}{2}\left(p - 1\right)\Omega_0{}^2 \quad \text{(A4.12)}$$